NATIONAL ADVISORY COMMITTEE FOR AERONAUTICS

REPORT No. 586

AIRFOIL SECTION CHARACTERISTICS AS AFFECTED BY VARIATIONS OF THE REYNOLDS NUMBER

By EASTMAN N. JACOBS and ALBERT SHERMAN

REPRINT OF REPORT No. 586, ORIGINALLY PUBLISHED SEPTEMBER 1937

1939

AERONAUTIC SYMBOLS

1. FUNDAMENTAL AND DERIVED UNITS

	Symbol	Metric		English	
		Unit	Abbreviation	Unit	Abbreviation
Length	l	meter	m	foot (or mile)	ft. (or mi.)
Time	t	second	s	second (or hour)	sec. (or hr.)
Force	F	weight of 1 kilogram	kg	weight of 1 pound	lb.
Power	P	horsepower (metric)		horsepower	hp.
Speed	V	kilometers per hour	k.p.h.	miles per hour	m.p.h.
		meters per second	m.p.s.	feet per second	f.p.s.

2. GENERAL SYMBOLS

W, Weight$=mg$

g, Standard acceleration of gravity$=9.80665$ m/s^2 or 32.1740 ft./sec.^{2}

m, Mass$=\frac{W}{g}$

I, Moment of inertia$=mk^2$. (Indicate axis of radius of gyration k by proper subscript.)

μ, Coefficient of viscosity

ν, Kinematic viscosity

ρ, Density (mass per unit volume)

Standard density of dry air, 0.12497 kg-m^{-4}-s^2 at 15° C. and 760 mm; or 0.002378 lb.-ft.$^{-4}$ sec.^{2}

Specific weight of "standard" air, 1.2255 kg/m^3 or 0.07651 lb./cu. ft.

3. AERODYNAMIC SYMBOLS

S, Area

S_w, Area of wing

G, Gap

b, Span

c, Chord

$\frac{b^2}{S}$, Aspect ratio

V, True air speed

q, Dynamic pressure$=\frac{1}{2}\rho V^2$

L, Lift, absolute coefficient $C_L=\frac{L}{qS}$

D, Drag, absolute coefficient $C_D=\frac{D}{qS}$

D_0, Profile drag, absolute coefficient $C_{D_0}=\frac{D_0}{qS}$

D_i, Induced drag, absolute coefficient $C_{D_i}=\frac{D_i}{qS}$

D_p Parasite drag, absolute coefficient $C_{D_p}=\frac{D_p}{qS}$

C, Cross-wind force, absolute coefficient $C_C=\frac{C}{qS}$

R, Resultant force

i_w, Angle of setting of wings (relative to thrust line)

i_t, Angle of stabilizer setting (relative to thrust line)

Q, Resultant moment

Ω, Resultant angular velocity

$\rho\frac{Vl}{\mu}$, Reynolds Number, where l is a linear dimension (e.g., for a model airfoil 3 in. chord, 100 m.p.h. normal pressure at 15° C., the corresponding number is 234,000; or for a model of 10 cm chord, 40 m.p.s., the corresponding number is 274,000)

C_p, Center-of-pressure coefficient (ratio of distance of c.p. from leading edge to chord length)

α, Angle of attack

ϵ, Angle of downwash

α_0, Angle of attack, infinite aspect ratio

α_i, Angle of attack, induced

α_a, Angle of attack, absolute (measured from zero-lift position)

γ, Flight-path angle

REPORT No. 586

AIRFOIL SECTION CHARACTERISTICS AS AFFECTED BY VARIATIONS OF THE REYNOLDS NUMBER

By EASTMAN N. JACOBS and ALBERT SHERMAN
Langley Memorial Aeronautical Laboratory

NATIONAL ADVISORY COMMITTEE FOR AERONAUTICS

HEADQUARTERS, NAVY BUILDING, WASHINGTON, D. C.

LABORATORIES, LANGLEY FIELD, VA.

Created by act of Congress approved March 3, 1915, for the supervision and direction of the scientific study of the problems of flight (U. S. Code, Title 50, Sec. 151). Its membership was increased to 15 by act approved March 2, 1929. The members are appointed by the President, and serve as such without compensation.

TECHNICAL COMMITTEES

AERODYNAMICS
POWER PLANTS FOR AIRCRAFT
AIRCRAFT MATERIALS

AIRCRAFT STRUCTURES
AIRCRAFT ACCIDENTS
INVENTIONS AND DESIGNS

Coordination of Research Needs of Military and Civil Aviation

Preparation of Research Programs

Allocation of Problems

Prevention of Duplication

Consideration of Inventions

LANGLEY MEMORIAL AERONAUTICAL LABORATORY

LANGLEY FIELD, VA.

Unified conduct, for all agencies, of scientific research on the fundamental problems of flight.

OFFICE OF AERONAUTICAL INTELLIGENCE

WASHINGTON, D. C.

Collection, classification, compilation, and dissemination of scientific and technical information on aeronautics.

REPORT No. 586

AIRFOIL SECTION CHARACTERISTICS AS AFFECTED BY VARIATIONS OF THE REYNOLDS NUMBER

By Eastman N. Jacobs and Albert Sherman

SUMMARY

An investigation of a systematically chosen representative group of related airfoils was made in the N. A. C. A. variable-density wind tunnel over a wide range of the Reynolds Number extending well into the flight range. The tests were made to provide information from which the variations of airfoil section characteristics with changes in the Reynolds Number could be inferred and methods of allowing for these variations in practice could be determined. This work is one phase of an extensive and general airfoil investigation being conducted in the variable-density tunnel and extends the previously published researches concerning airfoil characteristics as affected by variations in airfoil profile determined at a single value of the Reynolds Number.

The object of this report is to provide means for making available as section characteristics at any free-air value of the Reynolds Number the variable-density tunnel airfoil data previously published. Accordingly, the various corrections involved in deriving more accurate airfoil section characteristics than those heretofore employed are first considered at length and the corrections for turbulence are explained. An appendix is included that covers the results of an investigation of certain consistent errors present in test results from the variable-density tunnel. The origin and nature of scale effects are discussed and the airfoil scale-effect data are analyzed. Finally, methods are given of allowing for scale effects on airfoil section characteristics in practice within ordinary limits of accuracy for the application of variable-density-tunnel airfoil data to flight problems.

INTRODUCTION

When data from a model test are applied to a flight problem, the condition that should be satisfied is that the flows for the two cases be similar. The Reynolds Number, which indicates the ratio of the mass forces to the viscous forces in aerodynamic applications, is ordinarily used as the criterion of similarity. The practical necessity for having the flow about the model aerodynamically similar to the flow about the full-scale object in flight becomes apparent from the fact that aerodynamic coefficients, as a rule, vary with changes in the Reynolds Number. This phenomenon is referred to as "scale effect."

Early investigations of scale effect were made in small atmospheric tunnels at comparatively low values of the Reynolds Number and, for airfoils, covered a range of the Reynolds Number too limited and too remote from the full-scale range to permit reliable extrapolations to flight conditions. Attempts were made to bridge the gap between the two Reynolds Number ranges by making full-scale flight tests for comparison with model tests. These investigations of scale effect, however, proved disappointing owing partly to the difficulty of obtaining good flight tests and to the difficulty of reproducing flight conditions in the model tests and partly to the large unexplored Reynolds Number range between the model and flight tests with consequent uncertainties regarding the continuity of the characteristics over this range. Furthermore, the flight tests could not ordinarily include a sufficiently large range of the Reynolds Number to establish the character of the scale effects for certain of the airfoil characteristics over the full-scale range of the Reynolds Number, which may extend from values as low as a few hundred thousand to thirty million or more.

These limitations of the early investigations were first overcome by the N. A. C. A. through the use of the variable-density tunnel, which was designed to facilitate aerodynamic investigations over the entire range of Reynolds Numbers between the wind tunnel and flight values. Several miscellaneous and commonly used airfoils were investigated for scale effect in the variable-density tunnel during the first years of its operation. The results indicated that important scale effects for some airfoils may be expected above the usual wind-tunnel range and even within the flight range of values of the Reynolds Number. Later, when the N. A. C. A. full-scale tunnel was constructed, airfoil tests therein served to confirm the importance of scale effects occurring in the full-scale range and also provided valuable data for the interpretation of the variable-density-tunnel results, particularly in connection with the effects of the turbulence present in the

variable-density tunnel. The interpretation of the variable-density-tunnel results has consequently been modified to allow for the turbulence on the basis of an "effective Reynolds Number" higher than the test Reynolds Number.

In the meantime, the investigations of airfoils in the variable-density tunnel had been turned to an extensive study of airfoil characteristics as affected by airfoil shape. This phase, which resulted in the development of the well-known N. A. C. A. airfoils, involved the testing of a large number of related airfoils, but these tests were largely confined to one value of the Reynolds Number within the full-scale range. Such a procedure expedited the investigation and provided comparable data for the various airfoils within the full-scale range of the Reynolds Number but, of course, gave no information about scale effects.

As previously stated, the full-scale-tunnel results had provided information regarding the application of the variable-density-tunnel data to flight. Methods were accordingly developed for correcting the data and for presenting them in forms that would facilitate their use as applied to flight problems. Flight problems, however, require airfoil data at various values of the Reynolds Number between values as low as a few hundred thousand in some cases to thirty million or more in others. Obviously the results available from the tests of related airfoils at one value of the Reynolds Number (effective Reynolds Number=8,000,000) are inadequate for the purpose unless they can be corrected to other values of the Reynolds Number. The present investigation was therefore undertaken to study the scale effects for the related airfoil sections primarily with a view to the formulation of general methods for determining scale-effect corrections for any normal airfoil section so that the standard test results from the variable-density tunnel could be applied to flight at any Reynolds Number. For most practical uses it is considered desirable and sufficient to present airfoil test results in the form of tabular values giving certain important aerodynamic characteristics for each *airfoil section*. The primary object of this investigation, therefore, is to give information about the variation of these important airfoil section characteristics with Reynolds Number.

In regard to the scope of the experimental investigation, the Reynolds Number range was chosen as the largest possible in the variable-density tunnel and the airfoil sections were chosen to cover as far as possible the range of shapes commonly employed. Accordingly, groups of related airfoils (fig. 1) were tested to investigate the following variables related to the airfoil-section shape:

Thickness.
Camber.
Thickness and camber.
Thickness shape.
Camber shape.
Sections with high-lift devices.

The testing program was begun in May 1934 and extended several times as it became apparent that additional tests would be desirable. The final tests in the variable-density tunnel were made in September 1935.

TESTS AND MODELS

Descriptions of the variable-density wind tunnel and of the methods of testing are given in reference 1.

The tests herein reported were made for the most part for each airfoil at tank pressures of 1/4, 1/2, 1, 2, 4, 8, 15, and 20 atmospheres, covering a range of test Reynolds Numbers from 40,000 to 3,100,000. The 1/4- and 1/2-atmosphere runs were omitted for many of the airfoils and, in several cases, only the lift-curve peaks were obtained at the lower Reynolds Numbers. Runs at reduced speeds (1/5 and 1/2 the standard value of the dynamic pressure q) at 20 atmospheres were sometimes substituted for the tests at 8 and 15 atmospheres. Several check tests at 8 and 15 atmospheres and results from some earlier investigations have shown that the specific manner of varying the Reynolds Number with respect to speed or density is unimportant when the effects of compressibility are negligible. For all the airfoils, the air in the tunnel was decompressed and the airfoil repolished before running the higher Reynolds Number tests. Tares obtained at corresponding Reynolds Numbers were used in working up the results.

The airfoil models are of metal, usually of duralumin and of standard 5- by 30-inch plan form; the sections employed (see fig. 1), except for the slotted Clark Y, are members of N. A. C. A. airfoil families (references 2 and 3). The slotted Clark Y model is of 36-inch span and 6-inch chord (with the slot closed) and was made to the ordinates given in reference 4. For this airfoil, the coefficients are given as based on the chord and area corresponding to the slot-closed condition. The slat was made of stainless steel and fastened to the main wing in the position reported (reference 4) to result in the highest value of maximum lift coefficient. This model was tested at a much earlier date than the others, and the test data are somewhat less accurate. The main wing of the N. A. C. A. 23012 airfoil with external-airfoil flap is of 30-inch span and 4.167-inch chord. The flap is of stainless steel and is also of N. A. C. A. 23012 section having a chord of 20 percent that of the main airfoil. It was fastened to the main wing in the optimum hinge position reported in reference 5. Data for this airfoil combination are given herein for two angular flap settings: −3°, which corresponds to the minimum-drag condition; and 30°, which corresponds to the maximum-lift condition. The coefficients are given as based on the sums of the main wing and flap chords and areas.

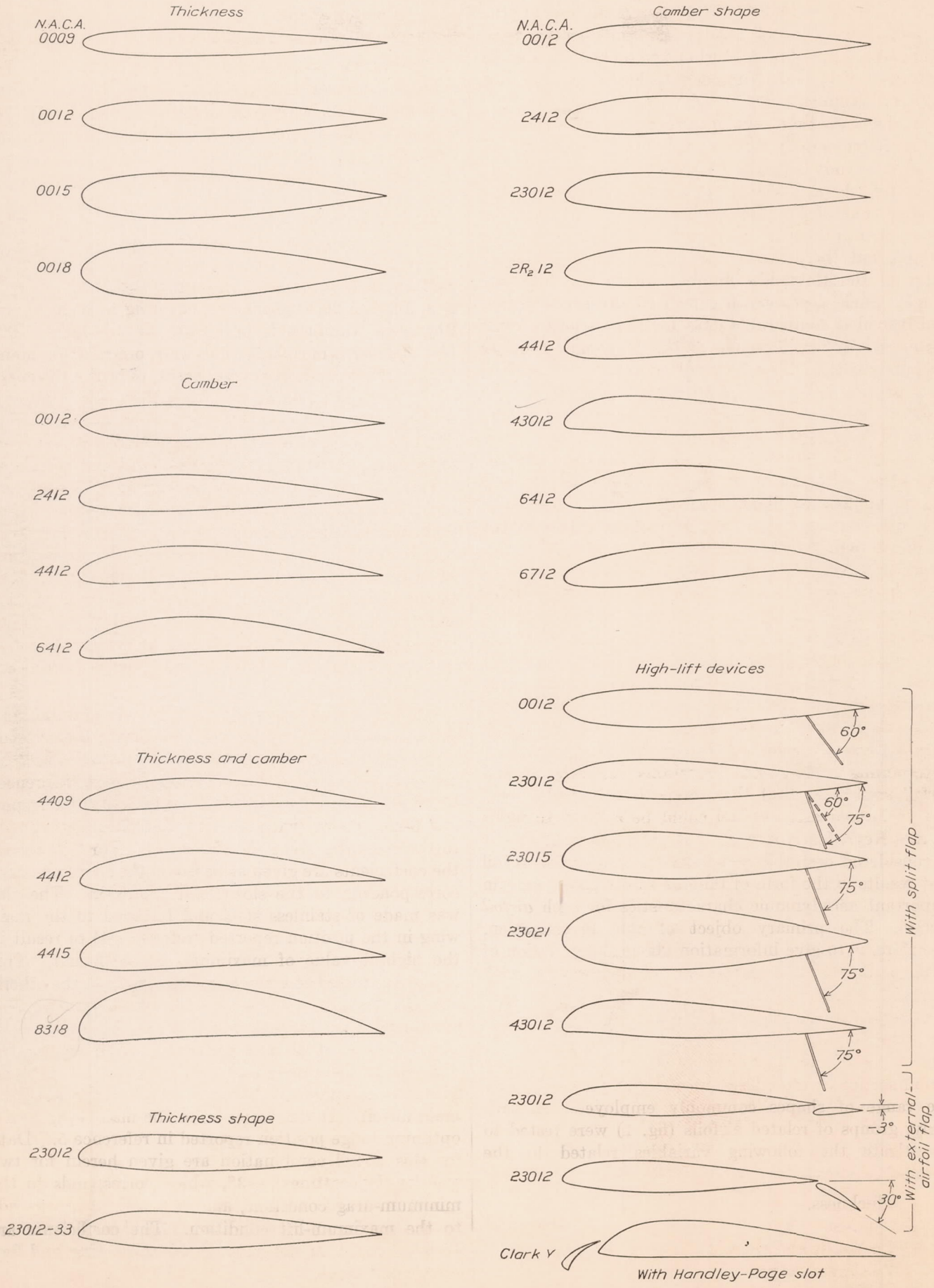

FIGURE 1.—Airfoil sections employed for the scale-effect investigation. The sections, except for the slotted Clark Y, are members of N. A. C. A. airfoil families.

ACCURACY

The accuracy of the experimental data of this investigation at the highest Reynolds Number is comparable with that of the standard airfoil test data as discussed in reference 2. The systematic errors of measurement therein mentioned, however, have since been investigated and the results are presented in the appendix to this report. The systematic errors of velocity measurement have hence been eliminated, the errors associated with support deflection have been largely removed, and the errors associated with model roughness have been minimized by giving careful attention to the model surfaces.

The remaining systematic errors are mainly those associated with the interpretation of the wind-tunnel results rather than the direct errors of measurement. These errors are associated, first, with the calculation of airfoil *section* characteristics from the tests of finite-aspect-ratio airfoils and, second, with the correction of the test results to zero turbulence or free-air conditions. Such errors will be more fully treated in the discussion where the methods of correction, including the interpretation of the results as involving the effective Reynolds Number, are considered.

The magnitude of the direct experimental errors, particularly of the accidental errors, increases as the Reynolds Number is reduced. Any variation of the support interference with the Reynolds Number was not taken into account in spite of the fact that the test results tend to indicate that the uncorrected part (see appendix) of the support interference may cease to be negligible at low test Reynolds Numbers. These errors may be judged by a study of the dissymmetry of the test results for positive and negative angles of attack for the symmetrical airfoils and by the scattering of the points representing the experimental data. (See figs. 2 to 24.) Such a study indicates that the results from tests at tank pressures at and above 4 atmospheres (effective Reynolds Numbers above 1,700,000) are of the same order of accuracy as those from the highest Reynolds Number tests. The drag and pitching-moment results for effective Reynolds Numbers below 800,000, however, become relatively inaccurate owing to limitations imposed by the sensitivity of the measuring equipment. In fact, it appears that the accuracy becomes insufficient to define with certainty the shapes of curves representing variations of these quantities with angle of attack or lift coefficient. Hence airfoil characteristics dependent on the shape of such curves, e. g., the optimum lift coefficient and the aerodynamic-center position, are considered unreliable and in most cases are not presented below an effective Reynolds Number of 800,000.

RESULTS

Figures 2 to 24 present the test results corrected after the methods given in reference 1 for approximating infinite-aspect-ratio characteristics. Curves are given (for each airfoil for different test Reynolds Numbers) of lift coefficient C_L against effective angle of attack α_0, and of profile-drag coefficient C_{D_0} and of pitching-moment coefficient about the aerodynamic center $C_{m_{a.c.}}$ against lift coefficient C_L. The x and y coordinates of the aerodynamic center from the airfoil quarter-chord point are also given where the data permit. Although not precisely *section characteristics*, characteristics so corrected have been used heretofore as section characteristics because of the lack of anything more exact.

Further corrections, however, to allow for the effects of wind-tunnel turbulence, airfoil-tip shape, and some of the limitations of the previous corrections based on airfoil theory were developed during the course of this investigation and, when applied, give results representing the most reliable section data now available from the variable-density wind tunnel. These additional corrections and their derivation are fully discussed later in this report. The more exact *section* characteristics have been distinguished by lower-case symbols, e. g., section lift coefficient c_l, section profile-drag coefficient c_{d_0}, section optimum lift coefficient $c_{l_{opt}}$, and section pitching-moment coefficient about the aerodynamic center $c_{m_{a.c.}}$. These values are then considered applicable to flight at the effective Reynolds Number, R_e.

Table I presents, for various Reynolds Numbers, the principal aerodynamic characteristics, in the form of these fully corrected section characteristics, of the airfoils tested. Cross plots of certain of these section characteristics against Reynolds Number are also given for use with the discussion. (See fig. 28 and figs. 32 to 43.)

DISCUSSION

Scale effects, or the variations of aerodynamic coefficients with Reynolds Number, have previously been considered of primary importance only in relation to the interpretation of low-scale test results from atmospheric wind tunnels. It now appears from variable-density and full-scale-tunnel data that important variations of the coefficients must be recognized within the flight range of values of the Reynolds Number, particularly in view of the fact that the flight range is continually being increased.

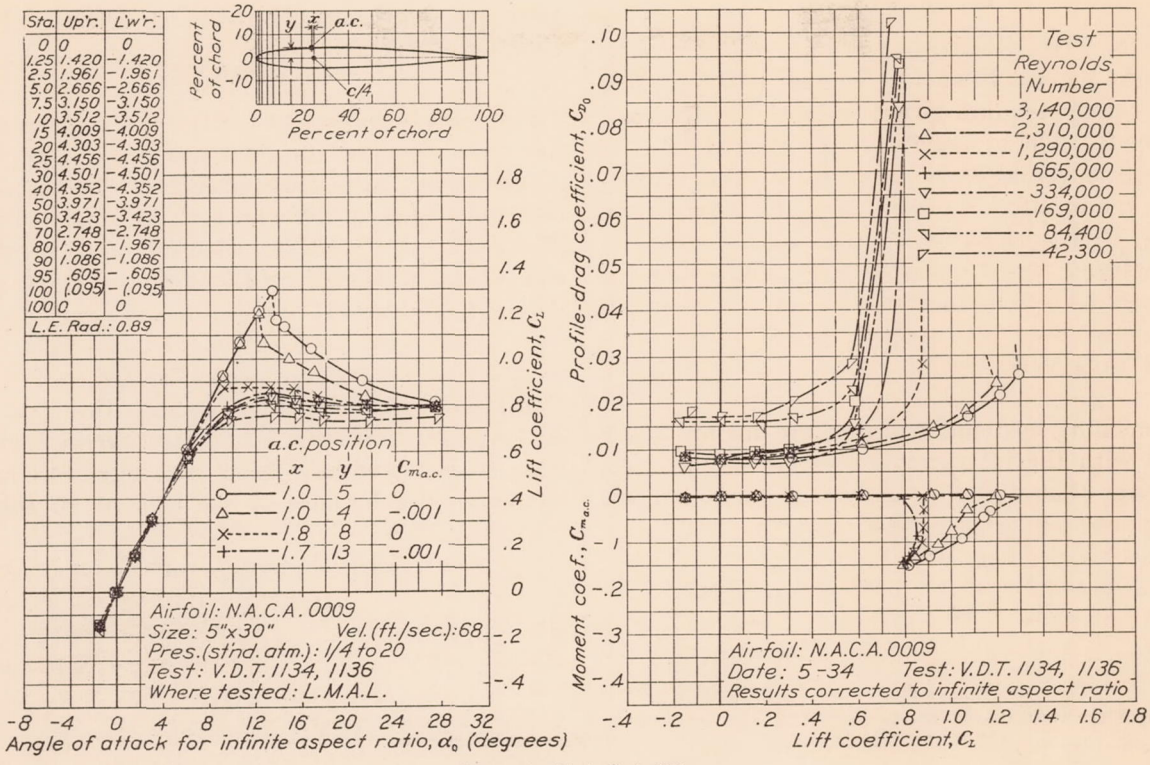

FIGURE 2.—N. A. C. A. 0009.

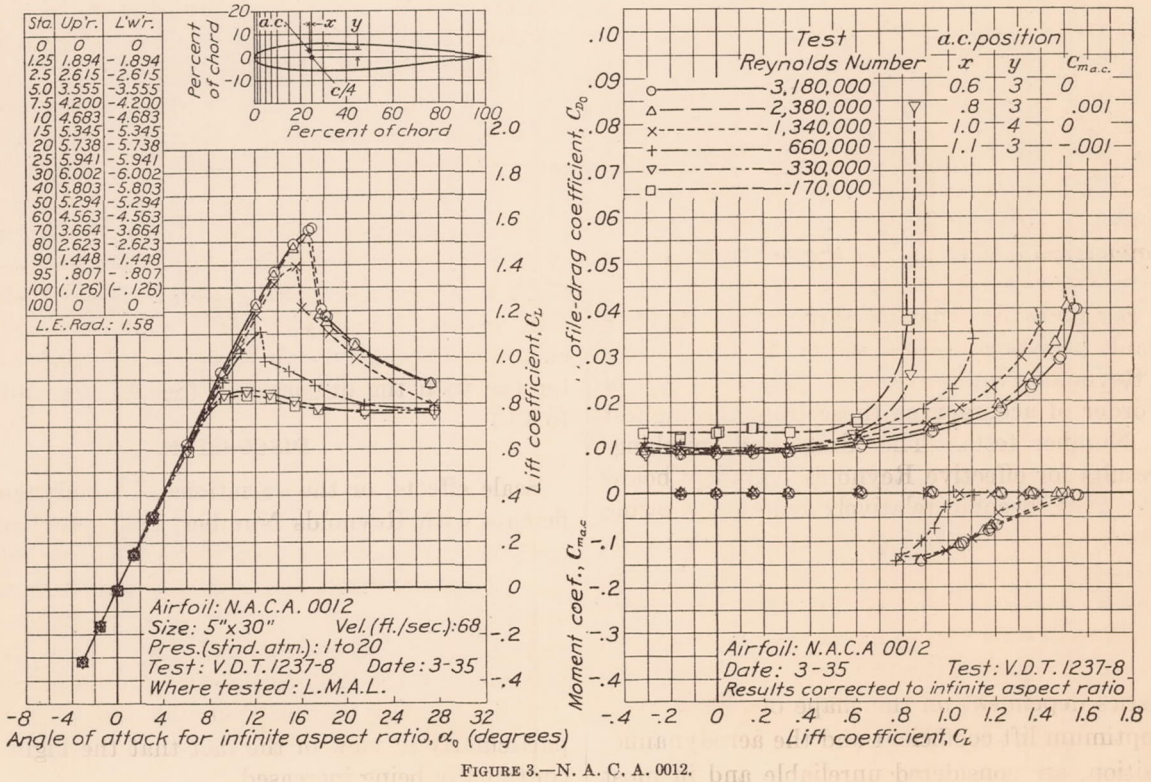

FIGURE 3.—N. A. C. A. 0012.

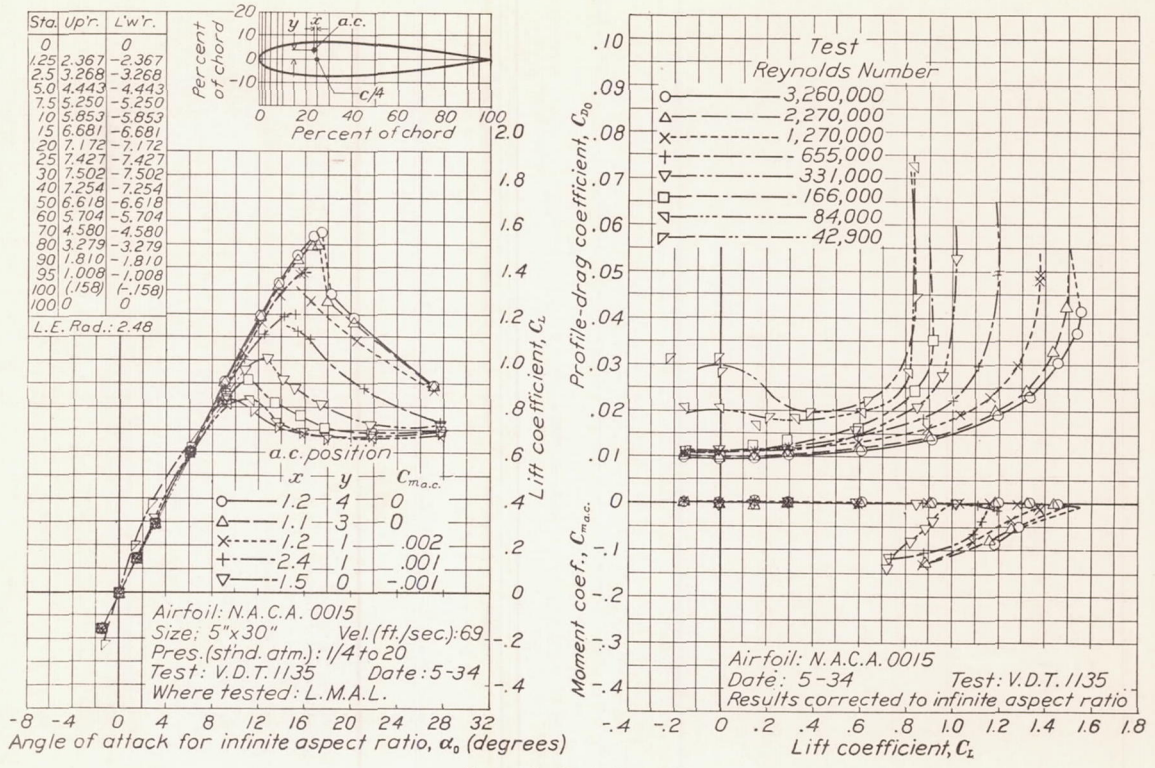

FIGURE 4.—N. A. C. A. 0015.

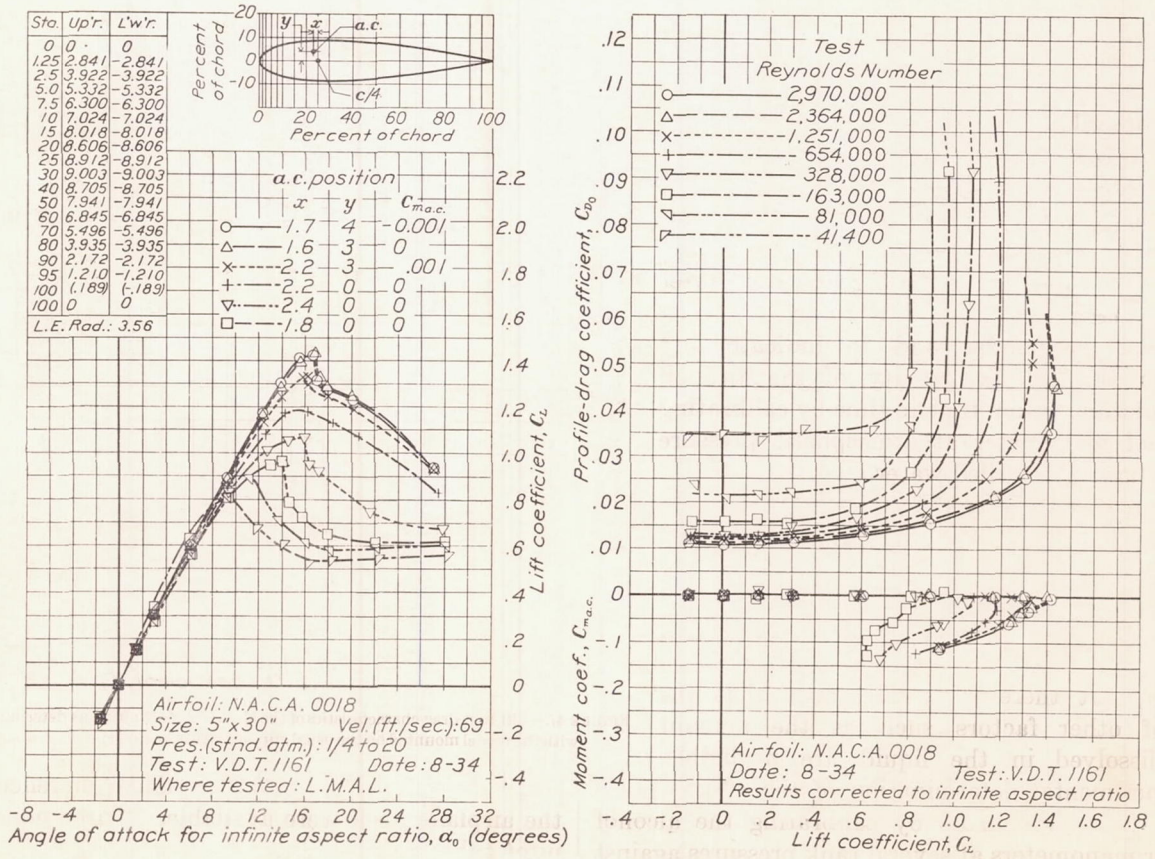

FIGURE 5.—N. A. C. A. 0018.

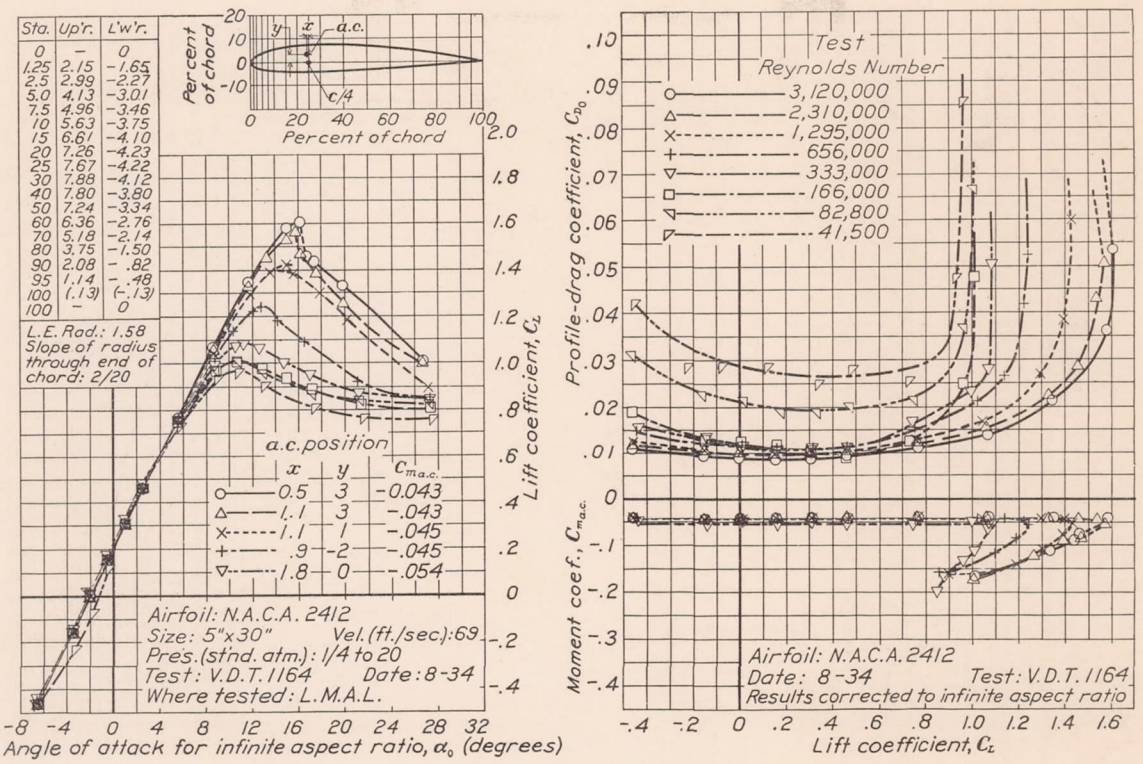

FIGURE 6.—N. A. C. A. 2412.

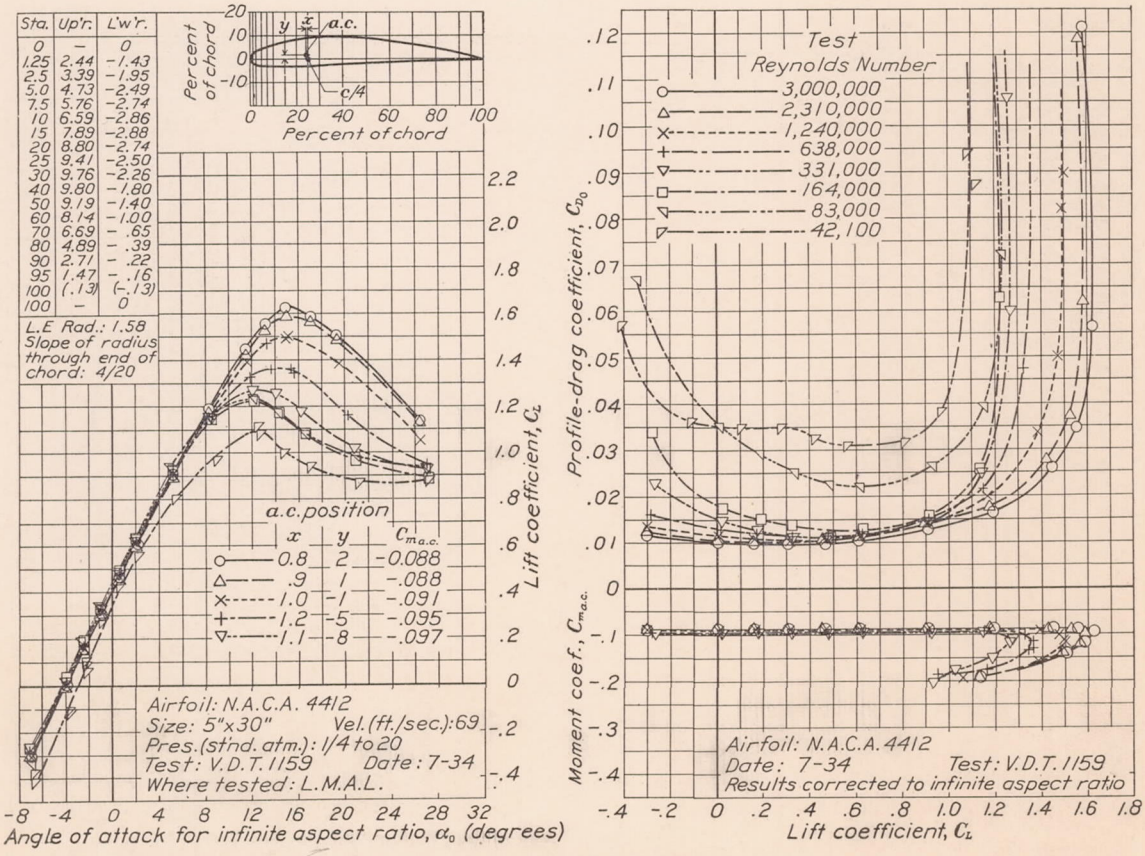

FIGURE 7.—N. A. C. A. 4412.

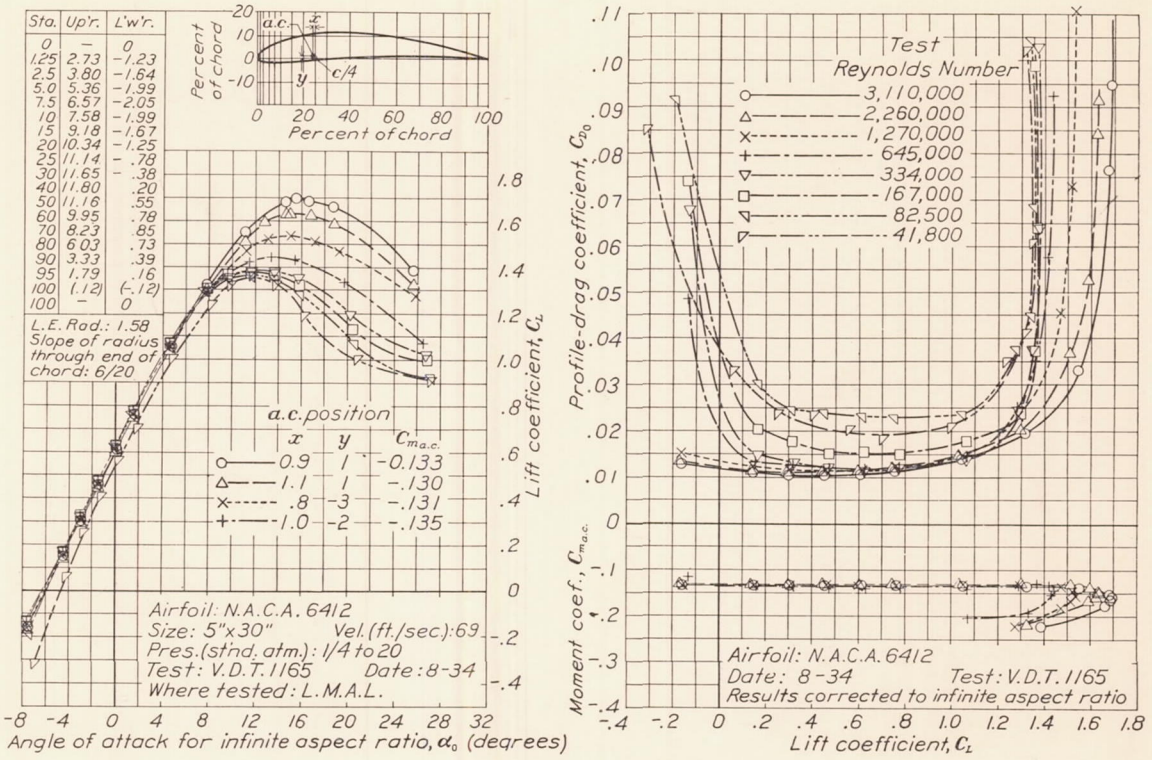

FIGURE 8.—N. A. C. A. 6412.

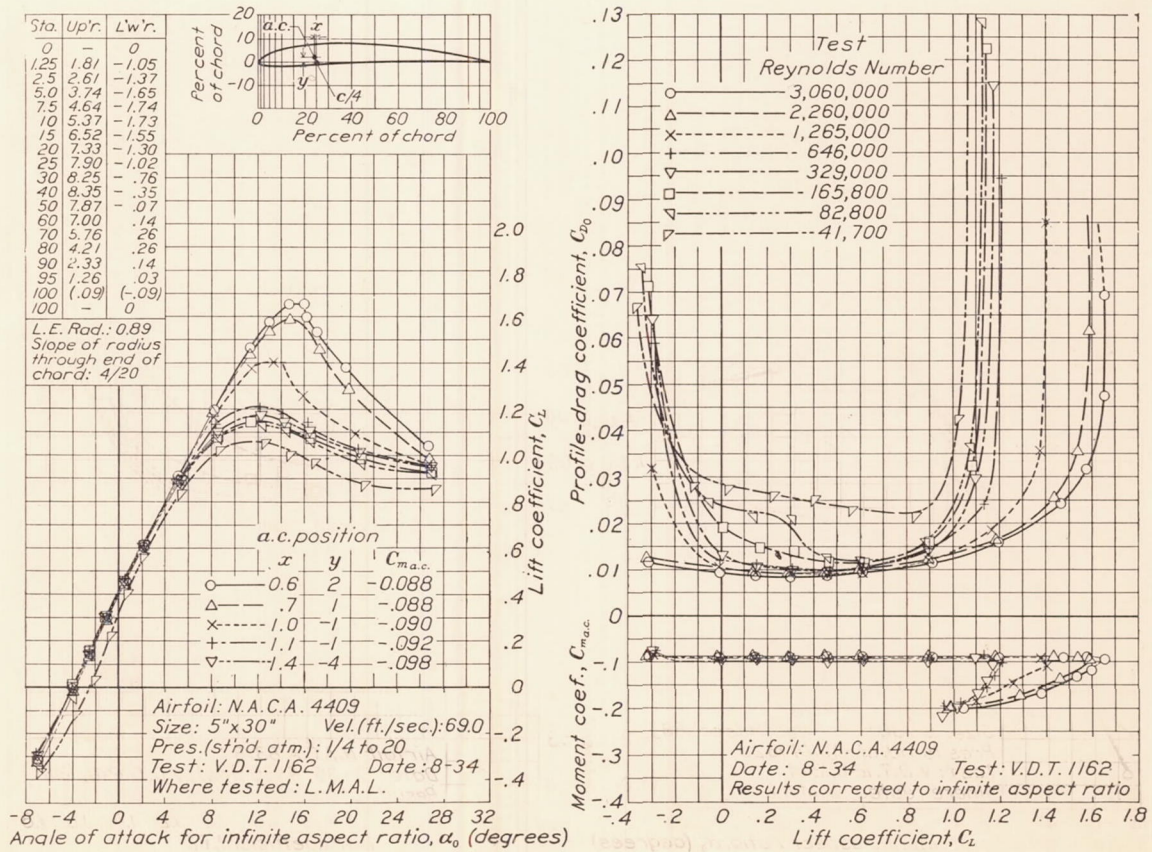

FIGURE 9.—N. A. C. A. 4409.

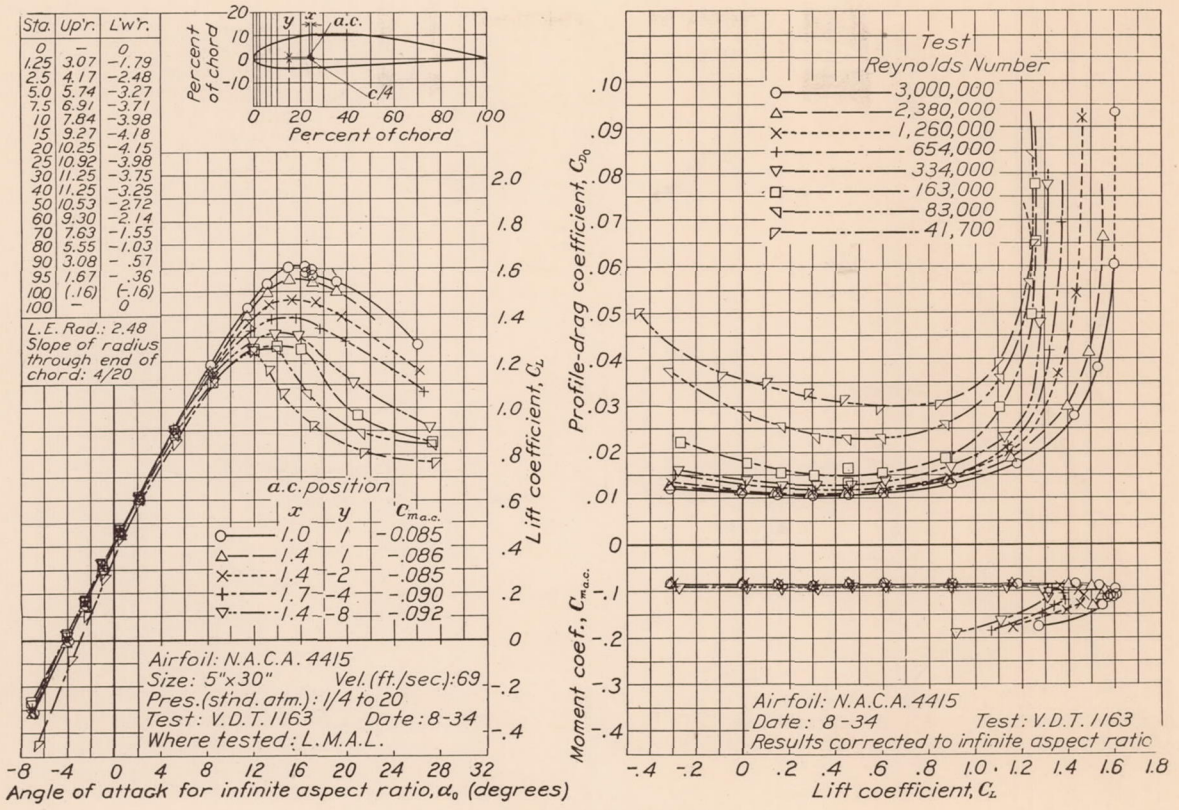

FIGURE 10.—N. A. C. A. 4415.

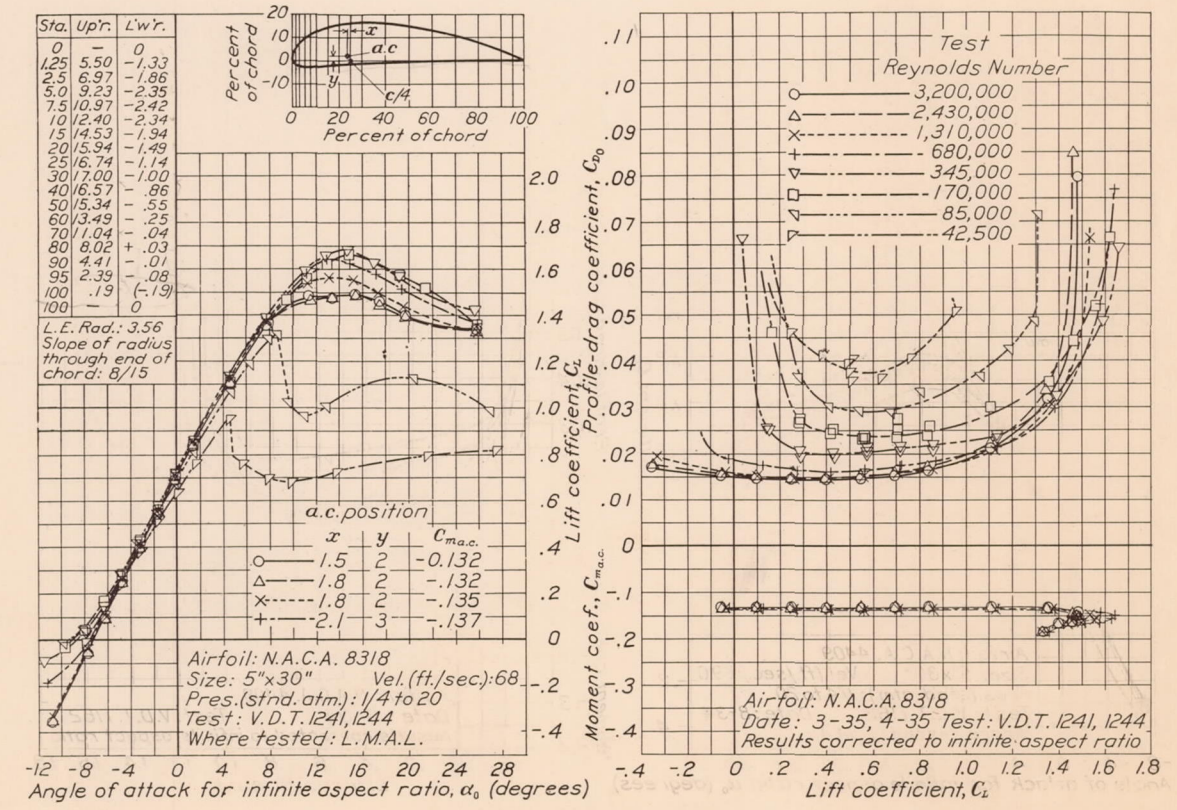

FIGURE 11.—N. A. C. A. 8318.

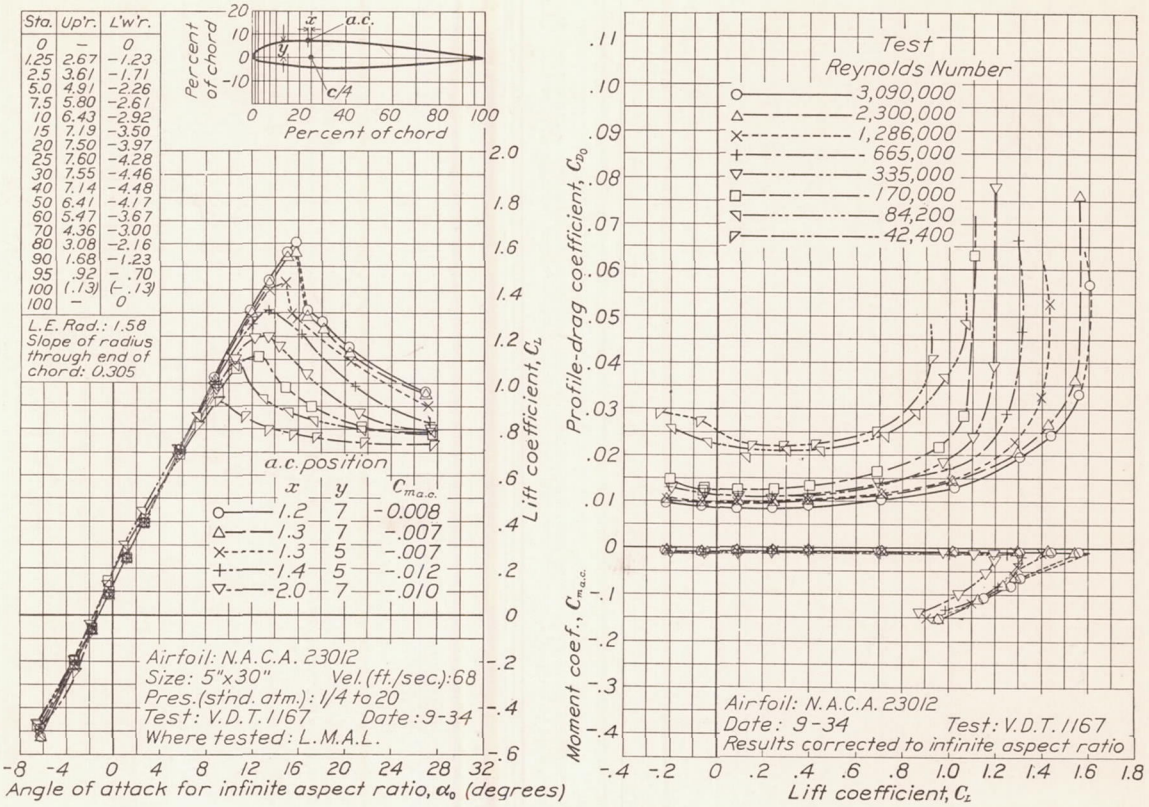

FIGURE 12.—N. A. C. A. 23012.

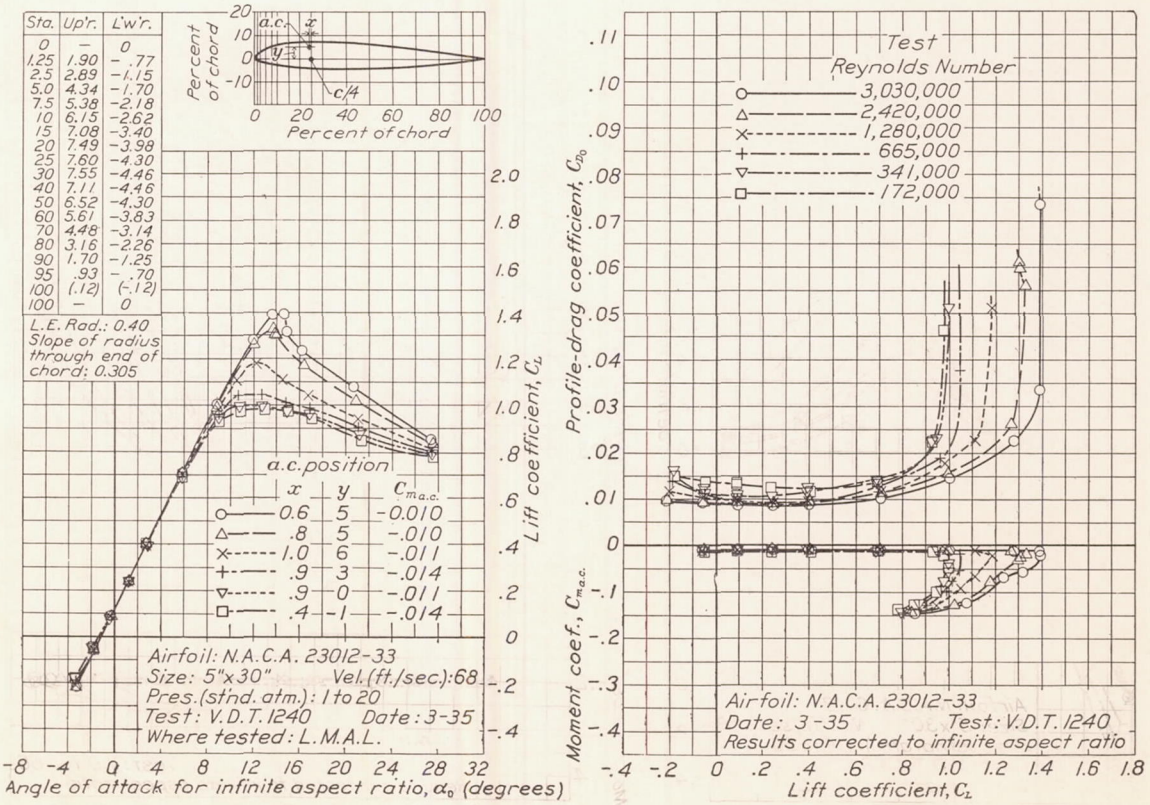

FIGURE 13.—N. A. C. A. 23012-33.

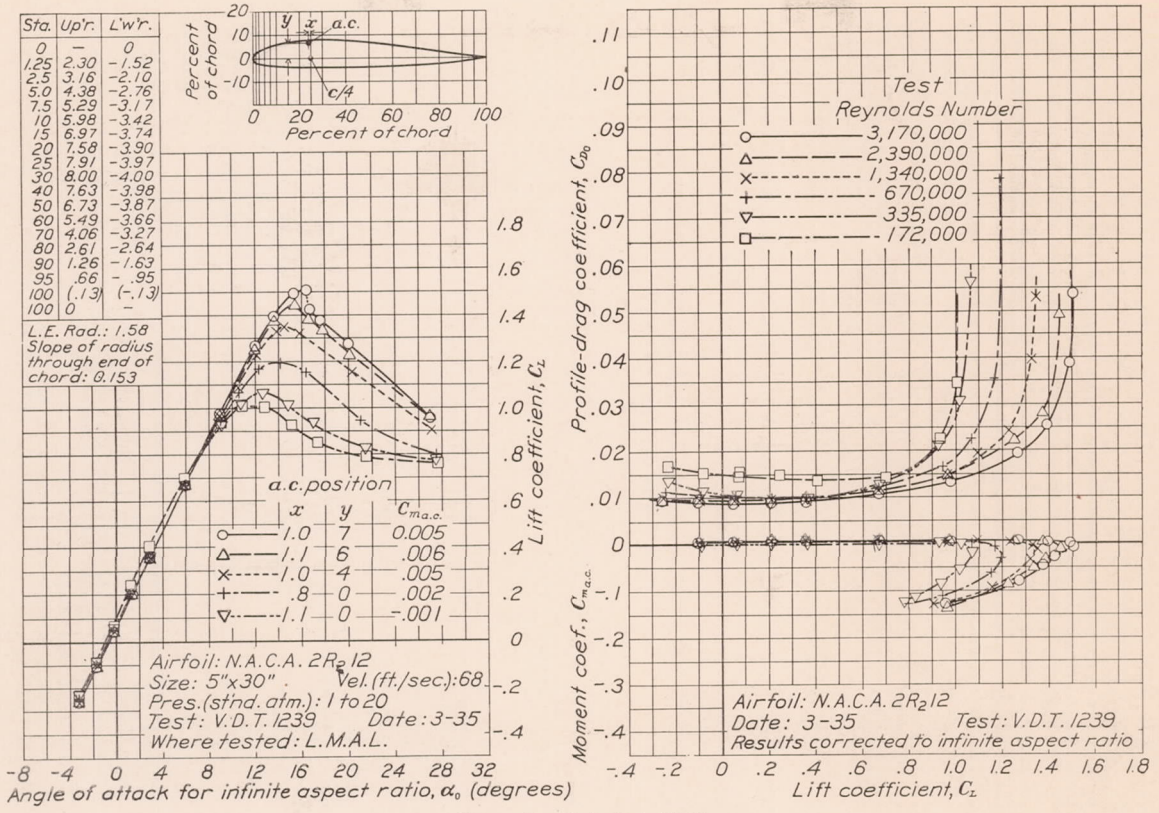

FIGURE 14.—N. A. C. A. 2R2 12.

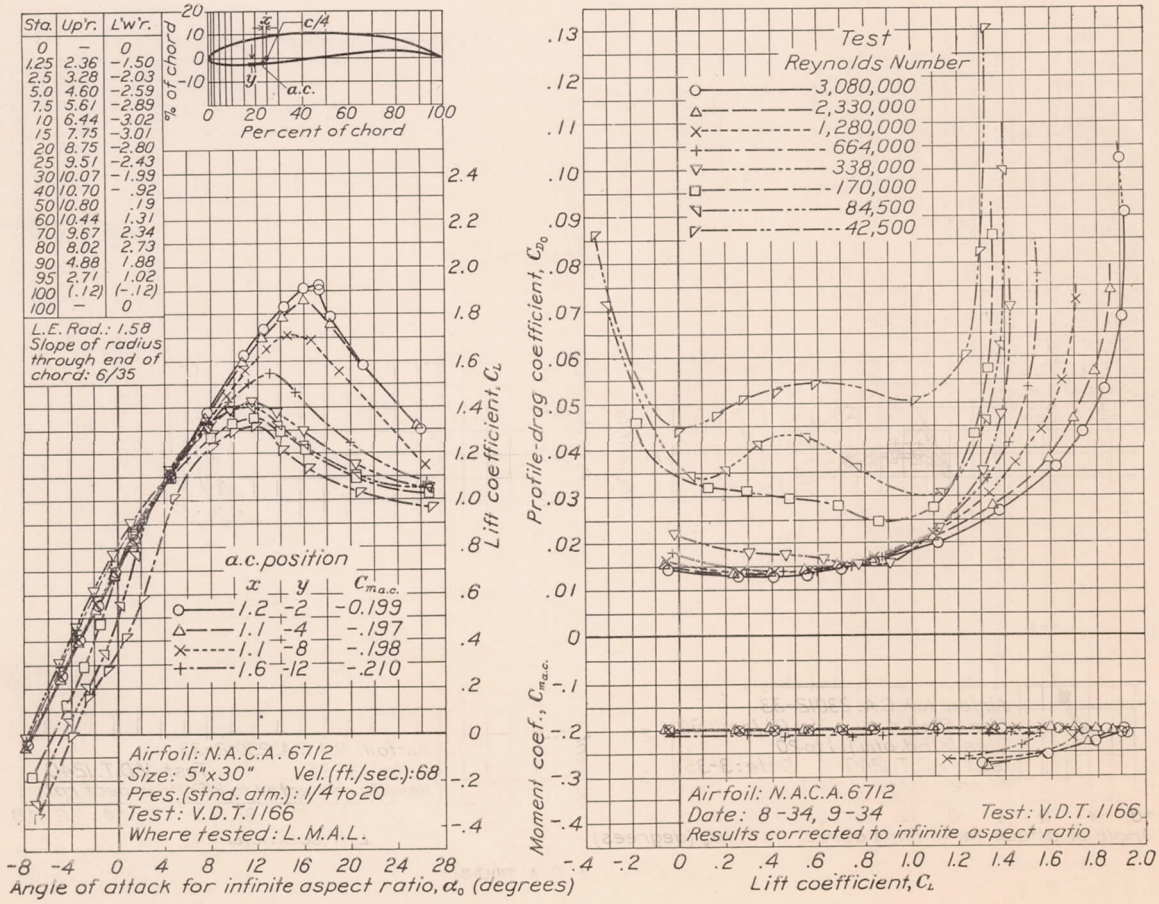

FIGURE 15.—N. A. C. A. 6712.

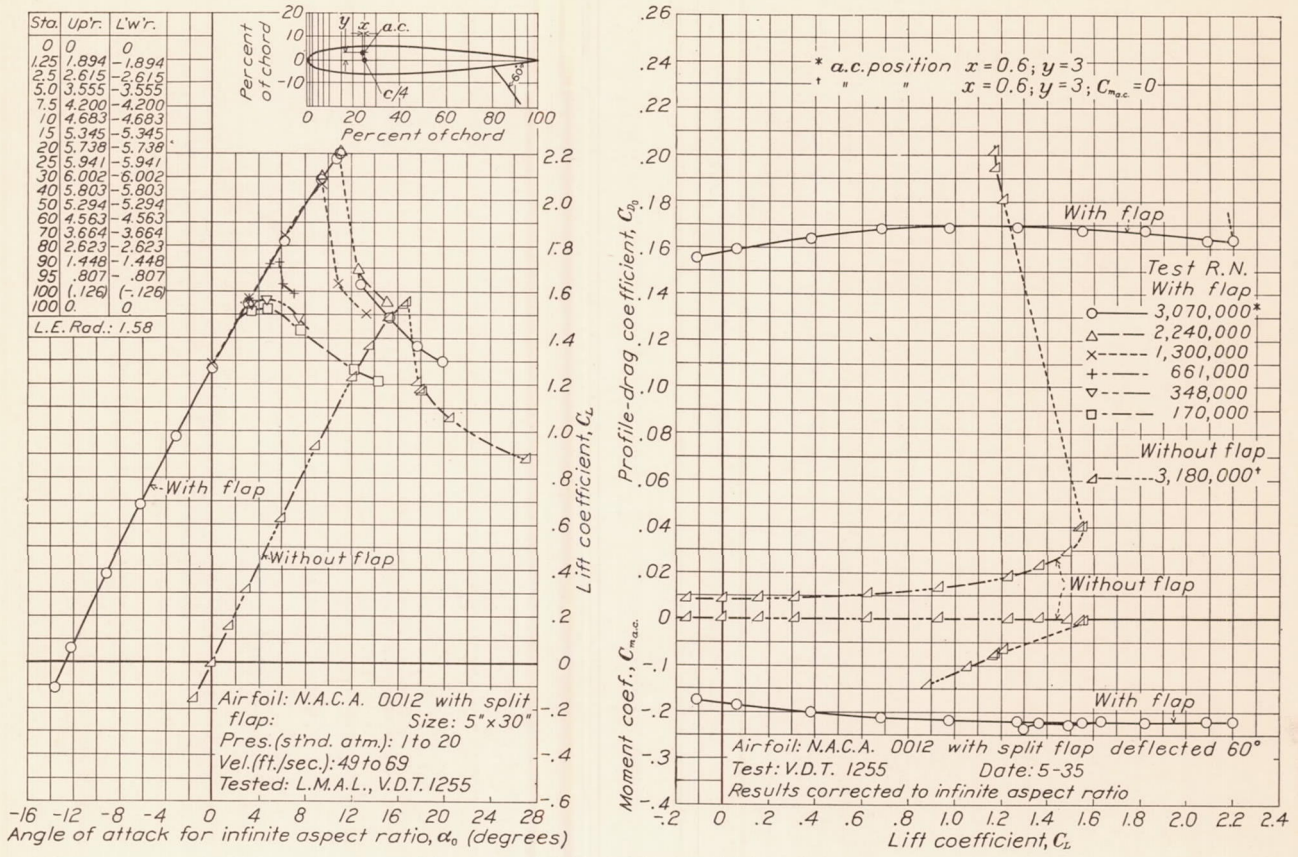

FIGURE 16.—N. A. C. A. 0012 with split flap deflected 60°.

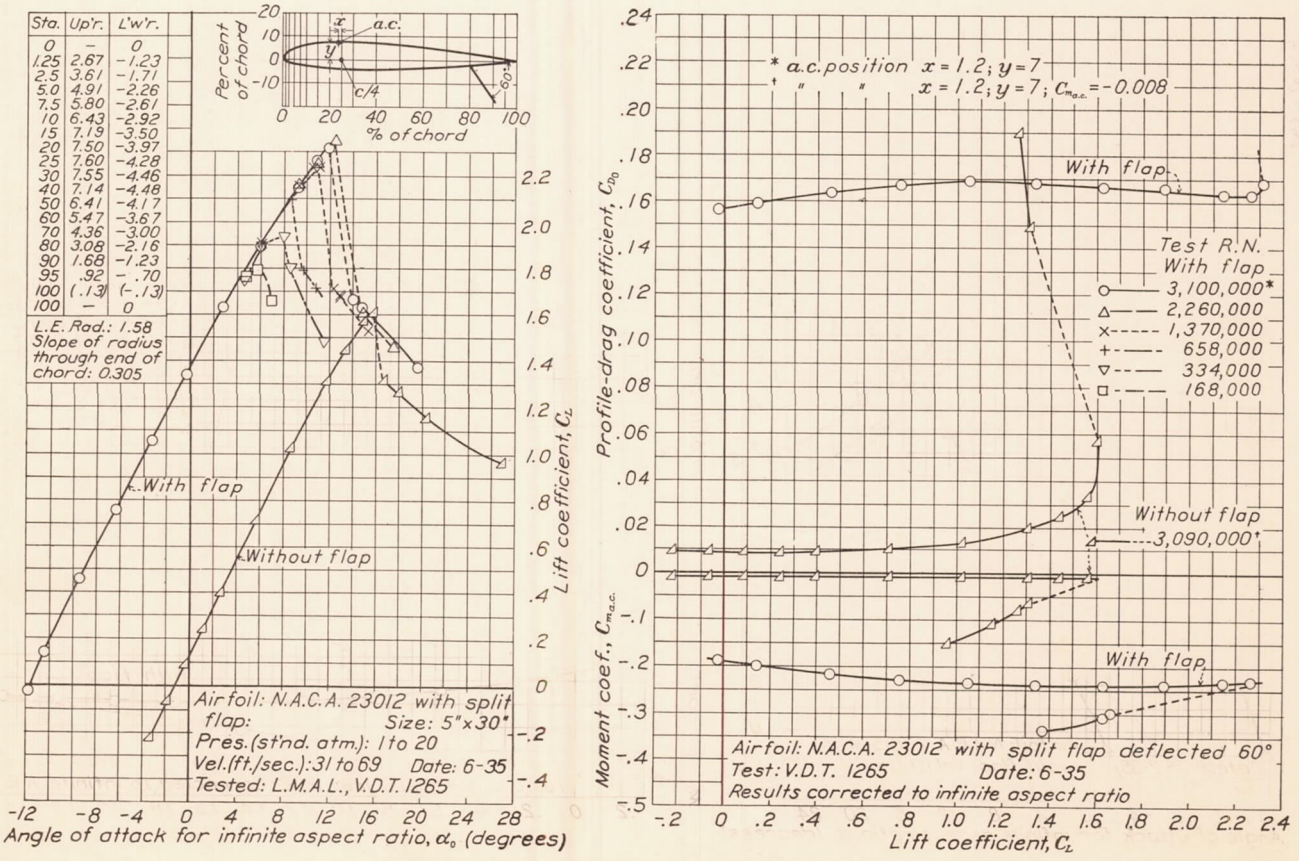

FIGURE 17.—N. A. C. A. 23012 with split flap deflected 60°.

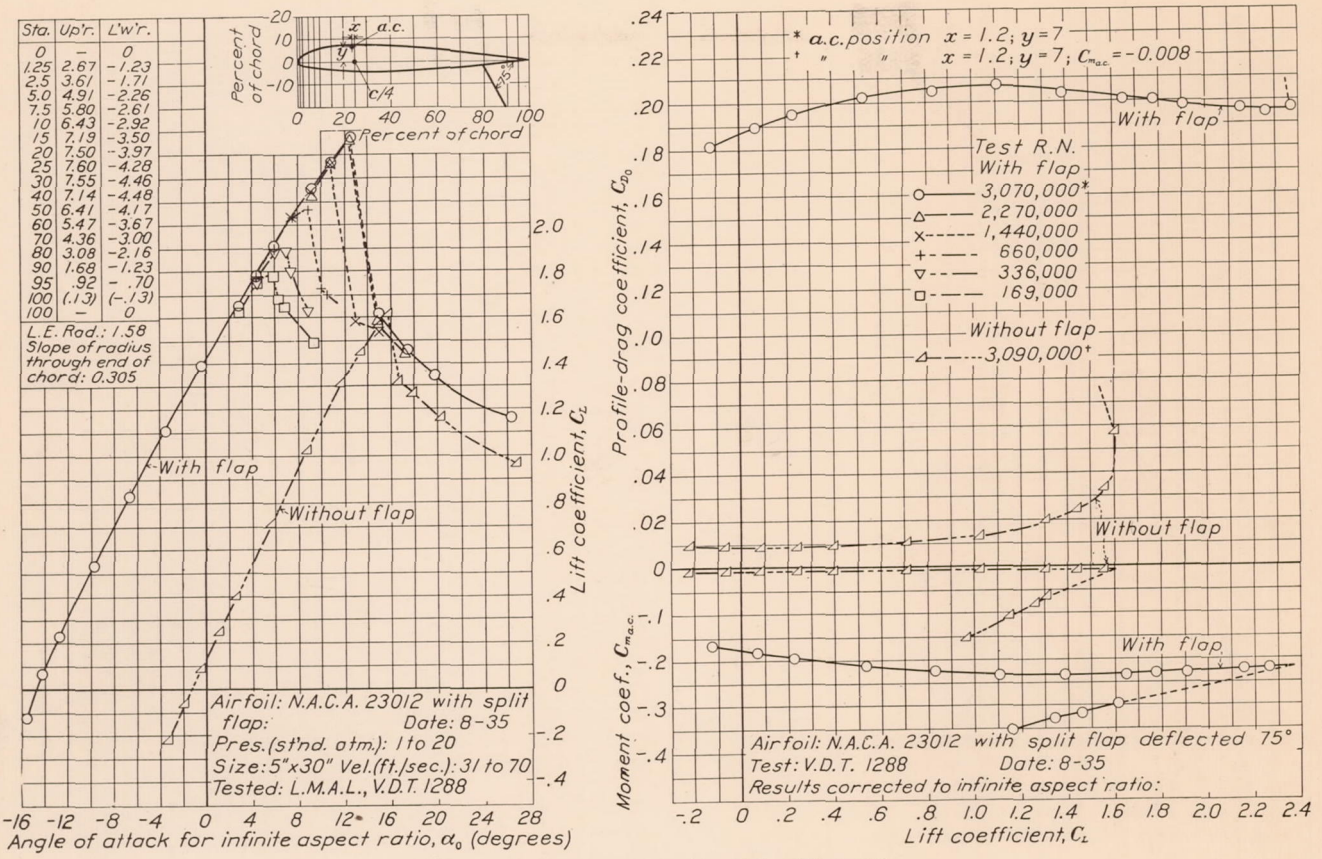

FIGURE 18.—N. A. C. A. 23012 with split flap deflected 75°.

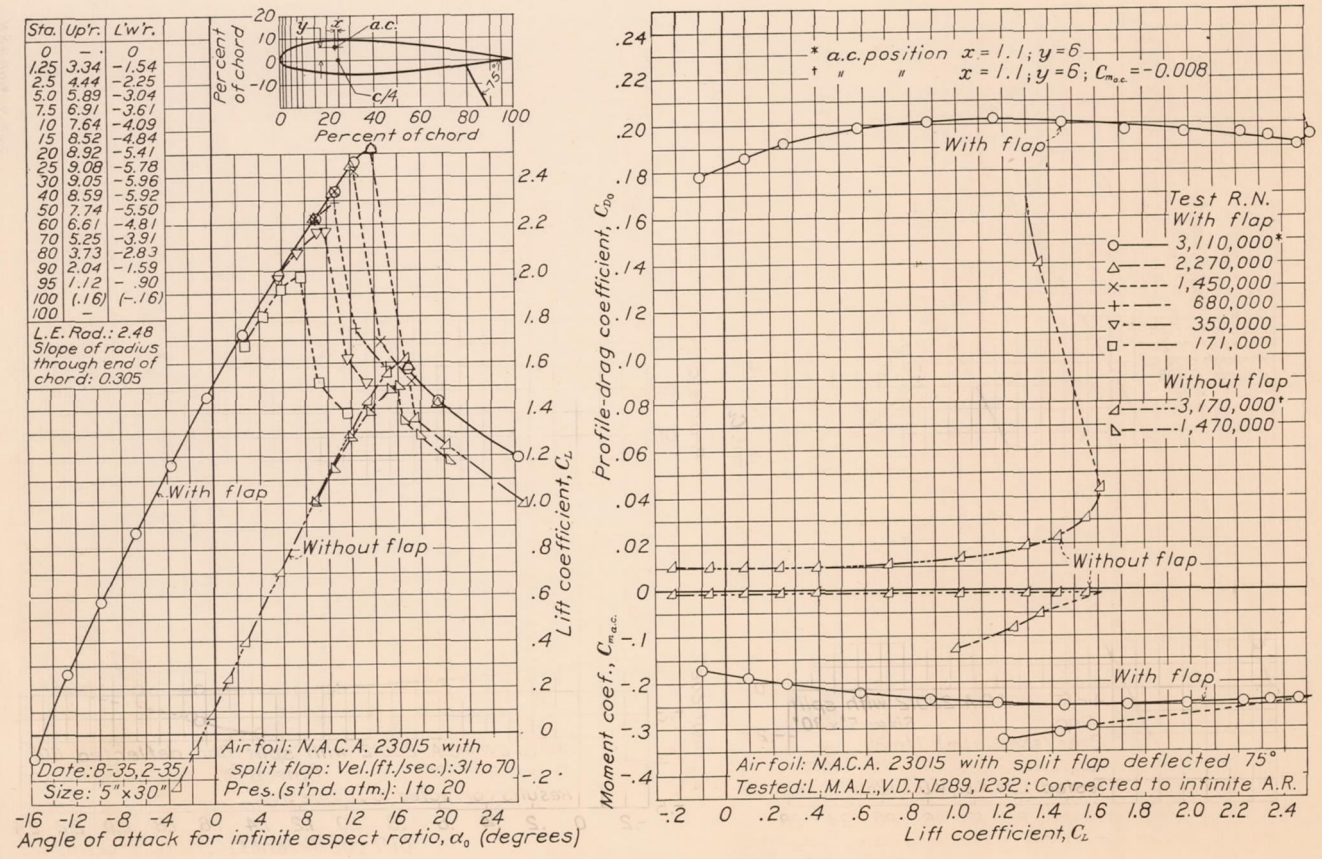

FIGURE 19.—N. A. C. A. 23015 with split flap deflected 75°.

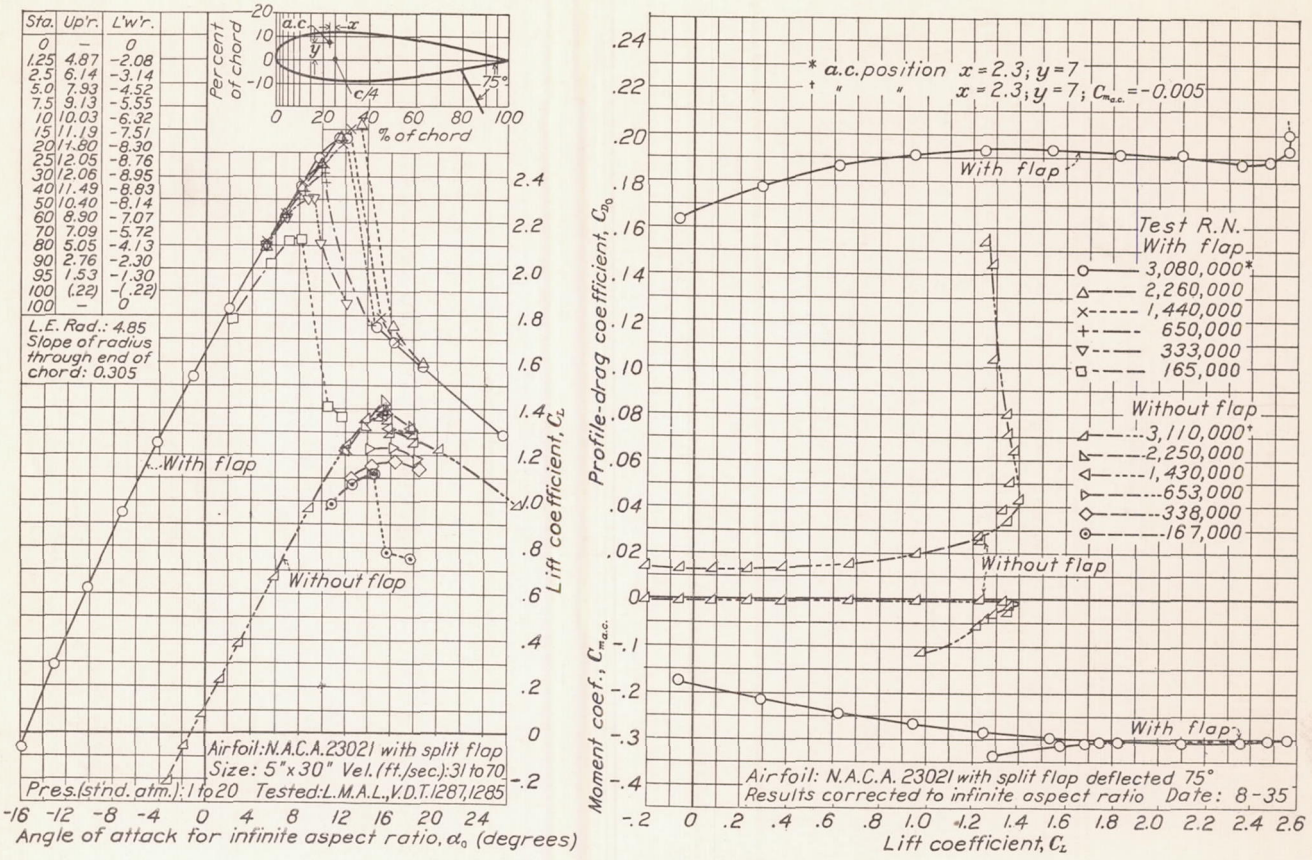

FIGURE 20.—N. A. C. A. 23021 with split flap deflected 75°.

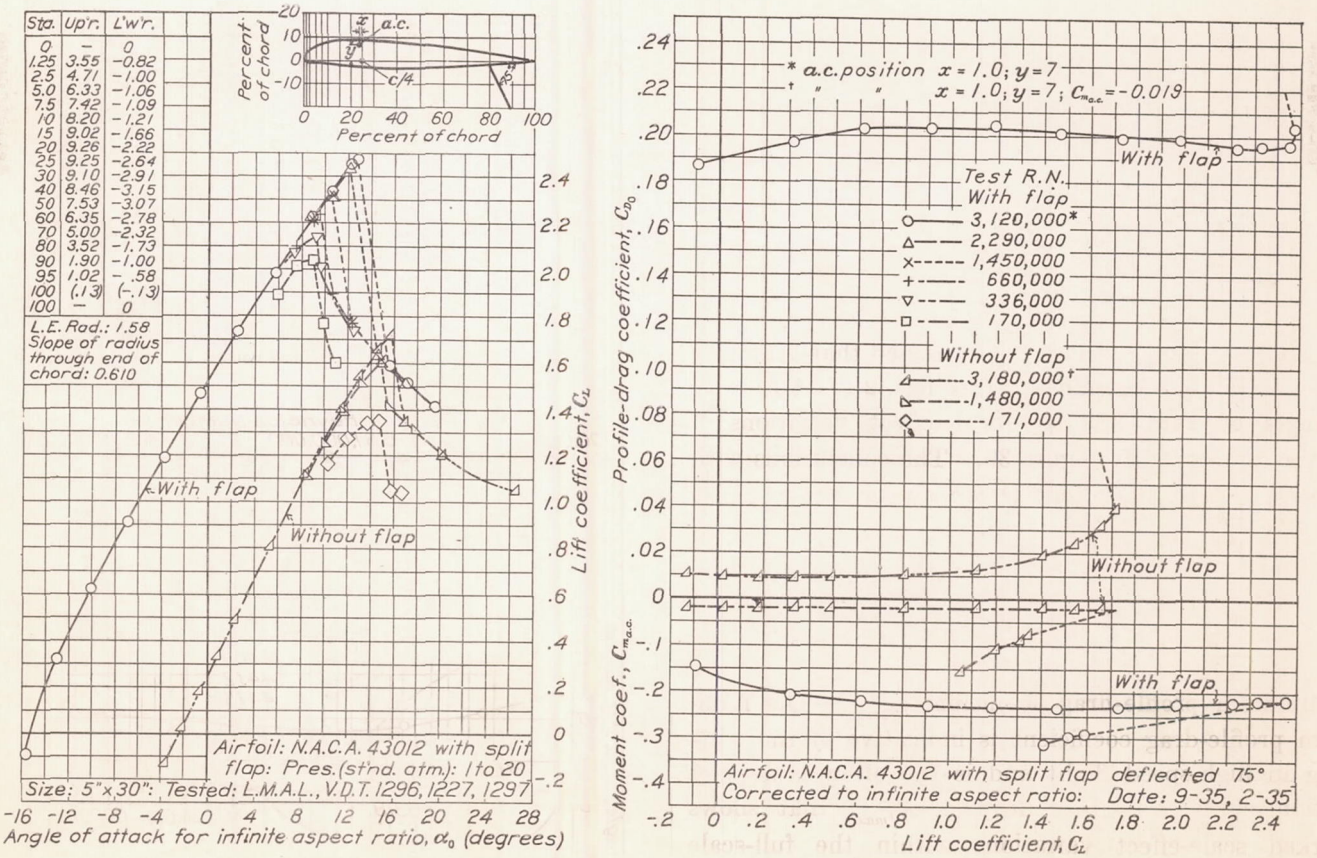

FIGURE 21.—N. A. C. A. 43012 with split flap deflected 75°.

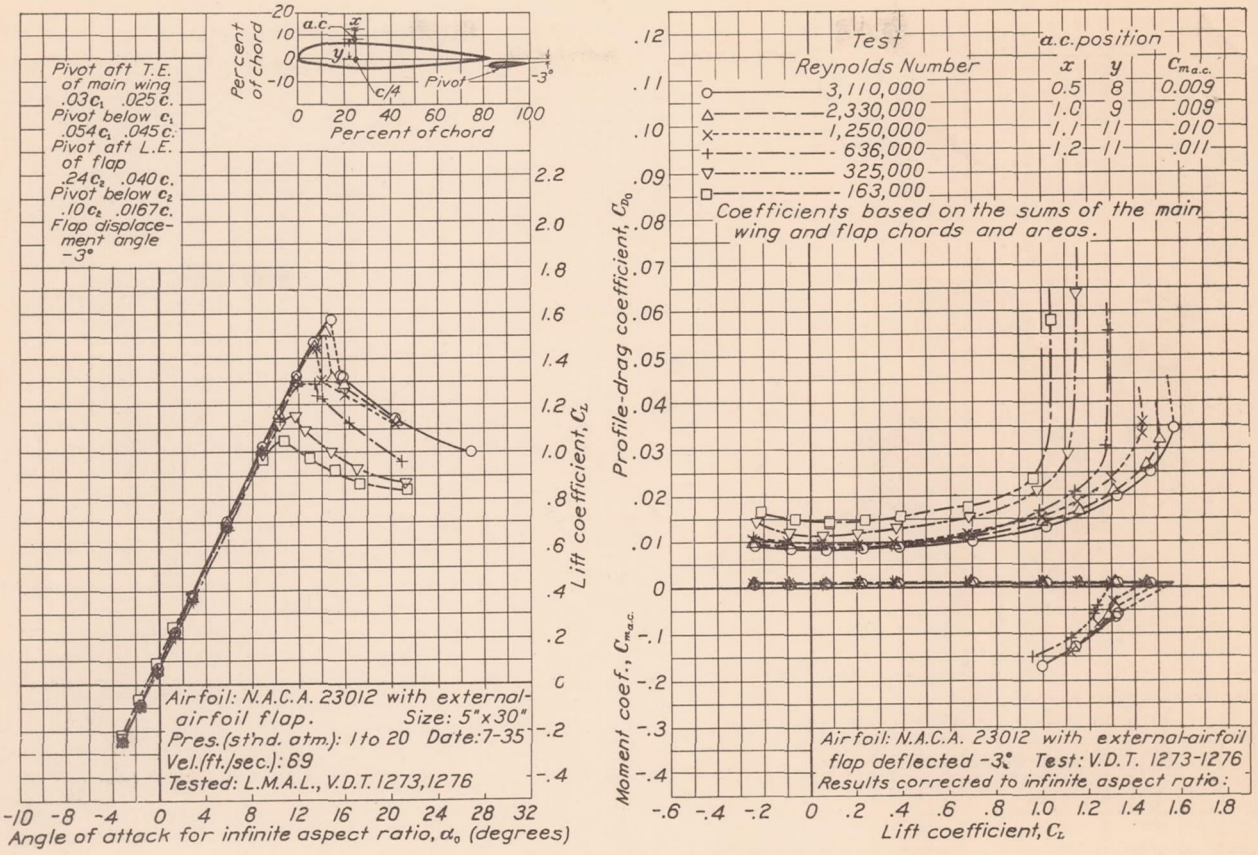

FIGURE 22.—N. A. C. A. 23012 with external-airfoil flap deflected −3°.

Main wing section	N. A. C. A. 23012	Main wing chord, c_1	0.833c	Datum chord, $c=c_1+c_2$.
Flap section	N. A. C. A. 23012	Flap chord, $c_2=0.2c_1$	.167c	

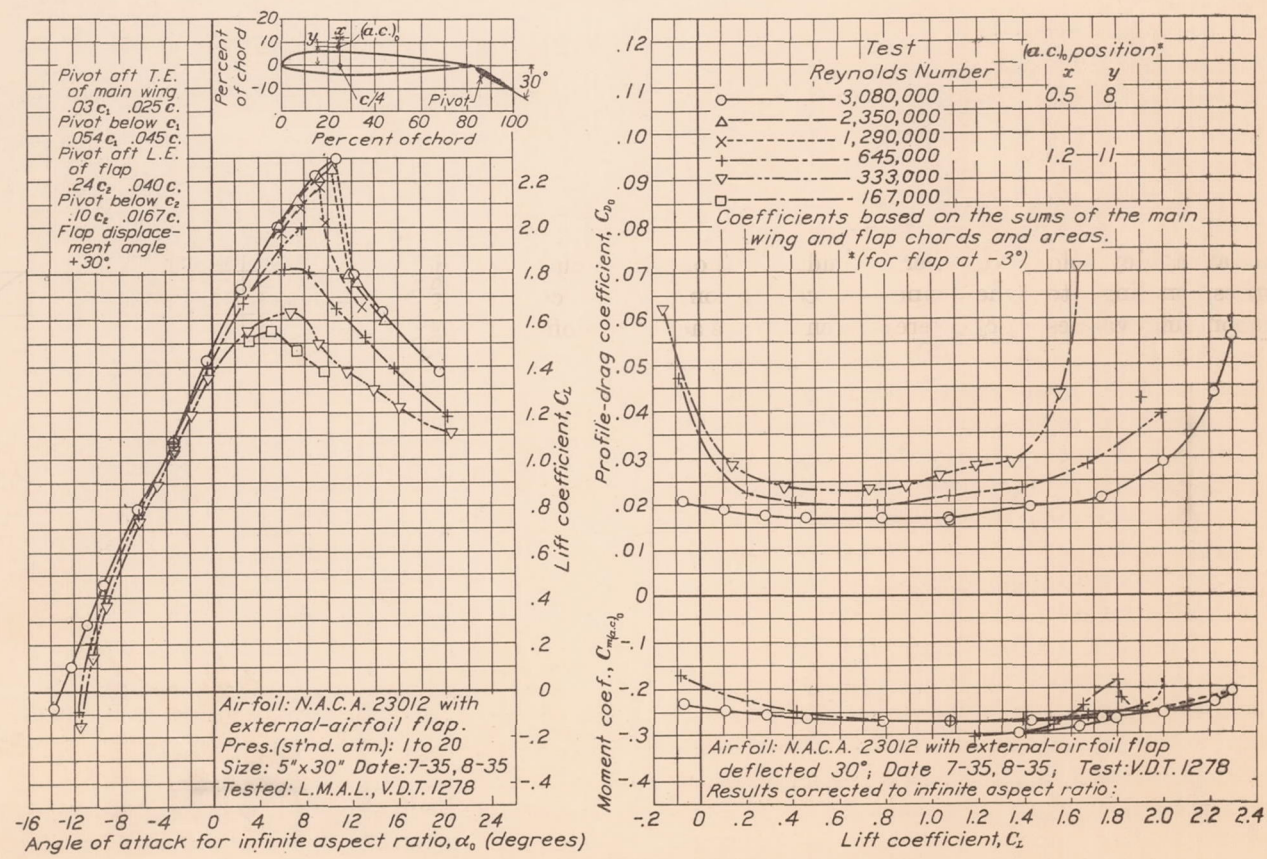

FIGURE 23.—N. A. C. A. 23012 with external-airfoil flap deflected 30°.

Main wing section	N. A. C. A. 23012	Main wing chord, c_1	0.833c	Datum chord, $c=c_1+c_2$.
Flap section	N. A. C. A. 23012	Flap chord, $c_2=0.2c_1$	.167c	

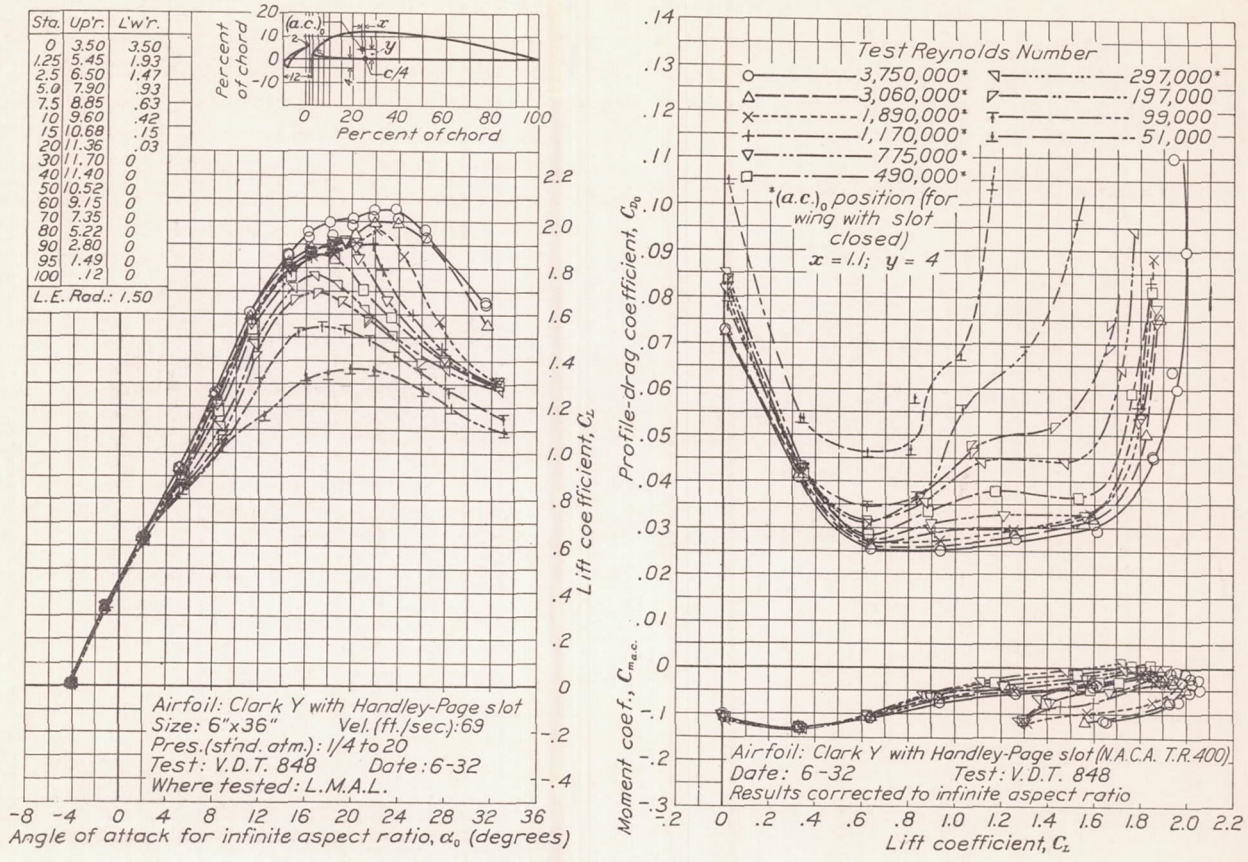

FIGURE 24.—Clark Y with Handley Page slot.

As an example of scale effects within the flight range, figure 25 has been prepared to show how the choice of an airfoil section for maximum aerodynamic efficiency may depend on the flight Reynolds Number at which the airfoil is to be employed. The efficiency is judged by the speed-range index $c_{l_{max}}/c_{d_0}$. Values of $c_{l_{max}}$ were determined for the airfoil sections (N. A. C. A. 230 series) with a deflected 20 percent chord split flap and at a Reynolds Number as indicated on each curve corresponding to the landing condition. The corresponding values of c_{d_0} were taken as the actual profile-drag coefficients associated with a high-speed lift coefficient suitable to an actual speed range of 3.5, but corrected by the methods of this report to the high-speed Reynolds Number (indicated landing Reynolds Number R times 3.5). Four curves were thus derived indicating the variation of speed-range index with section thickness for four values of the landing Reynolds Number: 1, 2, 4, and 8 million, the extremes corresponding to a small airplane and to a conventional transport airplane. The highest value shown, 414, of the speed-range index may appear surprisingly high, but it should be remembered that the corrections to section characteristics and for Reynolds Number, as well as the use of flaps, are all favorable to high values. The important point brought out by figure 25 is that the section thickness corresponding to the maximum aerodynamic efficiency is dependent on the Reynolds Number. The most efficient airfoil for a landing Reynolds Number of 1,000,000, for example, is definitely not the most efficient for a larger airplane landing at a Reynolds Number of 8,000,000. An analysis such as that of the foregoing example or further analyses such as those

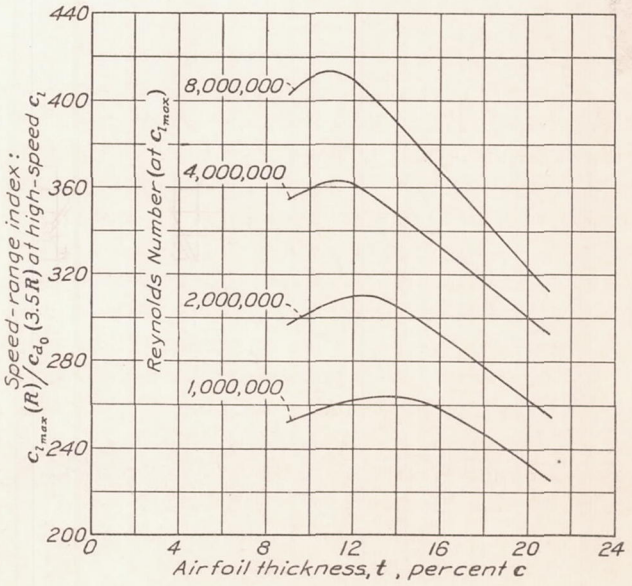

FIGURE 25.—Airfoil speed-range indexes for various Reynolds Numbers. N. A. C. A. 230 series sections; $c_{l_{max}}$ taken for airfoil with 0.20c split flap deflected 75°; c_{d_0} taken for airfoil with flap retracted for a high-speed value of c_l and at 3.5 times the R for the $c_{l_{max}}$.

discussed in reference 8 concerning the determination of the characteristics of wings evidently require a knowledge of the variation of airfoil *section* characteristics with profile shape over the practical range of flight Reynolds Numbers.

DETERMINATION OF *SECTION* CHARACTERISTICS APPLICABLE TO FLIGHT

The present analysis is intended primarily to supply a means of arriving at airfoil *section* characteristics that are applicable to flight at Reynolds Numbers within the practical flight range. This object is best accomplished by applying corrections to the standard airfoil test results from the variable-density tunnel.

The standard airfoil characteristics at large Reynolds Numbers are customarily defined in terms of a few parameters or important airfoil *section* characteristics that may be tabulated for each airfoil section. These important characteristics are:

$c_{l_{max}}$, the section maximum lift coefficient.

a_0, the section lift-curve slope.

α_{l_0}, the angle of zero lift.

$c_{d_{0\,min}}$, the minimum profile-drag coefficient.

$c_{l_{opt}}$, the optimum lift coefficient, or section lift coefficient corresponding to $c_{d_{0\,min}}$.

$c_{m_{a.c.}}$, the pitching-moment coefficient about the section aerodynamic center.

a. c., the aerodynamic center, or point with respect to the airfoil section about which the pitching-moment coefficient tends to remain constant over the range of lift coefficients between zero lift and maximum lift.

Essentially, the general analysis therefore reduces to an analysis of the variation of each of these important section characteristics with Reynolds Number. Before this analysis is begun, however, it will be necessary to consider how values of these *section* characteristics applicable to flight are deduced from the wind-tunnel tests of finite-aspect-ratio airfoils in the comparatively turbulent air stream of the tunnel. The variation of the important *section* characteristics with Reynolds Number will then be considered. Finally, consideration will be given to methods of arriving at complete airfoil characteristics after the important *section* characteristics have been predicted for flight at the desired value of the Reynolds Number.

Correction to infinite aspect ratio.—The derivation of the *section* characteristics from the test results uncorrected for turbulence will be discussed first; the turbulence effects will be considered later. The reduction to *section* characteristics is actually made in three successive approximations. First, the measured characteristics for the rectangular airfoil of aspect ratio 6 are corrected for the usual downflow and induced drag, using appropriate factors that allow at the same time for tunnel-wall interference. These induction factors are based on the usual wing theory as applied to rectangular airfoils. The methods of calculation are presented in reference 1. (Second-order influences have also been investigated; that is, refinement of the tunnel-wall correction to take into account such factors as the load grading and the influence of the tunnel interference on the load grading. (See reference 6.) For the conditions of the standard tunnel test such refinements were found to be unnecessary.) The results thus yield the first approximation characteristics, e. g., the profile-drag coefficient C_{D_0} that has been considered a section characteristic in previous reports (reference 2).

These first-approximation section characteristics are unsatisfactory, first, because the airfoil theory does not represent with sufficient accuracy the flow about the tip portions of rectangular airfoils and, second, because the measured coefficients represent average values for all the sections along the span whereas each section actually operates at a section lift coefficient that may differ markedly from the wing lift coefficient. The second approximation attempts to correct for the shortcomings of the wing theory as applied to rectangular airfoils.

It is well known that pressure-distribution measurements on wings having rectangular tips show humps in the load-distribution curve near the wing tips. These distortions of the load-distribution curve are not represented by the usual wing theory. The failure of the theory is undoubtedly associated with the assumption of plane or two-dimensional flow over the airfoil sections whereas the actual flow near the tips is definitely three-dimensional, there being a marked inflow from the tips on the upper surface and outflow toward the tips on the lower surface. This influence not only affects the induction factors and hence the over-all characteristics of the rectangular wing but also produces local disturbances near the tips that may be expected to affect the average values of the section profile-drag coefficients.

Theoretical load distributions for wings with well-rounded (elliptical) tips agree much more closely with experiment than do the distributions for rectangular-tip wings. Local disturbances near the tips should also be much less pronounced. Test results for rounded-tip wings were therefore employed to evaluate the rectangular-tip effects and hence to arrive at the second approximations. Four wings, having N. A. C. A. 0009, 0012, 0018, and 4412 sections, were employed for the purpose. The normal-wing airfoil sections were employed throughout the rounded-tip portion of the wing but the plan area was reduced elliptically toward each tip beginning at a distance of one chord length from the tip. Section characteristics were derived from tests of these wings in the usual way but using theoretical induction factors appropriate to the modified plan form. These section characteristics when compared

with the first approximation ones from tests of wings with rectangular tips served to determine the second approximations. These values indicated by double primes were given from this analysis in terms of the first approximation values indicated by single primes as follows:

$$C_{L_{max}}'' = 1.03 C_{L_{max}}'$$
$$a_0'' = 0.96 a_0'$$
$$\alpha_0'' = \alpha_0' + 0.39 C_L' \text{ (degrees)}$$
$$C_{D_0}'' = C_{D_0}' + 0.0016 C_L'^2 - \frac{1}{3}(t-6)0.0002 \quad (t \gtrless 6)$$

where t is the maximum section thickness in percent chord. In some recent reports on airfoil characteristics (references 3, 5, and 7) these values have been presented as section characteristics except that a small correction has in some cases been applied to the aerodynamic-center positions. This correction is no longer considered justifiable.

These corrections are, of course, entirely empirical. They must be considered as only approximately correct and as being independent of the Reynolds Number. The corrections themselves, however, are small so that they need not be accurately known. All things considered, it is believed that through their use the reliability of the *section* data is definitely improved, at least within the lower part of the range of lift coefficients. For lift coefficients much greater than 1, however, the profile-drag coefficients from the rounded tip and rectangular airfoil tests show discrepancies that increase progressively with lift coefficient and, of course, become very large near the maximum lift coefficient owing to the different maximum-lift values. This difference brings up the necessity for the third approximation. The second approximation values may, however, be considered sufficiently accurate to determine the section profile-drag coefficient c_{d_0} over the lower lift range and also the following important section parameters that are determined largely from the characteristics in the low lift range:

α_{l_0}
a_0
$c_{l_{opt}}$
$c_{d_{0\ min}}$
$c_{m_{a.c.}}$
$a.\ c.$

In this range of the lift coefficient the deviations from the mean of the c_l values along the span have been adequately taken into account. The mean values of c_l and c_{d_0} represent true values as long as the deviations along the span are within a limited range over which the quantities may be considered to vary lineally. Near the maximum lift, however, the deviations become larger and the rates of deviation increase so that the profile drag of the rounded-tip airfoil, for example, is predominantly influenced by the high c_{d_0} values of the central sections which, according to the theory, are operating at c_l values as much as 9 percent higher than the mean value indicated by the wing lift coefficient C_L. Moreover, the actual lift coefficient corresponding to the section stall (in this case the center section) might thus, in accordance with the theory, be taken as 9 percent higher than the measured wing lift coefficient corresponding to the stall.

Several considerations, however, indicate that this 9 percent increase indicated by the simple theory is too large. The simple theory assumes a uniform section lift-curve slope in arriving at the span loading and hence the distribution of the section lift coefficients along the span. Actually on approaching the maximum lift the more heavily loaded sections do not gain lift as fast as the more lightly loaded ones owing to the bending over of the section lift curves near the stall. This effect has also been investigated approximately. The results showed that for commonly used airfoil sections the center lift drops from 9 percent to 5 or 6 percent higher than the mean at the stall of rectangular airfoils with rounded tips. For some unusual sections that have very gradually rounding lift-curve peaks and with little loss of lift beyond the stall, this correction may practically disappear either because the lift virtually equalizes along the span before the stall or because the maximum lift is not reached until most of the sections are actually stalled. Omitting from consideration these sections to which no correction will be applied, the question as to whether or not such a correction should be applied to usual sections was decided by considering how it would affect predictions based on the $c_{l_{max}}$ values.

Maximum-lift measurements had been made for a number of tapered airfoils of various taper ratios and aspect ratios. The same airfoil *section* data presented in this report were applied (taking into account the reduced Reynolds Number of the sections near the tips of highly tapered wings) by the method indicated in reference 8 to predict the maximum lift coefficients of the tapered wings. These predictions appeared somewhat better when the *section* data were obtained on the assumption that the center-section lift coefficient at the stall of the rectangular airfoil with rounded tips is 4 percent higher than the wing lift coefficient. Hence the third approximation as regards the section maximum lift coefficients was obtained by increasing the maximum lift coefficients by 4 percent, although the value of the correction could not be definitely established because it appeared to be of the same order as possible errors in maximum lift measurements and predictions for tapered airfoils. The correction has been applied, however, except in the unusual cases previously mentioned where it obviously was not applicable, by increasing the maximum lift coefficients for the sections

by 4 percent. With the rounded-tip correction this increase makes the total maximum lift coefficient for the *section* 7 percent higher than the measured maximum lift coefficient for the rectangular airfoil of aspect ratio 6.

The correction of the important airfoil section parameters has thus been completed, but the curve of profile-drag coefficient against lift coefficient should now be modified at high lift coefficients owing to the change in $c_{l_{max}}$ and the variation of c_{d_0} along the span. Completely corrected c_{d_0} curves are not presented for the various airfoils in this report. The change resulting from the variation of c_{d_0} along the span has been applied only in a general way in the construction of a generalized c_{d_0} curve. From this curve, values of c_{d_0} at any c_l may be derived in terms of the presented airfoil section parameters. This "generalized section polar" (see fig. 45) was derived from tests of rounded-tip N. A. C. A. 0012 and 4412 airfoils, taking into account the variation of c_{d_0} along the span. For conventional airfoils of medium thickness, c_{d_0} values from this generalized section polar should be more nearly true section characteristics than the C_{D_0} values obtained directly from the test data. This conclusion is particularly important for lift coefficients above 1 where the second approximation correction becomes definitely unreliable and near $c_{l_{max}}$ where the C_{D_0} values are influenced by the variation of c_{d_0} along the span. A reference to figure 26 will show the relation of these successive approximations to the original measurements and to the final results.

Turbulence.—The correction for turbulence is made as in reference 9 by use of the concept of an effective Reynolds Number. Marked scale effects that have been experimentally observed are usually associated with a transition from laminar to turbulent flow in the boundary layer. As examples, consider the more or less sudden increase in the drag coefficient for skin-friction plates and airship models and the drop of the drag coefficient for spheres and cylinders with increasing Reynolds Numbers in the critical range. The latter scale effects are associated with the greater resistance to separation of the turbulent layer. The increase of maximum lift coefficient with Reynolds Number shown by most commonly used airfoils is a similar phenomenon. The drag scale effect for most airfoils, moreover, is at least comparable with the corresponding scale effect for the skin-friction plate.

This transition from laminar to turbulent flow in the boundary layer, as in Reynolds' classic experiments, is primarily a function of the Reynolds Number but, as he showed, the transition is hastened by the presence of unsteadiness or turbulence in the general air stream.

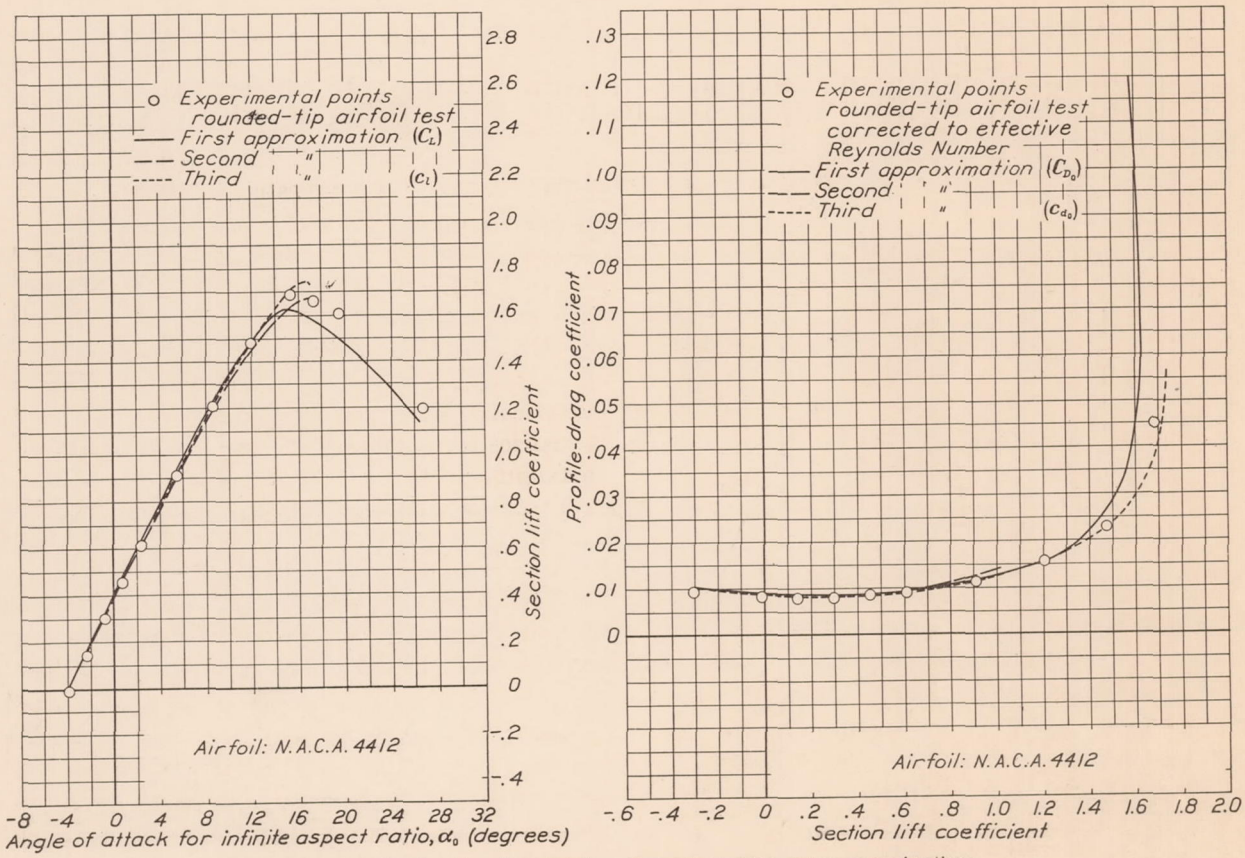

FIGURE 26.—Airfoil section characteristics. Comparison of the various approximations.

Likewise, the transition in the boundary layer is hastened by the turbulence in the air stream of a wind tunnel so that transition occurs at a given point on the model at a lower Reynolds Number in the tunnel than it would in free air. Likewise the associated scale effects that appear in the tunnel tend to correspond with those that would appear in flight at a higher Reynolds Number. This Reynolds Number may therefore be referred to as the "effective Reynolds Number" and is, of course, higher than the actual Reynolds Number of the test.

It appears that the effective Reynolds Number for practical purposes may be obtained by multiplying the test Reynolds Number by a factor referred to as the "turbulence factor." This factor was determined (reference 9) for the variable-density tunnel by a comparison of airfoil tests with tests in the N. A. C. A. full-scale tunnel and hence indirectly with flight. The value 2.64, which was thus obtained after a consideration of sphere tests in the full-scale tunnel and in flight, agrees with a subsequent determination (reference 10) by sphere tests in the variable-density tunnel that were compared directly with corresponding tests in flight.

An effective Reynolds Number is thus determined at which the tunnel results should, in general, be applied to flight. Flight conditions as regards the effects of the transition may then be considered as being approximately reproduced, but it should be remembered that the flow at the lower Reynolds Number cannot exactly reproduce the corresponding flow in flight. Both the laminar and turbulent boundary layers are relatively thicker than those truly corresponding to flight and both boundary layers have higher skin-friction coefficients at the lower Reynolds Number. Nevertheless the most important source of scale effects is taken into account, at least approximately, when the tunnel results are applied to flight at the effective Reynolds Number. The change in skin-friction drag coefficients in passing from the test to the effective Reynolds Number, moreover, is approximately allowed for by deducting a small correction increment from the measured airfoil profile-drag coefficients.

This correction increment was originally employed for tests at high values of the Reynolds Number when the boundary layer on an airfoil is largely turbulent. The correction was therefore estimated as the amount by which the drag coefficient representing the turbulent skin friction on a flat plate would decrease in passing from the test Reynolds Number to the effective Reynolds Number. The values of the increment thus deduced from Prandtl's analysis of the turbulent

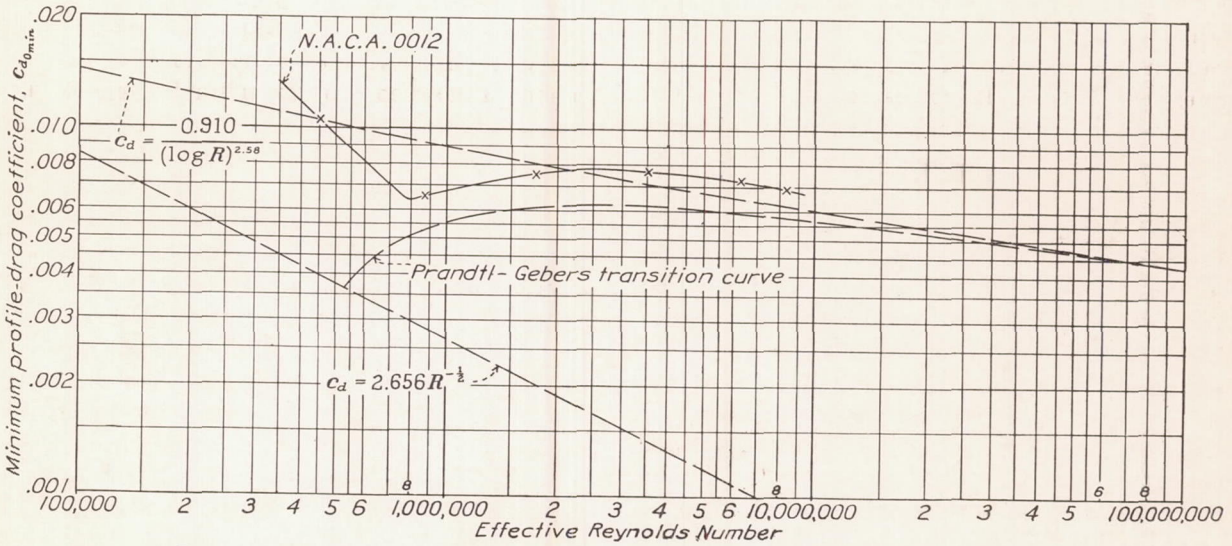

FIGURE 27.—Variation of $c_{d_{0min}}$ with R. Comparison of N. A. C. A. 0012 airfoil with skin-friction plates.

friction layer, which is substantially in agreement with von Kármán's original derivation, are as follows:

Test Reynolds Number	Effective Reynolds Number	Δc_d
300,000	792,000	0.0020
500,000	1,320,000	.0017
1,000,000	2,640,000	.0014
2,000,000	5,280,000	.0012
3,000,000	7,920,000	.0011

The objection might be raised that the increments Δc_d are based entirely on a turbulent skin-friction layer whereas the boundary layers on airfoils are actually laminar over a considerable part of the forward portion, particularly for the lower values of the Reynolds Number. The Δc_d correction was nevertheless employed over the complete range of Reynolds Numbers for several reasons: primarily for simplicity and consistency, because in the practical flight range the turbulent layer predominates; and secondarily because on most airfoils the boundary layer must be turbulent over a considerable part of the surface at any Reynolds Number sufficiently high to avoid separation. Reference to the corrected minimum-drag results for the N. A. C. A. 0012 section shown in figure 27 may

clarify these statements. Included in the figure are curves representing the variations with Reynolds Number of flat-plate drag coefficients for laminar and turbulent boundary layers and the Prandtl-Gebers transition curve, which represents a computed variation substantially in agreement with Gebers' measurements of the actual variation in drag coefficient for a flat plate towed in water at various Reynolds Numbers. The computed curve is the result of a calculation of the average drag coefficient for the plate when the forward part of the boundary layer is laminar and the after part turbulent and the transition is assumed to take place at a fixed value of the surface-distance Reynolds Number R_x. It is apparent that the airfoil curve tends to parallel the actual flat-plate curve throughout the flight range of values of the Reynolds Number.

In references 11 and 12 corresponding curves were presented for a very thin airfoil section. These results were uncorrected for the turbulence in the tunnel and hence, although they appear to parallel a transition curve like the present corrected results, the transition curve does not correspond to zero turbulence, or flight, but is displaced to the left. The correction increment could have been based on the difference between these two transition curves for flat plates, the one calculated for the tunnel and the other calculated for flight conditions. Such a correction increment would have been slightly different from the one actually employed, particularly in the range of the Reynolds Number below the flight range, owing to larger drag reductions in the laminar part of the boundary layer in passing to the higher Reynolds Number. Both the test results for the N. A. C. A. 0012 (fig. 27) and theoretical calculations for the same airfoil by the method of reference 13 indicate, however, that separation must occur as the Reynolds Number is reduced even in the case of this excellently streamlined form at zero lift. The separation is indicated by the abnormal increase of the drag coefficient shown by the experimental results below a Reynolds Number of 800,000. This separation may at first be a local phenomenon, the flow subsequently changing to turbulent and closing in again downstream from the separation point. In any case it is apparent that the flow will either be to a considerable extent turbulent or will separate so that a correction increment based mainly on a laminar layer would have little significance.

The applied correction increment based on the turbulent layer is thus justifiable as being conservative over the flight range of the Reynolds Number and the influences not considered in its derivation will henceforth be considered as sources of error in the experimental results. Admittedly it would be of interest to give further consideration to the results in the range of Reynolds Number below the usual flight range where the influences of extensive laminar boundary layers and separation are of primary importance, but the relatively poor experimental accuracy of the test data for these low Reynolds Numbers and the lack of practical applications tend to discourage an extensive analysis of the low-scale data.

The accuracy of the final results as applied to flight is best judged from a comparison of the results with those from the N. A. C. A. full-scale tunnel. Such comparisons have been made in references 9 and 10. The agreement for both the maximum lift and minimum drag for the Clark Y is easily within the accuracy of the experiments. For the other airfoil for which a comparison is possible, the N. A. C. A. 23012, the results show similar satisfactory agreement for maximum lift, within 4 percent, and for the drag coefficient at zero lift, within 5 percent. The polar curve of the profile-drag coefficients from the full-scale tunnel, however, tended to show a marked drop for a small range of lift coefficients near that for minimum profile drag. Although the same phenomenon was apparent from the variable-density-tunnel tests, it was less marked. The fact that the minimum drag shown by the full-scale-tunnel test was 17 percent lower than shown by the variable-density-tunnel test thus appears less significant than it otherwise would. Furthermore, it might be expected that this localized dip in the profile-drag curve would tend to disappear at the higher Reynolds Numbers common to flight at low lift cofficients. In spite of the fact that the above-mentioned difference between the results is but slightly outside the limit of *possible* experimental errors, the difference does tend to show how much the turbulence corrections applied to the variable-density-tunnel data may be in error, particularly for a condition like the one considered for which rather extensive laminar boundary layers may be present. Comparatively high velocities over the lifting airfoil as contrasted with the flat plate may also tend to increase the value of the correction increment so that all these considerations are in agreement in indicating that the correction increment applied may be considerably too conservative in some instances, particularly for the lower range of flight Reynolds Numbers.[1] The greatest uncertainty, however, in regard to the application of the drag data to flight is due to the possibility that under certain favorable conditions in flight, corresponding to very smooth surfaces and to practically zero turbulence, the transition may be

[1] Since the writing of this report, the results of comparative experiments made in the less turbulent British C. A. T. on the N. A. C. A. 0012 airfoil have come to the attention of the authors. For the model with the most carefully finished surface, the results do show lower drags over the lower range of flight Reynolds Numbers than the data in this report.

Still more recently the results of tests from England and Germany at moderately large Reynolds Numbers have added further support to the conclusion that the correction increments applied herein are too small. Furthermore, as indicated by the foregoing discussion, the increments should probably increase with the airfoil thickness or drag. For example, better agreement is obtained if, instead of the increment 0.0011 subtracted from the usual large-scale profile-drag results, a correction as a factor applied to the measured profile drag is employed. This factor is 0.85, as similarly determined from the flat plate with completely turbulent boundary layer. Final conclusions, however, must await further information on the transition as it actually occurs in flight.

abnormally delayed. For example, Dryden (reference 14) found very large values of R_x corresponding to transition on a flat plate. The conditions are reminiscent of those of supersaturation in solutions. Following this analogy, it may be impossible to set an upper limit of R above which transition must occur. Unusually low drags would, of course, be associated with the presence of this type of abnormally extensive laminar boundary layer; but, while this possibility should be recognized, it is probable that in most practical applications conditions such as slight surface irregularities, vibration, or self-induced flow fluctuations will operate against it. The present results may therefore be used in flight calculations as conservative for wings that are not aerodynamically rough.

VARIATION OF IMPORTANT SECTION CHARACTERISTICS WITH REYNOLDS NUMBER

Maximum lift coefficient $c_{l_{max}}$.—The maximum lift coefficient is one of the most important properties of the airfoil section. It largely determines not only the maximum lift coefficient of wings and hence the stalling speed of airplanes but also, for example, influences how and where tapered wings stall and hence the character of the stall in relation to lateral stability and damping in roll. The maximum lift coefficient, moreover, indicates the useful lift range of the section and tends to define the nature of the variation of profile drag with lift. Finally, the maximum lift coefficient is the important aerodynamic characteristic that usually shows the largest scale effects.

It is not surprising to find large variations of $c_{l_{max}}$ with Reynolds Number because $c_{l_{max}}$ is dependent entirely on the boundary-layer behavior, which in turn is directly a function of viscosity as indicated by the value of the Reynolds Number. In other words, potential-flow theory alone is totally incapable of any predictions concerning the value of $c_{l_{max}}$.

The following discussion traces the mechanism of the stall with a view to reaching an understanding of how the stall, and consequently the maximum lift, is affected by variations of the Reynolds Number. Basically, the discussion is concerned mainly with air-flow separation. The pressure distribution over the upper surface of the conventional airfoil section at lift coefficients in the neighborhood of the maximum is characterized by a low-pressure point at a small distance behind the leading edge and by increasing pressures from this point in the direction of flow to the trailing edge. Under these conditions the reduced-energy air in the boundary layer may fail to progress against the pressure gradient. When this air fails to progress along the surface, it accumulates. The accumulating air thereby produces separation of the main flow. The separation, of course, reduces the lift.

Whether or not separation will develop is dependent on the resistance to separation of the boundary layer. The turbulent layer displays much more resistance to separation than the laminar boundary layer. This dependence of separation on the character of the boundary-layer flow was first observed in sphere-drag tests. At low Reynolds Numbers separation of the boundary layer develops near the equator of the sphere. When the boundary layer on the sphere is made turbulent, however, as it is when the Reynolds Number is sufficiently increased, the separation shifts to a position considerably aft.

The occurrence of separation for airfoils, as affected by the transition from laminar to turbulent flow in the boundary layer, is indicated by the scale effects on $c_{l_{max}}$ (fig. 28) for symmetrical sections of varying thickness. For these airfoils at any considerable lift coefficient the low-pressure point on the upper surface tends to occur just behind the nose, on the leading-edge-radius portion of the airfoil. When the boundary layer is laminar behind this point, separation may be expected

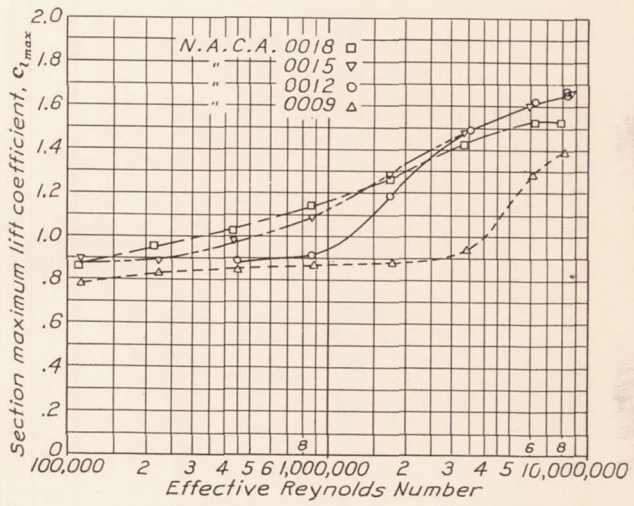

FIGURE 28.—Section maximum lift coefficient, $c_{l_{max}}$. Symmetrical airfoils of varying thickness.

to occur very quickly behind or almost at the low-pressure point owing to the presence of large adverse pressure gradients. In fact, the von Kármán-Millikan method of calculating the incipient separation point for laminar boundary layers (reference 13) has been applied by Millikan to estimate the position of the separation point and also its relation to the transition point as it is assumed to influence the scale effect on the maximum lift coefficient. The number and character of the assumptions involved in such an analysis, however, are such that the results may be expected to yield only qualitative predictions. Elaborate calculations in such cases are of doubtful necessity as indicated by the fact that qualitative predictions, perhaps more reliable, had previously been reached without them. (See references 12, 15, and 16.) Exact methods of calculation are unquestionably desirable but are definitely not a matter for the present but for a time when much more experimental data concerning both separation and transition shall have been secured.

For the present discussion it is sufficient to consider that, if the boundary layer remains laminar, separation will occur very close behind the low-pressure point on the upper surface. Incidentally, the actual separation point is expected, in general, to be forward of the calculated incipient separation point; that is, nearer the low-pressure point. It should not, however, be assumed that the occurrence of separation defines the maximum lift coefficient. For example, at very low Reynolds Numbers, separation on the N. A. C. A. 0012 airfoil occurs even at zero lift, which on this assumption would define zero as the maximum lift. Motion pictures have been made showing the air flow and separation for airfoils at low values of the Reynolds Number. Three photographs from the smoke tunnel are included in figures 29, 30, and 31 to indicate the position and character of the laminar separation for a cambered airfoil. The first two pictures show well-developed separation even at zero angle of attack; the third shows how laminar separation occurs just behind the nose at higher angles of attack.

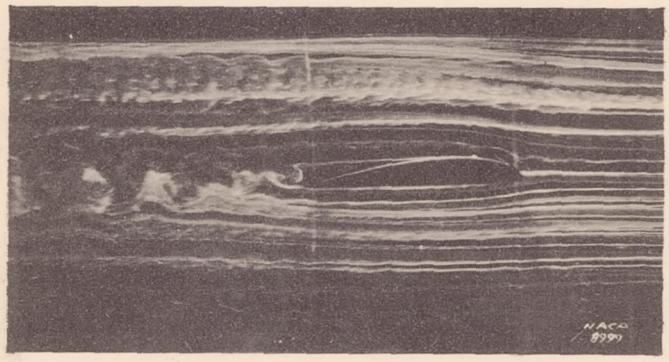

FIGURE 29.—Separation occurring on an airfoil at a low angle of attack.

It is thus apparent that separation of the laminar boundary layer will always be present at a point near the nose at any moderately high lift coefficient if the Reynolds Number is not sufficiently high to make the flow turbulent at that point. This condition certainly exists for the results in figure 28 over the lower range of the Reynolds Number; that is, separation near the nose must have occurred at angles of attack well below that of $c_{l_{max}}$ owing to the very small Reynolds Number associated with the short distance from the nose to the laminar separation point. In this range of R the $c_{l_{max}}$ values are of the order of 0.8 and change little with either R or the section thickness. (See fig. 28.) This value of $c_{l_{max}}$ corresponds approximately to that for a flat plate.

Now consider the character of the flow as the Reynolds Number is increased. The effects are shown very clearly by a comparison of figure 29 and figure 30. Figure 30 corresponds to a higher Reynolds Number and shows turbulence forming at a "transition point" along the separated boundary layer behind the laminar separation point. Incidentally, it should be remembered that the transition point is not really a point but is a more or less extended and fluctuating region in which the laminar layer is progressively changing to the fully

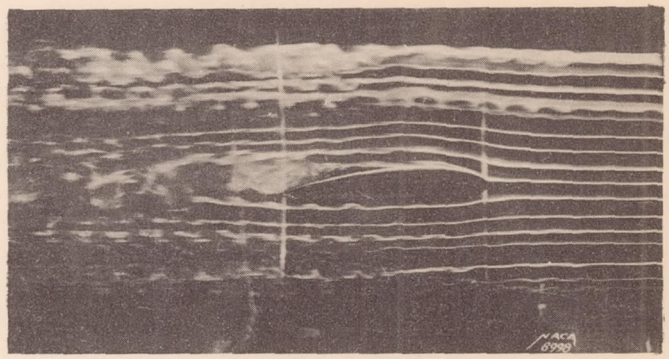

FIGURE 30.—Separation occurring on an airfoil at a low angle of attack (fig. 29) but at an increased Reynolds Number.

developed turbulent layer. This transition region now moves forward toward the separation point as the Reynolds Number is further increased. The formation of turbulence results in a thickening of the boundary layer between the dead air and the overrunning flow until the turbulent mixing extends practically to the airfoil surface. The separated flow may then be considered reestablished. This process would leave a bubble of "dead air" between the separation point and the transition region, the existence of which was predicted several years ago. Subsequently Jones and Farren (reference 17) have actually observed this phenomenon.

As the Reynolds Number is further increased, the transition region progresses toward the leading edge, approaching the region of the laminar separation point. Consider now, for example, the flow about the N. A. C. A. 0012 at a value of R in the neighborhood of R_c, the critical Reynolds Number, where the maximum lift

FIGURE 31.—Separation occurring on an airfoil at a high angle of attack.

increases rapidly with R. As shown in figure 28, $c_{l_{max}}$ for the N. A. C. A. 0012 begins to increase rapidly with R at approximately R_c=1,000,000. Consider therefore two flows, one at R_c=1,000,000 just at the attitude of $c_{l_{max}}$, and the other at the same attitude but at a higher

effective Reynolds Number, say 1,750,000. For the former, separation is probably occurring near the low-pressure point, but the turbulence is forming closely enough behind the separation point so that the flow over the upper surface is partly reestablished. An increase of angle of attack fails to increase the lift, however, because the turbulence is forming so late that the local separation and its resulting adverse effect on the thickening or separation of the turbulent layer farther aft prevent a further gain of lift. Now as the Reynolds Number is increased the transition region moves to a position nearer the separation point, the extent of the separated region is reduced and, as shown by reference to figure 3, C_L at the same angle of attack is increased from 0.85 to 1.05 (for the approximately corresponding test Reynolds Numbers of 330,000 and 660,000). Furthermore, the angle of attack may now be increased until C_L reaches 1.1 before the flow following the upper surface fails. The failure now occurs

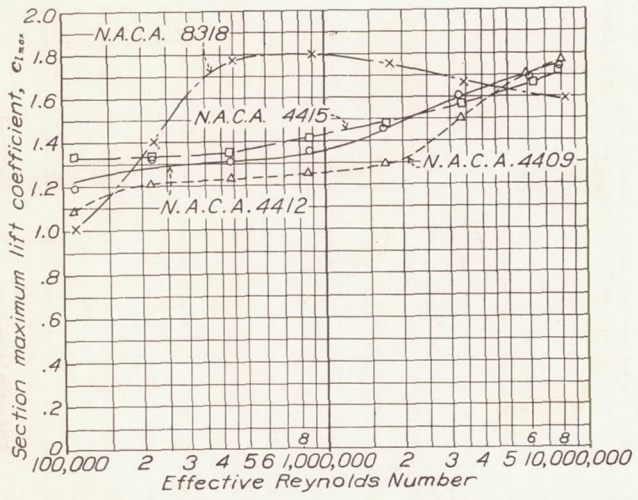

FIGURE 32.—Section maximum lift coefficient, $c_{l_{max}}$. Camber and thickness series.

suddenly, causing a break in the lift curve, but again may be delayed by a further increase of the Reynolds Number.

In such cases the scale effect evidently varies with the shape of the nose of the airfoil. If the leading-edge radius is reduced by making the airfoil thinner, the local Reynolds Number for the separation point or the transition region, either R_δ based on boundary-layer thickness or R_x based on the distance along the surface, is reduced with respect to R because the local dimensions near the nose are reduced with respect to the airfoil chord. Higher values of R are therefore required to reach the critical R_x or R_δ values in the neighborhood of the nose. This result is indicated by the higher critical Reynolds Number R_c for the N. A. C. A. 0009 than for the N. A. C. A. 0012, as shown in figure 28. Likewise, the 15 and 18 percent thick airfoils show progressively lower values of R_c than the N. A. C. A. 0012, but the critical range tends to disappear as the thickness is increased.

The range of R is limited by the wind tunnel so that in most instances the scale effect above the critical range could not be determined. It is probable, however, that the highest maximum lift coefficients are reached when the Reynolds Number corresponds to the occurrence of fully developed turbulence practically at the laminar separation point but that this condition occurs above the highest Reynolds Numbers reached except possibly for the thickest airfoil, N. A. C. A. 0018.

High local Reynolds Numbers at the laminar separation point could, however, be reached by employing a thick, highly cambered airfoil. The N. A. C. A. 8318 airfoil was included for this reason. The results (see fig. 32) indicate, as expected, a very low critical Reynolds Number. With increasing Reynolds Number, $c_{l_{max}}$ rises to a maximum at $R=900{,}000$ and then falls off slowly. In this instance, at the highest Reynolds Numbers transition probably occurs ahead of any point at which laminar separation could occur. The maxi-

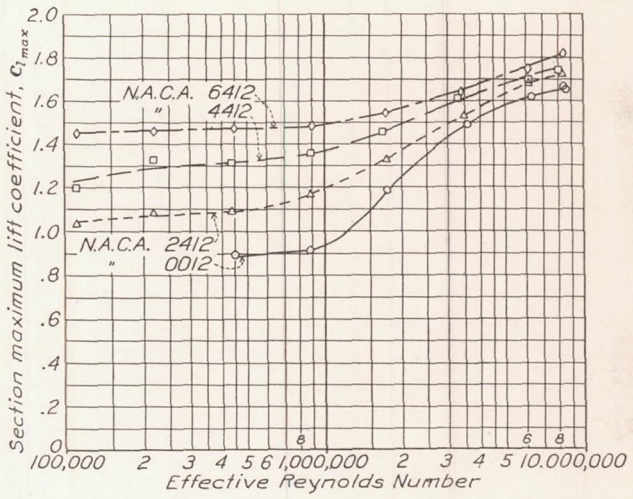

FIGURE 33.—Section maximum lift coefficient, $c_{l_{max}}$. Camber series.

mum lift coefficient must therefore be determined by the behavior of the turbulent layer. The significant conclusion is that $c_{l_{max}}$ then decreases with increasing R. Another significant observation is that under these conditions stalling is progressive as indicated by the rounded lift-curve peaks in figure 11. This type of stalling corresponds to a progressive separation or thickening of the turbulent layer in the region of the trailing edge.

The process of stalling in general is more complex than either of the two distinct processes just discussed. It has been compared by Jones (reference 17) to a contest between laminar separation near the nose and turbulent separation near the trailing edge, one or the other winning and thus producing the stall. Actually it appears from these scale-effect data that, for commonly used airfoils at a high Reynolds Number, the forward separation usually wins but that it is largely conditioned and brought about by the thickening or separation of the turbulent boundary layer near the

trailing edge, which, in turn, may be largely influenced by the local separation near the leading edge. The reasons for these statements will become clear from the consideration of the scale effects for the different types of airfoil.

Consider first the maximum lift of the conventional type of cambered airfoil. Where stalling is determined largely by separation near the leading edge, the maximum lift would be expected to be a function of the curvature near the leading edge and also a function of the mean camber because the effect of the camber is to add a more or less uniformly distributed load along the chord. At some angle of attack above that of zero lift the flow over the nose part of the cambered airfoil approximates that over the nose of the corresponding symmetrical airfoil at zero lift. This correspondence of flows at the leading edges between the symmetrical and cambered airfoils continues as the angles of attack of both are increased. If the stalling were determined largely by the flow near the nose, the two airfoils would stall at the same time, but the lift of the cambered airfoil would be higher than that of the symmetrical airfoil by the amount of the initial lift increment. Reference to figure 33 shows that this expected change of $c_{l_{max}}$ with camber is approximately that shown by the results from tests in the lower range of the Reynolds Number. At high Reynolds Numbers, however, the change of $c_{l_{max}}$ with camber is much smaller than would be expected if the stall were controlled only by conditions near the leading edge. On the other hand, some of the cambered airfoils show a sudden loss in lift at the maximum indicating that separation is occurring near the leading edge but, as the camber is increased, the lift curves become rounded. (See figs. 6, 7, and 8.) For the N. A. C. A. 2412, which shows a sharp break in lift at the maximum but a small gain in $c_{l_{max}}$ due to camber at the high Reynolds Numbers, the boundary-layer thickening or turbulent separation must become pronounced near the trailing edge at the higher Reynolds Numbers before the flow breakdown occurs near the leading edge. This alteration of the flow results in higher angles of attack for a given lift and consequently more severe flow conditions over the nose of the airfoil. These flow conditions, which really originate near the trailing edge, thus bring about the flow breakdown near the leading edge that finally produces the actual stall. It must not, however, be concluded that more gradually rounding lift-curve peaks with increasing R should be the result; actually, the opposite is usually true (e. g., figs. 6, 7, and 8). The explanation is probably that increasing the Reynolds Number reduces the extent of the local separation near the leading edge, which influences the boundary-layer thickening near the trailing edge, at least until the transition region reaches the separation point. That $c_{l_{max}}$ continues to be influenced by the flow conditions near the leading edge, even for highly cambered sections, is shown by the fact that the critical Reynolds Number is little affected by increasing the camber to that of the N. A. C. A. 6412 in spite of the fact that the actual gain in $c_{l_{max}}$ throughout the critical range becomes less for the more highly cambered airfoils. This conclusion is an important one because it can be extended to predict that the critical Reynolds Number will not be affected by flaps and other high-lift dev ces placed near the trailing edge, which act much like a camber increase.

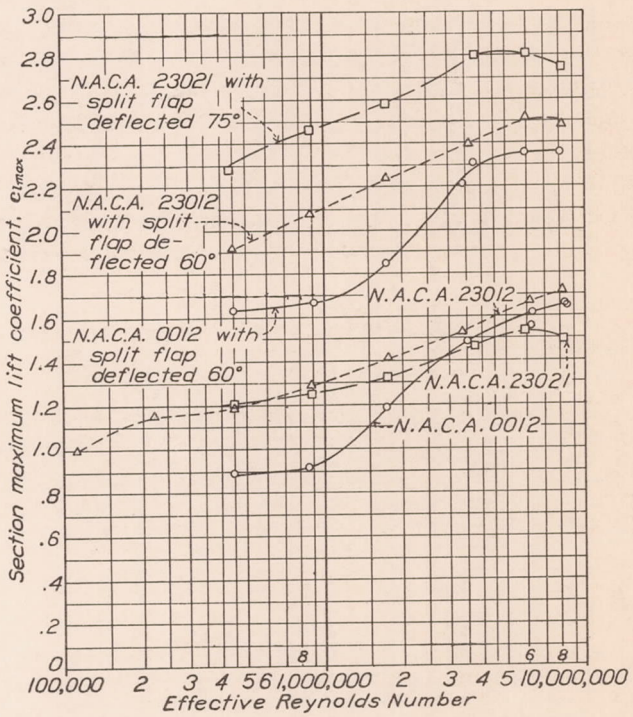

FIGURE 34.—Section maximum lift coefficient, $c_{l_{max}}$. Airfoils with and without flaps.

Reference to figure 34 shows the correctness of this conclusion. It will be noted, moreover, that each scale-effect curve representing an airfoil with a split flap tends to parallel the corresponding curve for the same airfoil without a flap. The split flap thus simply adds an increment to the maximum lift without otherwise changing the character of the scale effect. In this respect the behavior with the flap differs from the behavior with increasing camber. With the split flap, the distribution of pressures over the upper surface is apparently not affected in such a way as to increase the tendency toward trailing-edge stalling, otherwise the scale-effect variations would not be similar with and without the flaps. Incidentally, it is of interest to note that the maximum lift increment due to the split flap is not independent of the airfoil section shape but, for example, increases with the section thickness. (Cf. the N. A. C. A. 230 series, with and without split flaps, table I.)

As regards flaps other than split flaps, recent tests have shown that the maximum lifts attainable are approximately equal for either the ordinary or the split flap. This result might have been expected because the

results of references 18 and 19 had indicated that the flow does not follow the upper surface of an ordinary flap except for small angles of flap deflection. It should therefore make little difference whether or not the upper surface of the flap is deflected with the lower. Furthermore, the same reasoning might be applied to predict the effects of camber, when the mean line is of such a shape that the maximum camber occurs near the trailing edge so that the separation associated with increasing camber is localized in this region. Thus it might have been predicted that the scale effect as shown in figure 35 for the N. A. C. A. 6712 airfoil would be more like that of an airfoil with a split flap than like that of the usual type of cambered airfoil.

Another important conclusion can be deduced from the results in figure 35 showing the scale effects for airfoils having various mean-line shapes. When a mean-line shape like that of the N. A. C. A. 23012 is em-

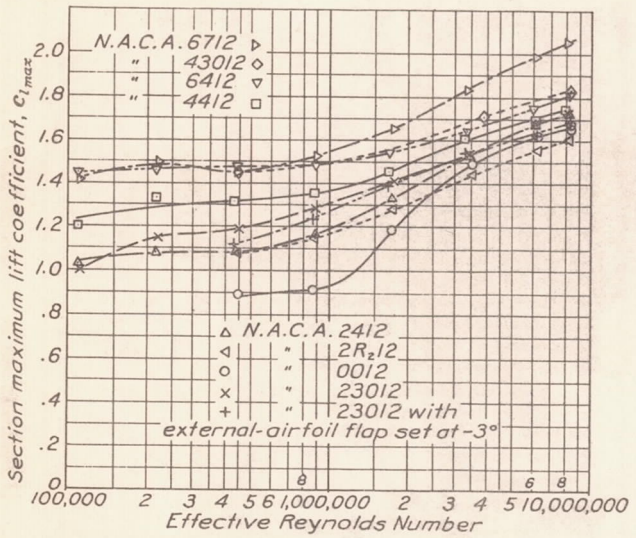

FIGURE 35.—Section maximum lift coefficient, $c_{l_{max}}$. Airfoils with various mean-line shapes.

ployed—that is, one having marked curvature near the nose and a forward camber position—the effect is to alter the conditions of the leading-edge stall. The critical Reynolds Number is thus shifted to the left and the general character of the scale effect becomes more like that of the usual airfoil of 15 instead of 12 percent thickness.

The opposite effect on the nose stall is shown in figure 36 where the critical Reynolds Number is shifted to the right by decreasing the leading-edge radius, that is, by changing from the N. A. C. A. 23012 section to the 23012–33. Thus it appears, in general, that the character of the $c_{l_{max}}$ scale effect, particularly in relation to the value of the critical Reynolds Number, depends mainly on the shape of the airfoil near the leading edge.

The two remaining airfoils not covered by the previous discussion (fig. 37) have slotted high-lift devices. Both the Clark Y airfoil with Handley Page slot and the airfoil with external-airfoil flap show unusual scale effects. The airfoil with Handley Page slot shows an increasing $c_{l_{max}}$ throughout the Reynolds Number range but shows a peculiar change in the character of the stall in the full-scale range near R_e=3,000,000. (See also fig. 24.) The airfoil with the external-airfoil flap shows a break in the scale-effect curve. Two values of $c_{l_{max}}$ were measured for the condition corresponding to R_e=1,700,000 (fig. 23, test R=645,000), one lift curve having a sharp break at the maximum and the other being rounded. It is believed that the change is associated with the action of the slot at the nose of the external-airfoil flap. It is particularly interesting because it represents one of the cases mentioned under the interpretation of the wind-tunnel data for which the failure of the tunnel flow to reproduce exactly at the effective Reynolds Number the corresponding flow in flight becomes of practical importance. A comparison of these tests with tests in the 7- by 10-foot tunnel (reference 5) indicated that such scale effects may be due primarily to the action

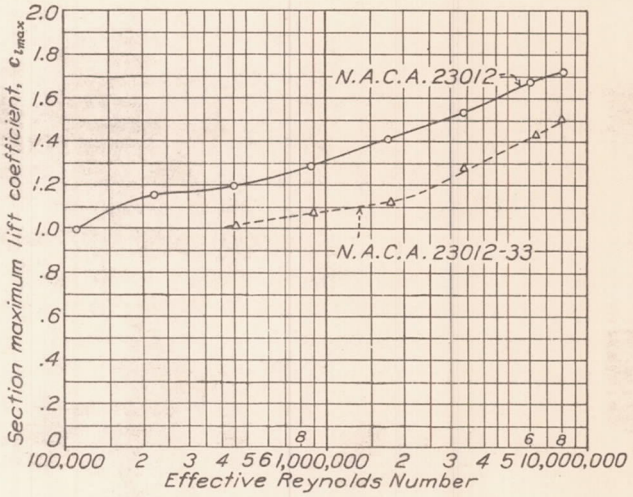

FIGURE 36.—Section maximum lift coefficient, $c_{l_{max}}$. Thickness-shape variation.

of the slot as affected by the boundary-layer thickness relative to the slot width, which is a function of both the test and the effective Reynolds Number, rather than to the transition from laminar to turbulent flow. When interpreted on the basis of the test rather than the effective Reynolds Number as regards the occurrence of the break in the low Reynolds Number range, better agreement with the results from the variable-density tunnel was obtained. On this basis the discontinuity shown in figure 37 as occurring at R_e= 1,700,000 would be expected to occur in flight at a considerably lower Reynolds Number outside the usual flight range.

With regard to $c_{l_{max}}$ scale effects for conventional types of airfoils, it now appears in the light of the preceding discussion that a position has been reached from which the scale effects appear rational and sufficiently regular and systematic so that general scale-effect corrections may be given for such airfoils. This position represents a marked advance. In a later

section of this report such generalized scale-effect corrections for $c_{l_{max}}$ are presented for engineering uses.

Lift variation near $c_{l_{max}}$.—The variation of the lift near the maximum as indicated by the shape of the lift curve is of some importance because it often affects the character of the stall and the corresponding lateral control and stability of the airplane in flight. The character of the stall for the airfoils may be inferred approximately from the preceding discussion of $c_{l_{max}}$ and is indicated by the lift curves in figures 2 to 24. The moderately thick symmetrical airfoils in the critical or flight range of R show sudden losses of lift beyond the maximum. Efficient airfoils of moderate thickness and camber, for example, N. A. C. A. 2412 and 23012, likewise usually show sudden breaks in the lift curve at the maximum for the higher Reynolds Numbers. When the influence of trailing-edge stalling becomes sufficiently marked as it does with airfoils N. A. C. A. 4412 and 6412, the breaks in the lift curves disappear and the lift curve becomes rounded at the maximum. It is interesting to note that breaks occur at comparatively low values of the Reynolds Number for the N. A. C. A. 8318. In this case the breaks appear in the critical range of R, where critical leading-edge stalling occurs, and disappear at higher and lower Reynolds Numbers. (See figs. 11 and 32.)

Lift-curve slope a_0.—The scale effects for a_0 are represented in figure 38. It will be noted that, within the full-scale range, the airfoils show little variation of a_0 with either airfoil shape or with R. In this range most of the airfoils show a slight tendency toward increasing a_0 with R but, for engineering purposes, the variation of a_0 may usually be considered negligible within the flight range. The lift-curve slope, like several of the other section characteristics, begins to display abnormal variations below a Reynolds Number of approximately 800,000. For the lowest values of R the lift curves often became so distorted that lift-curve slopes were not determined. (See figs. 2 to 24.)

Angle of zero lift α_{l_0}.—Scale-effect variations of α_{l_0} are represented in figure 39. The conclusions with respect to this characteristic are almost the same as for the lift-curve slope a_0. Symmetrical airfoils, of course, give $\alpha_{l_0}=0$ at all values of R. The cambered airfoils, in general, show a small decrease in the absolute value of the angle with increasing R above the value at which the variations are abnormal.

Minimum profile-drag coefficient $c_{d_{0min}}$.—The minimum profile-drag coefficient is indicative of the wing drag in high-speed flight and is the other important section characteristic, aside from $c_{l_{max}}$, that shows marked scale-effect variations within the full-scale range which must be taken into account in engineering work.

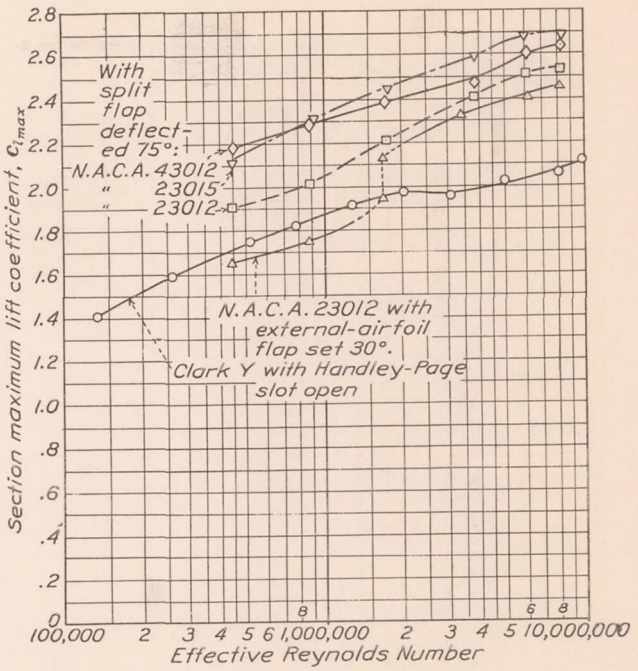

FIGURE 37.—Section maximum lift coefficient, $c_{l_{max}}$. Airfoils with high-lift devices.

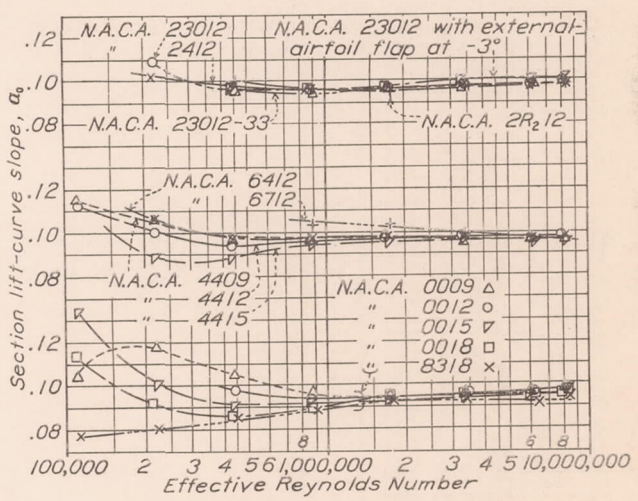

FIGURE 38.—Lift-curve slope, a_0.

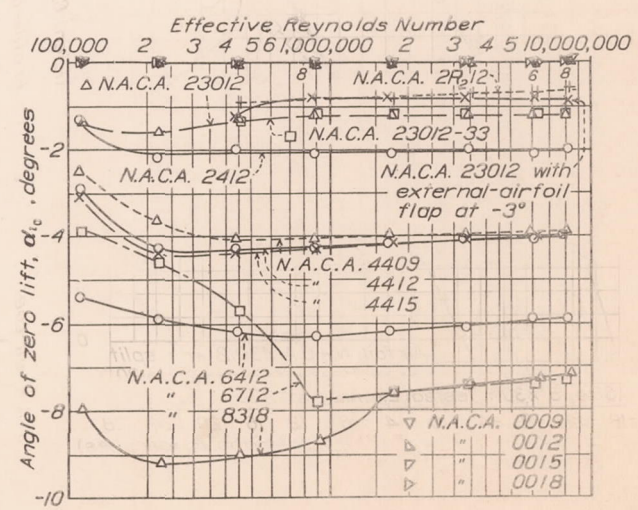

FIGURE 39.—Angle of zero lift, α_{l_0}.

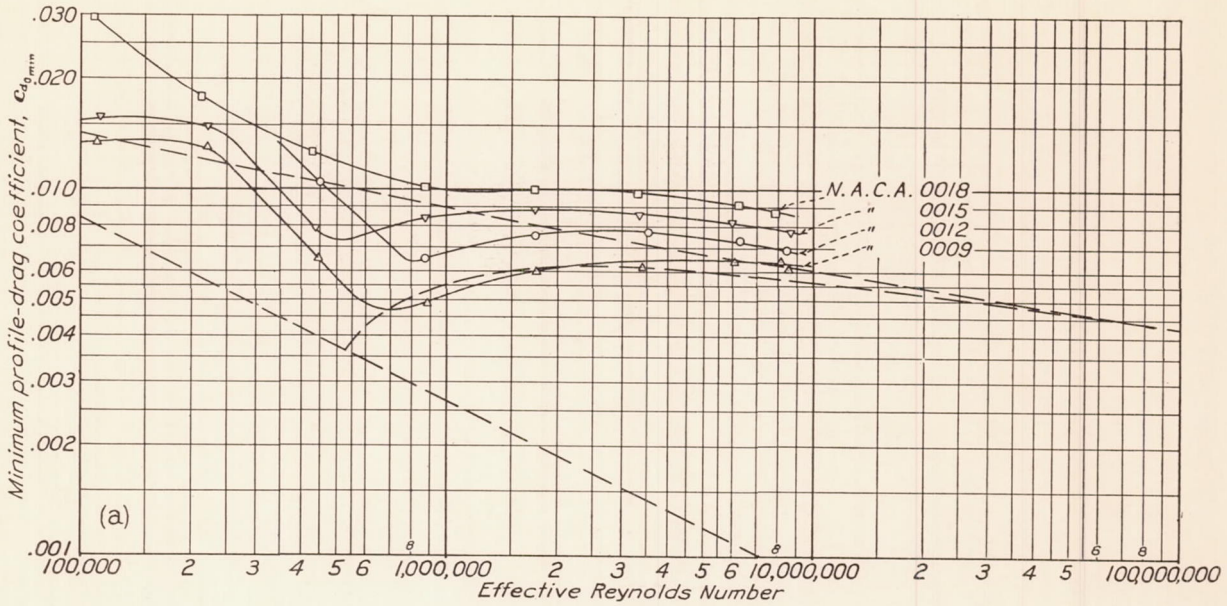

(a) Symmetrical airfoils of varying thickness.

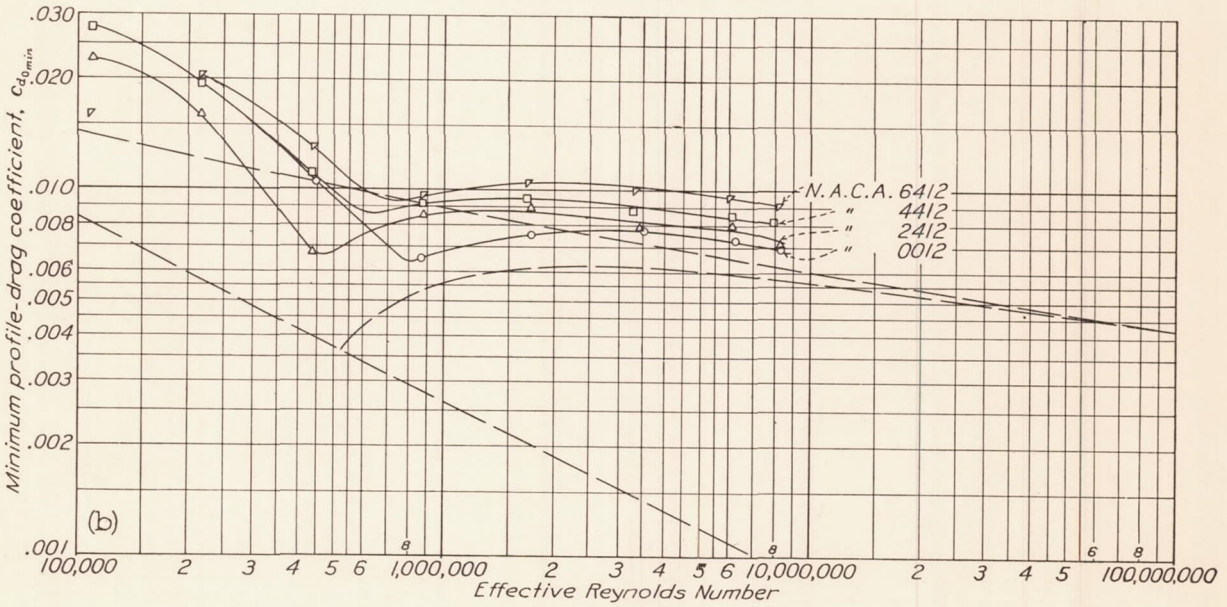

(b) Camber series.

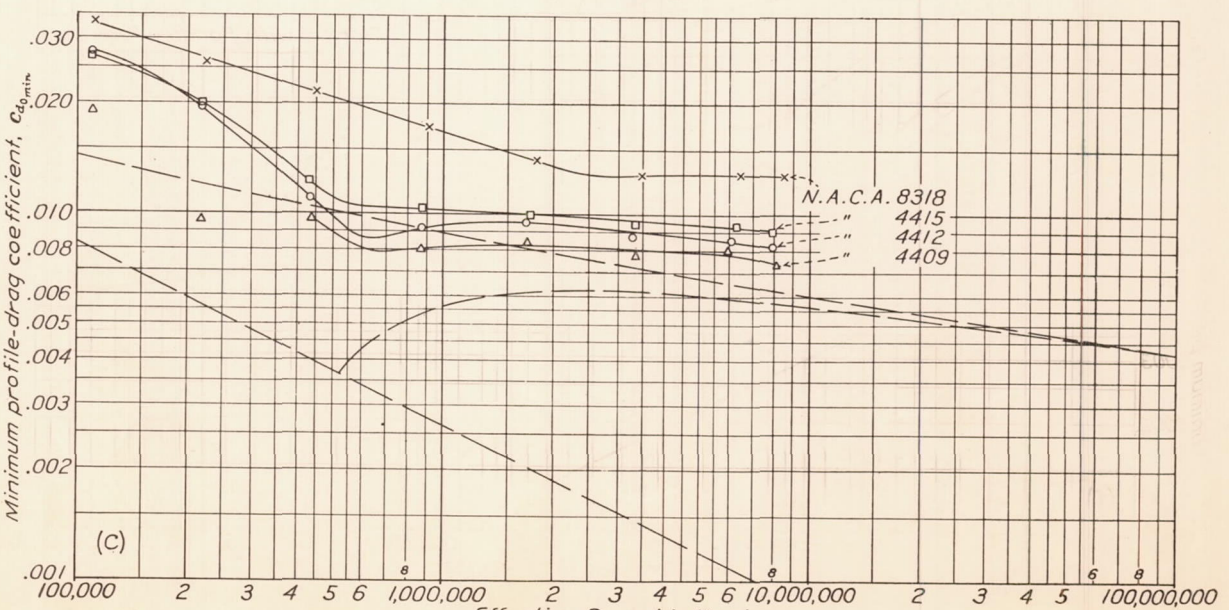

(c) Thickness and camber.

FIGURE 14.—Minimum profile-drag coefficient, $c_{d_{0_{min}}}$.

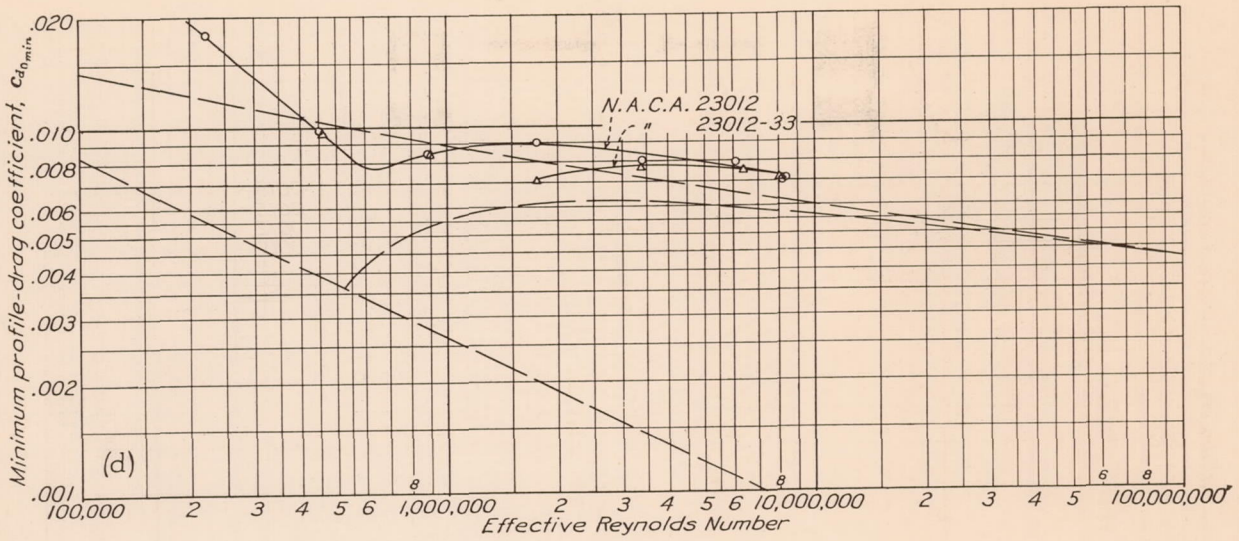

(d) Thickness shape.

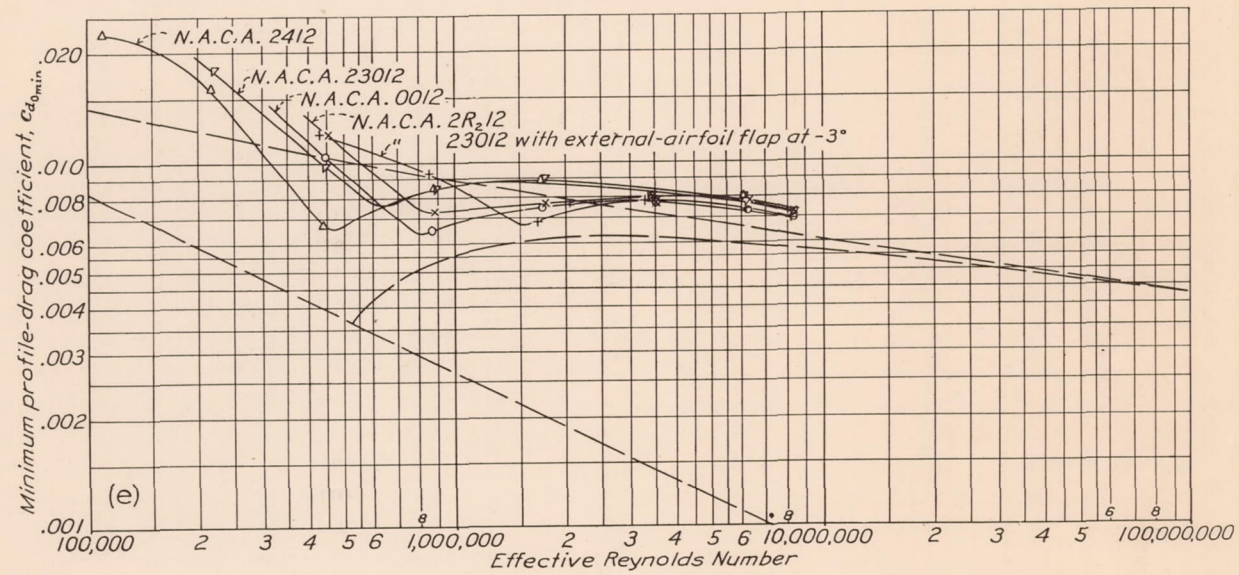

(e) Camber shape.

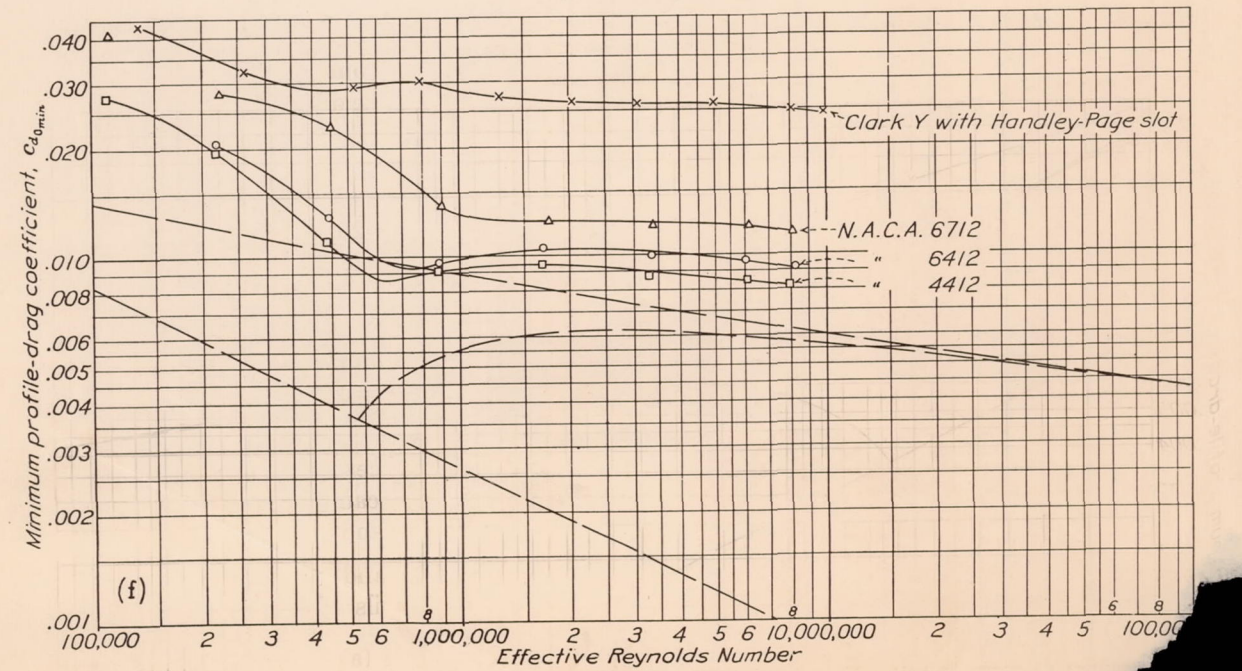

(f) Camber shape.

FIGURE 40 (continued.)—Minimum profile-drag coefficient, $c_{d0\ min}$.

The experimental drag results are presented by means of logarithmic plots with the well-known laminar and turbulent skin-friction curves and the Prandtl-Gebers transition curve shown for comparison. (See figs. 40 (a) to 40 (f).) At the higher Reynolds Numbers a striking similarity exists between the minimum profile-drag coefficients for the airfoils and the transition curve representing the drag coefficient variation with R for a flat plate towed in water. The other striking feature of the drag curves is their departure from regularity at Reynolds Numbers below a certain critical value. This critical value of the Reynolds Number usually lies in the range between 400,000 and 800,000, but a study of the experimental results will show that the critical value itself is irregular, that is, does not vary systematically with the airfoil shape. The results appear as though two or more drag values were possible within this Reynolds Number range and accidental disturbances determined whether a high or a low value of the drag was measured at a given value of R within this range. One is reminded of Baker's experiments towing airship models in water in a towing basin where measurements could not be repeated until transition was definitely brought about by the use of a cord passing around the model near the nose.

The shape of the scale-effect curve for the N. A. C. A. 0012 airfoil at zero angle of attack (fig. 40 (a)) was studied in the light of boundary-layer calculations. The results indicated that the computed skin-friction drag coefficients to give scale-effect variations in agreement with the measured ones required the presence of rather extensive laminar boundary layers in this critical range of the Reynolds Number. In fact, for the N. A. C. A. 0012 airfoil, the laminar boundary layer was found to have become so extensive when R was reduced to the experimentally determined critical value that a further reduction of R would have required the laminar boundary layer to extend behind the computed laminar separation point, which would have involved at least local separation. It seems evident, therefore, that the increased drag coefficients below the critical range are the result of this condition, which is probably associated with laminar separation and a resulting increase of the pressure or form drag of the section. Fortunately, however, this phenomenon seems to appear below the usual flight range of R.

When designers are concerned with the minimum drag of an airfoil section, it is usually for high-speed or cruising flight, which for modern transport airplanes may correspond to a Reynolds Number of 20,000,000 or more for some of the wing sections. The drag coefficients for the Reynolds Number range above the highest reached in the tunnel are therefore of more interest than those well within the experimental range. Unfortunately, [illegible] sion of the measurements permits only an [illegible]e determination of the shape of these scale-[illegible]s even in the higher experimental range of [illegible]polations into the higher flight range will necessarily be unreliable. Nevertheless, much engineering work requires a knowledge of airfoil drag coefficients within this range so that the engineer *must* resort to extrapolation. For this purpose the data may be studied in relation to the slopes of the curves for the various airfoils (fig. 40) in the highest range of R reached in the experiments. Such a study indicates that the airfoils, excluding the unusual airfoils N. A. C. A. 8318, N. A. C. A. 6712, and the Clark Y with Handley Page slot, show a decreasing $c_{d_{0\,min}}$ with R that seems, in general, to parallel approximately the corresponding curve for the flat plate. Thus, in general, the slope of the $c_{d_{0\,min}}$ scale-effect curves in the neighborhood of a Reynolds Number of 8,000,000 may be taken as approximately -0.11, which leads to the following extrapolation formula:

$$c_{d_{0\,min}} = \left(c_{d_{0\,min}}\right)_{std}\left(\frac{R_{std}}{R}\right)^{0.11}$$

where the subscript *std* refers to the standard airfoil-test results from the variable-density tunnel corresponding to an effective Reynolds Number of approximately 8,000,000. In such extrapolation formulas, values of the exponent have been used between 1/5, taken from Prandtl's original analysis of the completely turbulent skin-friction layer, and 0.15, which agreed better with experiments with pipes and flat plates at very high values of R and agrees better with von Kármán's recent analysis of the completely turbulent layer in this range of R. It should be emphasized, however, that these comparatively large exponents are not conservative and would be expected to lead to predictions of large-scale drag values much too low, particularly when the extrapolation is made from measurements made in the transition region; for example, in figure 40 (a) measurements in the range between 1,000,000 and 2,000,000 should not be extrapolated by such methods to 20,000,000. Extrapolations from $R=8{,}000{,}000$ using the comparatively low exponent 0.11 are, however, considered reasonably conservative for aerodynamically smooth airfoils.

In regard to profile-drag coefficients at lift coefficients other than the optimum, figure 41 (a) shows the scale effects for c_{d_0} at $c_l=0.8$ for the symmetrical series of airfoils. The drop in the scale-effect curves in the transition region has disappeared and the two thinner airfoils show evidences of the approaching stall. Curves for members of the camber series of airfoils, N. A. C. A. 0012, 2412, 4412, and 6412 at *zero lift* are shown in figure 41 (b). Here the symmetrical airfoil is operating at its optimum lift and the departure from the optimum for the other airfoils increases with camber. A progressive transition from the $c_{d_{0\,min}}$ type of scale effect to that of figure 41 (a) is apparent. Results (reference 10) from other wind tunnels for the Clark Y airfoil, which is in a sense similar to the N. A. C. A. 4412 but has slightly less camber, are also indicated in figure

41 (b) for comparison. The comparison of the results from the various tunnels should serve to indicate the limitations of accuracy that must be accepted when any of the data are extrapolated to the higher full-scale Reynolds Numbers.

Optimum lift coefficient $c_{l_{opt}}$.—The optimum lift coefficients are presented in figure 42. This characteristic is of importance mainly in relation to c_{d_0} values at other values of c_l. It is not possible, nor essential for this purpose, to evaluate $c_{l_{opt}}$ very accurately. In fact,

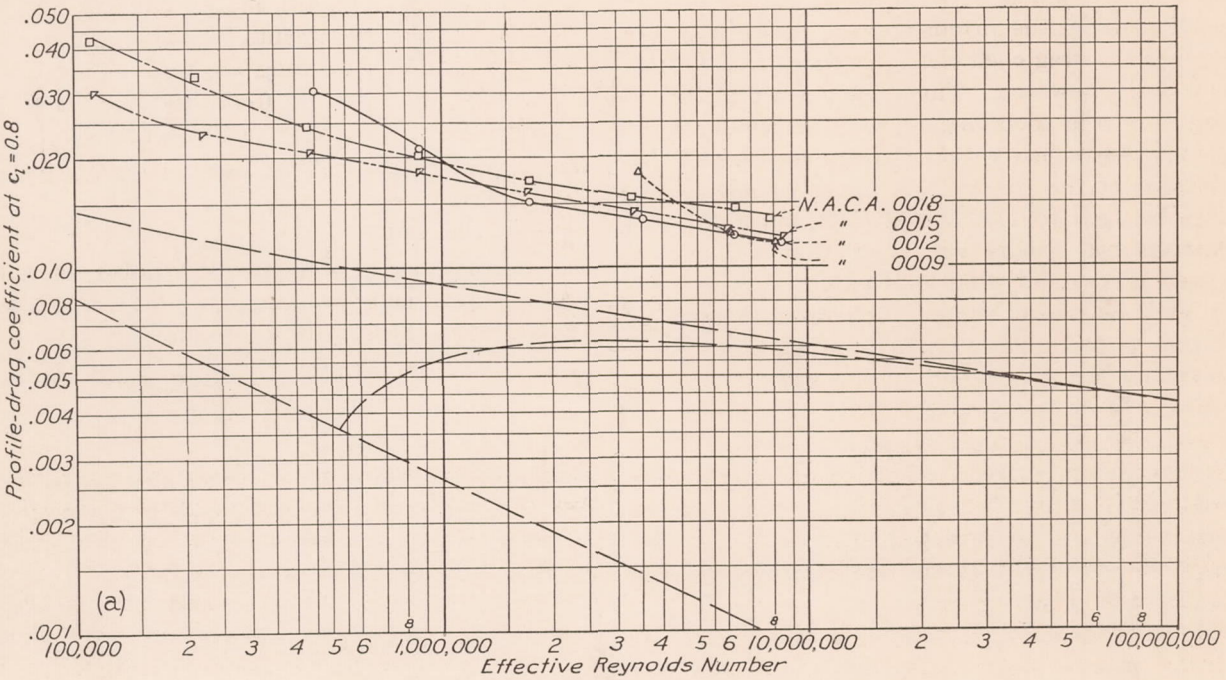

(a) Symmetrical airfoils of varying thickness; c_l=0.8.

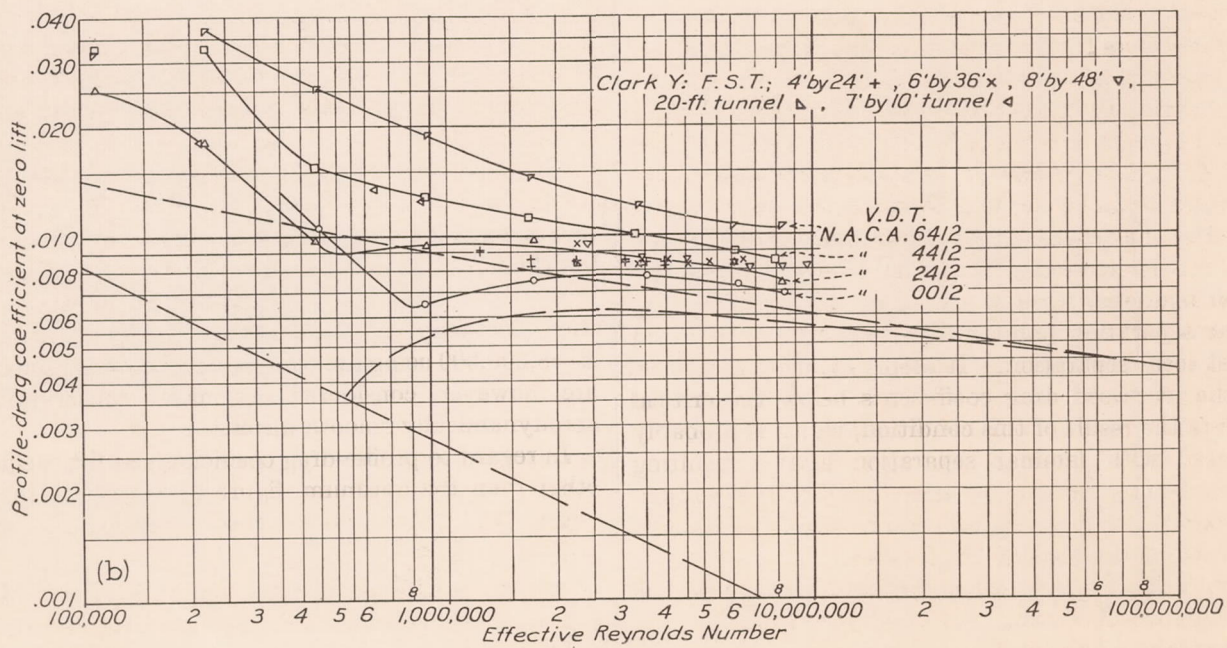

(b) Camber series; c_l=0.

FIGURE 41.—Profile-drag coefficient.

The determination of c_{d_0} values at various lift coefficients in engineering work is best accomplished by a consideration of increments from $c_{d_{0\,min}}$. The method of a "generalized polar" discussed in a later section of this report gives such increments in terms of the departure of c_l from $c_{l_{opt}}$ as compared with the departure of $c_{l_{max}}$ from $c_{l_{opt}}$.

the accuracy of the experimental data is not sufficient to establish the scale-effect variations with certainty. Nevertheless, the results show a definite tendency toward a decreasing $c_{l_{opt}}$ with increasing R. Thus values measured in small atmospheric tunnels may be expected to be too high. Values from the standard airfoil tests in the variable-density tunnel may usually

be taken as approximately correct within the usual full-scale range but may be somewhat too high for the higher flight range of R.

Pitching-moment coefficient $c_{m_{a.c.}}$ and aerodynamic-center position a. c.—The values of the pitching-moment coefficient and the aerodynamic-center position establish the pitching-moment characteristics of the airfoil section in the normal operating range between zero lift and the stall. In this range the pitching moment about the aerodynamic-center point may be considered constant for conventional airfoils. The accuracy of the low-scale data did not permit the evaluation of aerodynamic-center positions for values of R much below the flight range, and the variations found in the higher range showed little consistency. Values are indicated in figures 2 to 24 and in table I, but it is not considered advisable in practice to allow for a variation of aerodynamic center with R. The $c_{m_{a.c.}}$ values corresponding to these aerodynamic-center positions are plotted in figure 43. The values are nearly independent of R at high values of R but usually show a tendency to increase numerically as R is reduced toward the lower extremity of the flight range. Thus low-scale tunnel tests may be expected to give pitching moments that are numerically too large.

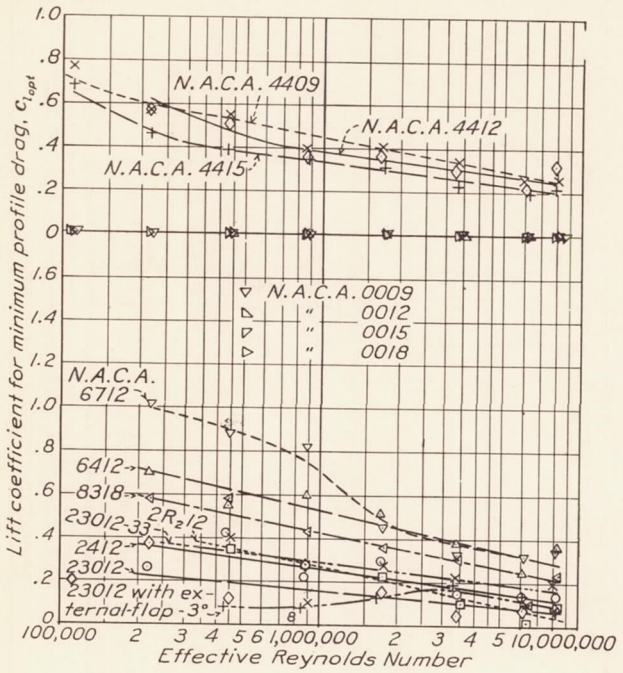

FIGURE 42.—Optimum lift coefficient, $c_{l_{opt}}$.

PREDICTION OF AIRFOIL CHARACTERISTICS AT ANY REYNOLDS NUMBER FOR ENGINEERING USE

In the consideration of methods of predicting wing characteristics, it should be remembered that the scope of this report is confined to the prediction of the *airfoil section* characteristics. Actual *wing* characteristics are obtained from these section characteristics by integrations along the span with suitable allowances for the induced downflow and the corresponding induced drag. Such calculations as applied to tapered wings are fully discussed in reference 8. It remains therefore to predict the airfoil *section* characteristics at any value of the flight Reynolds Number. The preceding discussion has shown that for engineering purposes many of the important airfoil section characteristics may be considered independent of R within the flight range, so that for application to flight at any value of R these characteristics may be taken directly from the tabulated values from the standard airfoil tests in the variable-density tunnel. There remain then the two important *section* characteristics $c_{l_{max}}$ and c_{d_0}, which in general will require correction to the design Reynolds Number before they are employed.

Section maximum lift.—For the prediction of the *section* maximum lift coefficient $c_{l_{max}}$ at values of R other than the R_e value for which they are commonly tabulated, the correction-increment curves of figure 44 have been prepared from the data in this report. In this figure, curves giving the corrections $\Delta c_{l_{max}}$ are grouped in families corresponding to the measured scale-effect variations for various types of airfoils. In general, for normal airfoils the curves in figure 44 marked 0 for types B, C, D, and E correspond to the symmetrical airfoil sections of different thickness and the curves indicated by increasing numbers correspond to airfoil sections of increasing camber.

In practice, the particular curve to be employed for a given airfoil will be indicated in the standard tables of airfoil characteristics such as table II of this report (see also reference 3) under: "Classification, SE."

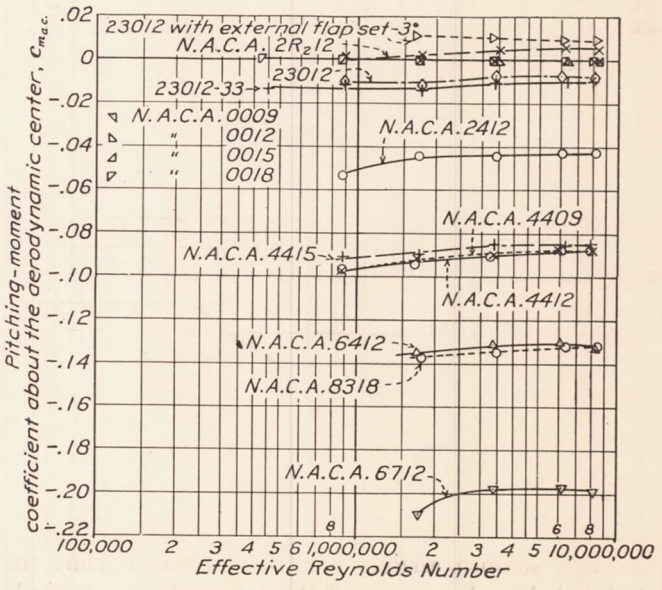

FIGURE 43.—Pitching-moment coefficient about the aerodynamic center, $c_{m_{a.c.}}$.

From the curve thus designated, the correction increment is read at the design Reynolds Number. The required $c_{l_{max}}$ for the section at the particular Reynolds Number is then obtained by adding this increment to the tabulated $c_{l_{max}}$ value.

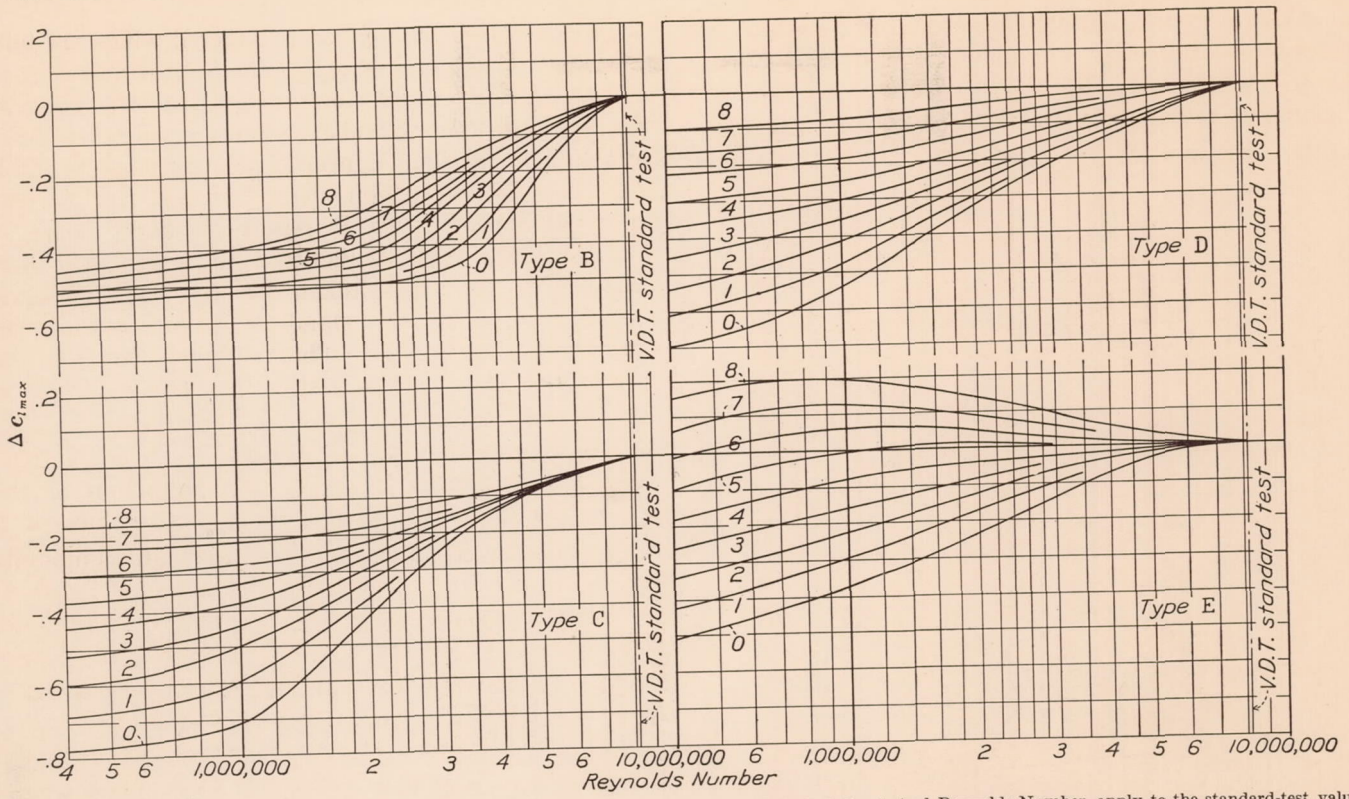

FIGURE 44.—Scale-effect corrections for $c_{l_{max}}$. In order to obtain the section maximum lift coefficient at the desired Reynolds Number, apply to the standard-test value the increment indicated by the curve that corresponds to the scale-effect designation of the airfoil.

Airfoil section drag.—In design work, values of the *section* minimum drag coefficient $c_{d_0\,min}$ for aerodynamically smooth airfoils are first obtained from the tabulated data by means of the extrapolation formula previously given,

$$c_{d_0\,min} = \left(c_{d_0\,min}\right)_{std} \left(\frac{R_{std}}{R}\right)^{0.11}$$

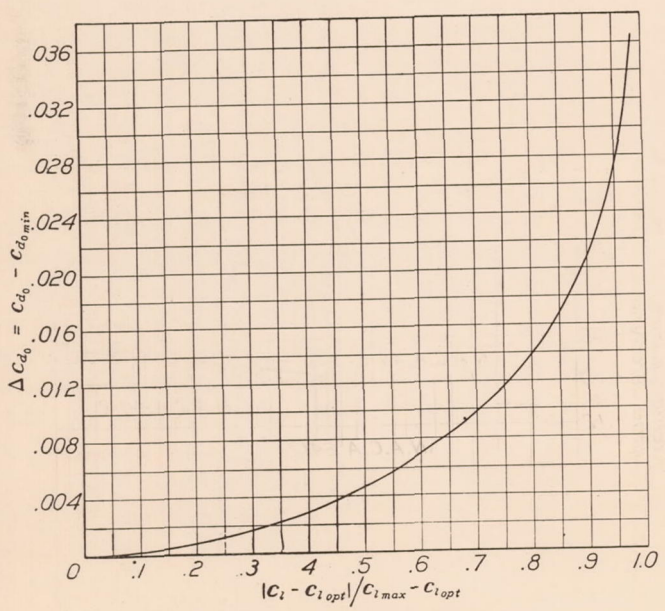

FIGURE 45.—Generalized variation of Δc_{d_0}.

The c_{d_0} values at other lift coefficients may now be obtained from the generalized variation of Δc_{d_0} with $\frac{|c_l - c_{l_{opt}}|}{c_{l_{max}} - c_{l_{opt}}}$ presented in figure 45, where the standard airfoil characteristic table is again employed to find $c_{l_{opt}}$. The $c_{l_{max}}$ value employed should, of course, correspond to the Reynolds Number of the c_{d_0} value being calculated. This procedure may involve the use of $c_{l_{max}}$ values corresponding to very high Reynolds Numbers. These values, however, may be estimated by extrapolating the maximum-lift scale-effect curves, little accuracy being required because c_l will usually be near $c_{l_{opt}}$ and Δc_{d_0} therefore small. A series of Δc_{d_0} values may thus be derived for various lift coefficients and Reynolds Numbers. The corresponding values of c_{d_0} are then obtained by adding these increments to the $c_{d_0\,min}$ value calculated from the preceding extrapolation formula for the corresponding Reynolds Number. In practice, a series of values of c_{d_0} may thus be derived to form a curve of c_{d_0} against c_l along which the Reynolds Number varies with lift coefficient as in flight.

LANGLEY MEMORIAL AERONAUTICAL LABORATORY,
NATIONAL ADVISORY COMMITTEE FOR AERONAUTICS,
LANGLEY FIELD, VA., *June 24, 1936.*

APPENDIX

INVESTIGATION OF CERTAIN CONSISTENT ERRORS PRESENT IN TEST RESULTS FROM THE VARIABLE-DENSITY TUNNEL

By Ira H. Abbott

INTRODUCTION

An investigation has been made to evaluate three corrections that were not applied to the data, obtained in the variable-density wind tunnel, and published in reference 2 and earlier reports. The need for these corrections had been recognized, and possible errors in the data resulting from the lack of these corrections have been listed as consistent errors (reference 2) due to the following effects:

1. Aerodynamic interference of the model supports on the model.

2. Effect of the compressed air on the effective weight of manometer liquids used to measure the dynamic pressure.

3. Combined effects on the measured dynamic pressure of blocking due to the model and to errors in pitot-tube calibration arising from differences in dynamic scale and turbulence between conditions of use in the variable-density tunnel and conditions of calibration. These effects result in errors in the calibration of the static-pressure orifices used to determine the dynamic pressure.

INTERFERENCE OF MODEL SUPPORTS

The model supports used in the variable-density tunnel and the method of determining the tare forces are described in reference 1. The usual tare tests determine the tare forces on the supports including the interference of the model on the supports. In addition, the usual method of determining the balance alinement with respect to the air-flow direction by testing an airfoil erect and inverted includes any interference of the supports on the model that is equivalent to a change in air-flow direction. Earlier attempts to determine any additional interference of the supports on the model were inconclusive except to show that such interference was small.

Two airfoils of moderate thickness were chosen to be used in the present investigation, one being a symmetrical airfoil (N. A. C. A. 0012) and the other an airfoil of moderate camber (N. A. C. A. 4412). Tests were made of each airfoil using three methods of supporting the model. Besides the method using the usual support struts, tests were made with the models mounted on the usual supports with the addition of special wire supports and with the models mounted only on the wire supports. The wire supports consisted of three wires attached to the quarter-chord point of the model at each wing tip and of a sting and angle-of-attack strut so located as to be free from aerodynamic interference with the usual supports. The sting used was symmetrical with respect to the airfoil and was attached near the trailing edge instead of to the lower surface, as is usual.

The tares due to the wire supports were determined from the data obtained from the tests with the models on the usual supports with and without the wire supports. Some difficulty was experienced in obtaining sufficiently accurate tares because of the relatively large drag of the wires as compared with the drag of the model. Sufficient accuracy was obtainable only at the highest value of the test Reynolds Number ordinarily obtained (about 3,000,000). The profile-drag coefficients obtained for the two airfoils are plotted as solid lines in figures 46 and 47, together with data obtained from several tests made with the usual supports over a considerable period of time. The scattering of the points obtained from the tests with the usual supports about the solid line is within the limits of the accidental errors listed in reference 2, showing that there is no support interference within the accuracy of the results at high values of the Reynolds Number.

It is evident that the data obtained can be analyzed in different ways. For example, the data obtained with the models mounted on both the usual supports and the wire supports can be corrected for the usual support tares and compared with the data from tests with the models mounted only on the wire supports. The comparison was made correcting the data for the change in air-flow direction due to the usual supports and failed to show any support interference within the test accuracy.

Analysis of the data to determine the effects of the support interference on the measured pitching-moment coefficients was more difficult. The support wires stretched under the lift and drag loads, necessitating a correction to the measured pitching-moment coefficients, and the method of supporting the model at the wing tips allowed the model itself to deflect under the lift loads much more than when mounted on the usual supports. The correction due to the deflection of the model is difficult to evaluate with certainty because it involves integrations along the span after determination of the span load distribution. Accordingly, the effect of the support interference for the pitching moments

was determined only at zero lift where it was found that the measured pitching-moment coefficient was too large (algebraically) by 0.002. This same correction had been found previously from tests with symmetrical

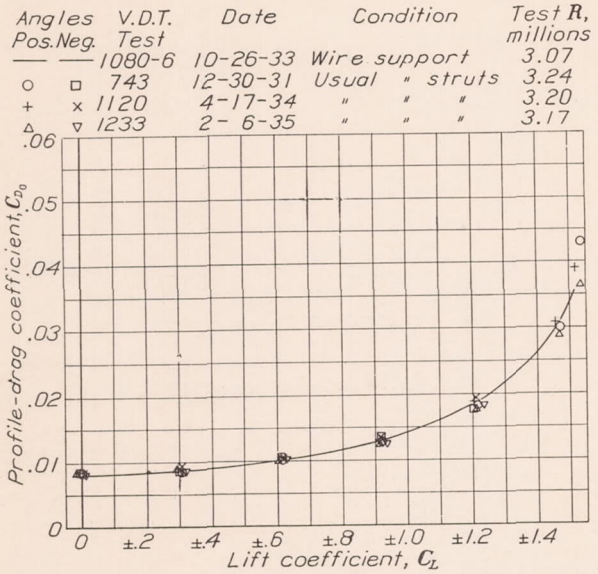

FIGURE 46.—Lift and drag characteristics of the N. A. C. A. 0012 airfoil as determined from tests with the model mounted on the usual support struts and on special wire supports.

airfoils and had been applied so that no new corrections were necessary.

EFFECTIVE WEIGHT OF MANOMETER LIQUIDS

The dynamic pressure is measured by two manometers connected to two sets of calibrated static-pressure orifices as described in reference 1. One manometer is filled with grain alcohol and the other with distilled water, the one filled with alcohol being ordinarily used to hold the dynamic pressure constant throughout a test because it is more easily read than the water manometer. Readings of the water manometer taken during each test serve to check the alcohol manometer and to indicate any change in the specific gravity of the alcohol, which is obtained from time to time by calibrating the alcohol manometer at atmospheric pressure against a head of distilled water.

It is apparent, as has been pointed out by Relf, that when the tank is filled with compressed air the increased density of the air reduces the effective weight of the alcohol or water in the manometers. This effect may be considered as a buoyancy of the air on the liquid and may be computed, but there is no assurance that the effects of other factors such as the amount of air dissolved in the liquid are negligible.

An experimental determination of the effect of the compressed air was made by calibrating the alcohol and water manometers at several tank pressures against a third manometer filled with mercury. The comparatively small buoyancy effect on the mercury was computed and applied to the results as a correction. The effects of other factors on the mercury were considered negligible. In addition to the correction determined in this way, a further small correction was applied to the specific gravity to compensate for the small change in balance calibration with air density due to the buoyancy of the air on the balance counterweights. The net correction at 20 atmospheres tank pressure was found to be 2.0 percent for the alcohol and 1.7 percent for the water, the dynamic pressure as measured being too high. It is planned to replace the manometers by a pressure balance in the near future. Measurements of dynamic pressure will then be independent of specific gravity.

CALIBRATION OF STATIC-PRESSURE ORIFICES

The static-pressure orifices used to measure the dynamic pressure are calibrated by making a velocity survey at the test section, using a calibrated pitot tube (reference 1). The calibration may be in error partly because of differences in dynamic scale and turbulence between conditions of pitot-tube calibration and of use in the variable-density tunnel and also because of possible blocking effects of the model. It is evident that a new method of calibration is necessary to eliminate these uncertainties.

These uncertainties may be largely eliminated by calibrating pitot tubes on an airplane in flight and by calibrating similar pitot tubes, similarly mounted on a model of the airplane in the tunnel. A detailed 1/20-scale model of the FC–2W2 airplane (reference 20) and the airplane itself were available. Three nonswiveling pitot tubes were mounted on the airplane as shown in figure 48. These pitot tubes were 2 inches in diameter

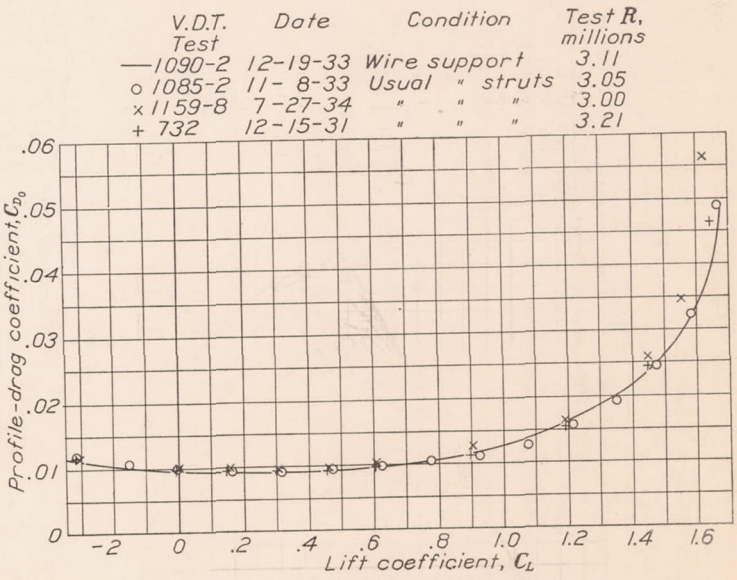

FIGURE 47.—Lift and drag characteristics of the N. A. C. A. 4412 airfoil as determined from tests with the model mounted on the usual support struts and on special wire supports.

with two staggered rows of static-pressure holes. Each row consisted of 12 equally spaced holes 0.22 inch in diameter. The pitot tubes were calibrated in flight against a previously calibrated trailing air-speed head. Three geometrically similar pitot tubes 0.10 inch in diameter were similarly mounted on the model and calibrated in the variable-density tunnel. Great care

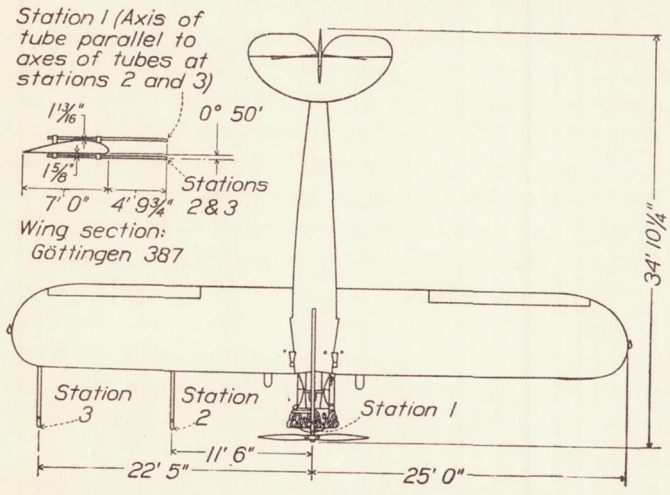

FIGURE 48.—Outline drawing showing location of pitot tubes on the FC-2W2 airplane.

was taken to make the small pitot tubes geometrically similar to the large ones and to mount them in the correct positions on the model.

The pitot tubes were calibrated in the tunnel over an angle-of-attack range from −8° to 14° and over a range of the test Reynolds Number from 1,000,000 to 2,500,000. Tests were made with three tail settings. All pressures were measured by a multiple-tube, photorecording manometer using a mixture of alcohol and water. Ratios of pressures were obtained directly from ratios of measured deflections and are independent of the specific gravity of the manometer liquid. A test was made with the pitot tubes interchanged as to position on the model to check the accuracy with which they were made. The results checked satisfactorily. Surveys were made upstream from the model with and without the model in place using a bank of 21 small pitot tubes mounted on a strut extending across the tunnel, surveys being made on the vertical center line and 6 and 12 inches to one side of the center line. The data obtained from these surveys are used to check the calibration of the static-pressure orifices from time to time as required. Force tests were also made on the model with and without the pitot tubes in place and with several tail settings.

The results obtained from the calibration of the pitot tubes are presented in figure 49. The data are presented as ratios of the dynamic pressures measured by the pitot tubes to the dynamic pressure as usually obtained from the static-pressure orifices. A fairly consistent variation of the results is shown with changes in Reynolds Number and tail settings. The results obtained from the calibration of the pitot tubes in flight are shown by outlined areas indicating the location of all points obtained.

Comparisons between the tunnel and flight results have been made on the basis of angles of attack, corrected in the case of the tunnel-

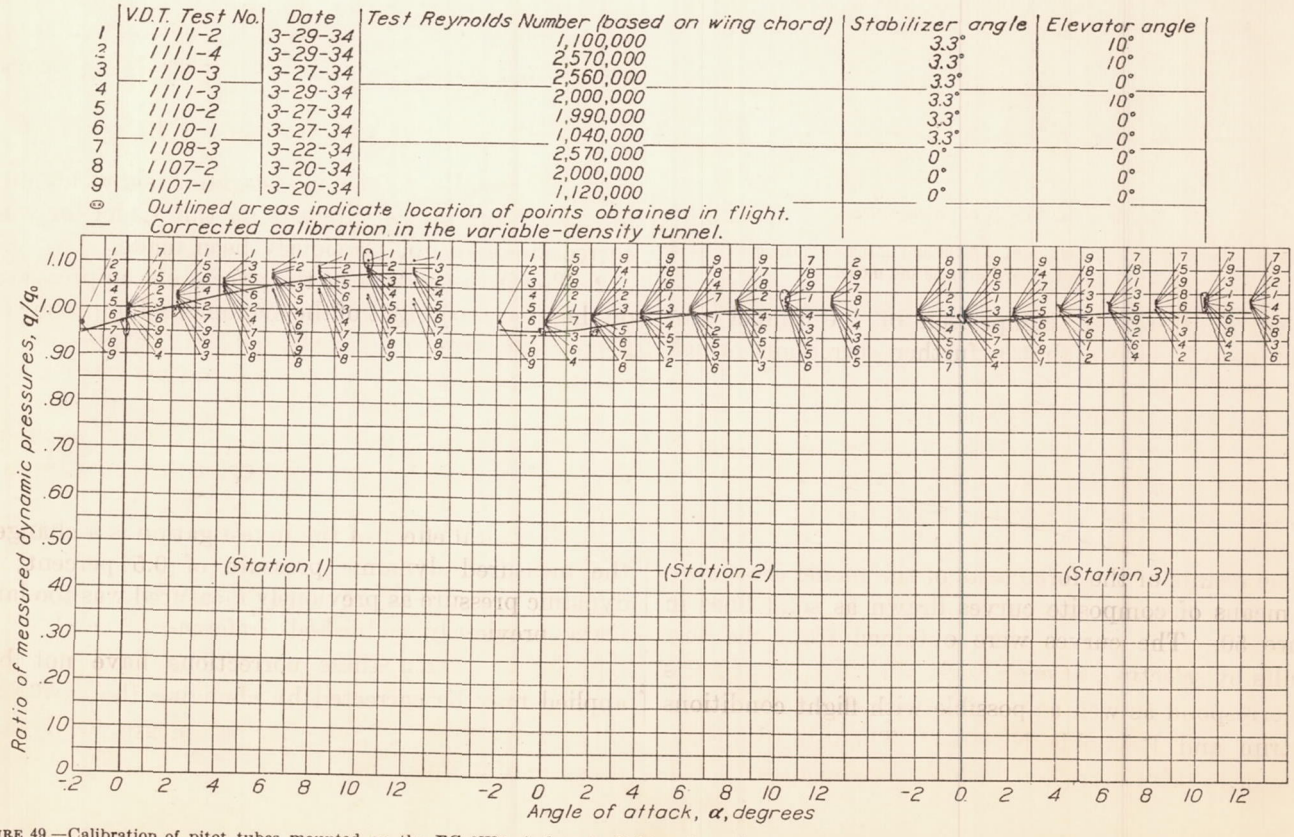

FIGURE 49.—Calibration of pitot tubes mounted on the FC-2W2 airplane in flight and on the FC-2W2 airplane model in the variable-density wind tunnel. Results corrected for tunnel-wall effect.

wall effect. Force tests made in the tunnel and in flight show that this method of comparison is very nearly equivalent to making the comparisons at equal lift coefficients. A value of the ratio q/q_0 was selected from the tunnel data to correspond as well as possible to flight conditions of trim and Reynolds Number for each pitot-tube position at each angle of attack. The values obtained were, in general, higher than the flight values at small angles of attack. Accordingly, the values obtained were reduced by increasing the value of q_0 by 1.5 percent, which is equivalent to a change in the static-pressure-orifice calibration factor from 1.172 to 1.190. The values of the ratio so obtained are plotted on the figure as solid lines, and the values agree reasonably well with the flight data at small

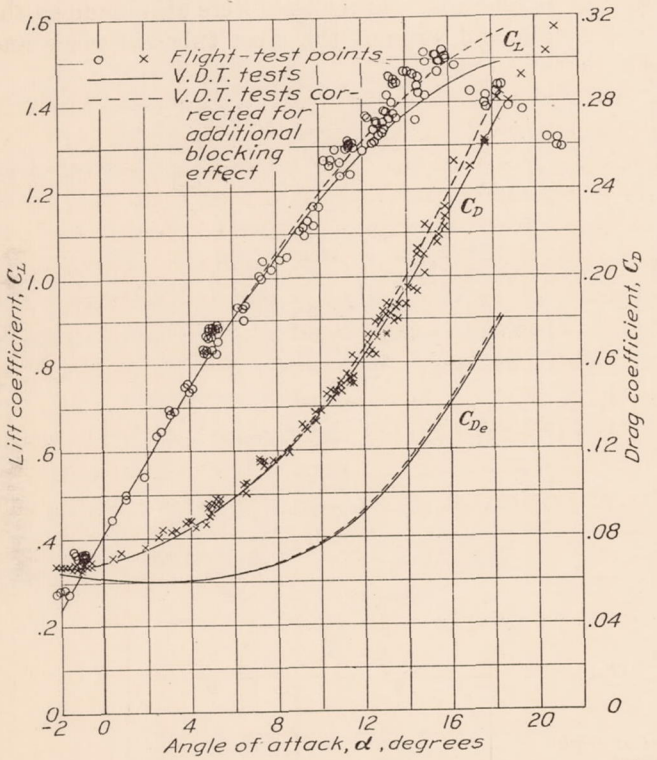

FIGURE 50.—Comparison of data obtained in flight and in the variable-density wind tunnel for the FC-2W2 airplane and model.

angles of attack. A comparison of the tunnel and flight data indicates that a further correction, which may be due to blocking effects, may be desirable at high angles of attack. The airplane model, however, had large drags at high angles of attack as compared with models normally used in the tunnel, making the application of this additional correction questionable for the usual airfoil tests.

The results of the force tests of the model are shown by means of composite curves drawn as solid lines in figure 50. The curves were obtained from the test results by selecting, at each angle of attack, test results to correspond as well as possible with flight conditions of trim and Reynolds Number. The tunnel results have been fully corrected including corrections to the effective Reynolds Number. Data obtained in flight tests (reference 20) are shown on the figure.

Although the model was much more detailed and accurate than is usual in wind-tunnel models, it was not considered before the tests to represent the airplane with sufficient accuracy and detail to give reliable drag results. Therefore too much emphasis should not be given to the good agreement of drag coefficients obtained in flight and in the tunnel. At lift coefficients less than 1.0 the agreement between flight and tunnel data is considered satisfactory. At higher lift coefficients some divergence of the tunnel and flight data is indicated. As previously stated, the results obtained from the pitot-tube calibration showed that an additional correction to the calibration factor of the static-pressure orifice might be desirable at high angles of attack. Such a correction has been determined from figure 49 and applied to the data. The results are plotted as dotted lines in figure 50 and show an improved agreement of the lift coefficients obtained in flight and in the tunnel at high angles of attack.

This additional correction is not ordinarily applied to the data obtained in the variable-density tunnel because it is doubtful whether the correction in most cases would give a better approximation to the actual conditions than no correction. The pitot-tube calibration tests were less accurate at high angles of attack than at low ones and, as previously stated, the drag of the model was larger than is the case for the models usually tested. Another fact indicating that this correction is small is that, up to the point of maximum lift, the lift curves obtained in the tunnel for some airfoils are very nearly straight. Any appreciable correction of this type would result in such lift curves being concave upward.

CONCLUSIONS

1. The results of the investigation show no interference of the model supports on the model for which corrections had not previously been made.

2. The investigation of the effects of compressed air on the effective weight of the manometer liquid showed a 2.0 percent error in the measured dynamic pressure; the dynamic pressure as previously measured was too large.

3. The investigation of the calibration of the static pressure orifices showed an error of 1.5 percent in this calibration; the dynamic pressure as previously measured was too small.

4. The total effect of the investigation is a change in the measured dynamic pressure of 0.5 percent; the dynamic pressure as previously measured was too large. Data previously published (reference 2 and earlier reports) to which these corrections have not been applied may be corrected by changing the coefficients to correspond to a reduction of measured dynamic pressure of 0.5 percent.

REFERENCES

1. Jacobs, Eastman N., and Abbott, Ira H.: The N. A. C. A. Variable-Density Wind Tunnel. T. R. No. 416, N. A. C. A. 1932.
2. Jacobs, Eastman N., Ward, Kenneth E., and Pinkerton, Robert M.: The Characteristics of 78 Related Airfoil Sections from Tests in the Variable-Density Wind Tunnel. T. R. No. 460, N. A. C. A., 1933.
3. Jacobs, Eastman N., and Pinkerton, Robert M.: Tests in the Variable-Density Wind Tunnel of Related Airfoils Having the Maximum Camber Unusually Far Forward. T. R. No. 537, N. A. C. A., 1935.
4. Wenzinger, Carl J., and Shortal, Joseph A.: The Aerodynamic Characteristics of a Slotted Clark Y Wing as Affected by the Auxiliary Airfoil Position. T. R. No. 400, N. A. C. A., 1931.
5. Platt, Robert C., and Abbott, Ira H.: Aerodynamic Characteristics of N. A. C. A. 23012 and 23021 Airfoils with 20-Percent-Chord External-Airfoil Flaps of N. A. C. A. 23012 Section. T. R. No. 573, N. A. C. A., 1936.
6. Millikan, Clark B.: On the Lift Distribution for a Wing of Arbitrary Plan Form in a Circular Wind Tunnel. Publication No. 22, C. I. T., 1932.
7. Jacobs, Eastman N., and Pinkerton, Robert M.: Tests of N. A. C. A. Airfoils in the Variable-Density Wind Tunnel. Series 230. T. N. No. 567, N. A. C. A., 1936.
8. Anderson, R. F.: Determination of the Characteristics of Tapered Wings. T. R. No. 572, N. A. C. A., 1936.
9. Jacobs, Eastman N., and Clay, William C.: Characteristics of the N. A. C. A. 23012 Airfoil from Tests in the Full-Scale and Variable-Density Tunnels. T. R. No. 530, N. A. C. A., 1935.
10. Platt, Robert C.: Turbulence Factors of N. A. C. A. Wind Tunnels as Determined by Sphere Tests. T. R. No. 558, N. A. C. A., 1936.
11. Stack, John: Tests in the Variable-Density Wind Tunnel to Investigate the Effects of Scale and Turbulence on Airfoil Characteristics. T. N. No. 364, N. A. C. A., 1931.
12. Toussaint, A., and Jacobs, E.: Experimental Methods–Wind Tunnels. Vol. III, div. I of Aerodynamic Theory, W. F. Durand, editor, Julius Springer (Berlin), 1935, p. 332.
13. von Kármán, Th., and Millikan, C. B.: On the Theory of Laminary Boundary Layers Involving Separation. T. R. No. 504, N. A. C. A., 1934.
14. Dryden, H. L.: Air Flow in the Boundary Layer Near a Plate. T. R. No. 562, N. A. C. A., 1936.
15. Dryden, H. L., and Kuethe, A. M.: Effect of Turbulence in Wind Tunnel Measurements. T. R. No. 342, N. A. C. A., 1930.
16. Jacobs, Eastman N.: The Aerodynamic Characteristics of Eight Very Thick Airfoils from Tests in the Variable-Density Wind Tunnel. T. R. No. 391, N. A. C. A., 1931.
17. Jones, B. Melvill: Stalling. R. A. S. Jour., vol. XXXVIII. No. 285, Sept. 1934, pp. 753–769.
18. Higgins, George J., and Jacobs, Eastman N.: The Effect of a Flap and Ailerons on the N. A. C. A. –M6 Airfoil Section. T. R. No. 260, N. A. C. A., 1927.
19. Jacobs, Eastman N., and Pinkerton, Robert M.: Pressure Distribution over a Symmetrical Airfoil Section with Trailing Edge Flap. T. R. No. 360, N. A. C. A., 1930.
20. Thompson, F. L., and Keister, P. H.: Lift and Drag Characteristics of a Cabin Monoplane Determined in Flight. T. N. No. 362, N. A. C. A., 1931.

TABLE I

IMPORTANT AIRFOIL SECTION CHARACTERISTICS

N. A. C. A. airfoil	R_e (millions)	α_{l_0} (deg.)	a_0	$c_{l_{max}}$ [1]	$c_{l_{opt}}$	$cd_{0_{min}}$	$c_{m_{a.c.}}$	a. c.	
								x (percent c)	y (percent c)
0009	8.470					[2] 0.0061			
	8.290	0	0.098	A1.39	0	.0064	0	1.0	5
	6.100	0	.097	A1.28	0	.0064	0	1.0	4
	3.410	0	.097	D.94	0	.0062	0	1.8	8
	1.760	0	.096	D.88	0	.0060	0	1.7	13
	.882	0	.096	D.86	0	.0049	0		
	.446	0	.105	D.85	0	.0065	0		
	.223	0	.117	D.83	0	.0131	0		
	.112	0	.104	D.78	0	.0135	0		
0012	8.370	0	.099	A1.66	0	.0069	0	.6	3
	8.450	0	.100	A1.65	0	.0069	0	.6	3
	6.280	0	.097	A1.62	0	.0073	0	.8	3
	3.540	0	.097	A1.49	0	.0077	0	1.0	4
	1.740	0	.096	A1.18	0	.0075	0	1.1	3
	.871	0	.094	D.91	0	.0065			
	.449	0	.098	D.89	0	.0105			
0015	8.610	0	.097	A1.66	0	.0077	0	1.2	4
	5.990	0	.096	A1.60	0	.0082	0	1.1	3
	3.350	0	.094	C1.48	0	.0086	0	1.2	1
	1.730	0	.093	C1.28	0	.0088	0	2.4	1
	.874	0	.092	C1.09	0	.0084	0	1.5	0
	.438	0	.091	D.98	0	.0079			
	.222	0	.101	D.89		.0149			
	.113	0	.134	D.90		.0158			
0018	7.840	0	.096	A1.53	0	.0088	0	1.7	4
	6.240	0	.096	A1.53	0	.0092	0	1.6	3
	3.300	0	.096	C1.42	0	.0098	0	2.2	3
	1.730	0	.095	D1.26	0	.0100	0	2.2	0
	.866	0	.090	C1.15	0	.0102	0	2.4	0
	.430	0	.086	A1.03	0	0127	0	1.8	0
	.214	0	.092	D.96	0	.0179			
	.109	0	.114	D.86	0	.0297			
2412	8.240	−2.0	.098	A1.72	.14	.0071	−.043	.5	3
	6.100	−2.1	.097	A1.68	.14	.0080	−.043	1.1	3
	3.420	−2.0	.098	C1.53	.15	.0079	−.045	1.1	1
	1.730	−2.1	.096	D1.33	.30	.0089	−.045	.9	−2
	.879	−2.1	.096	D1.16	.22	.0085	−.054	1.8	0
	.438	−2.0	.098	D1.08	.42	.0067			
	.218	−2.2	.102	D1.08	.26	.0159			
	.110	−1.3		D1.03		.0227			
23012	8.370					[3] .0071			
	8.160	−1.2	.100	A1.72	.08	.0070	−.008	1.2	7
	6.070	−1.2	.098	A1.67	.08	.0079	−.007	1.3	7
	3.400	−1.2	.098	A1.53	.05	.0080	−.007	1.3	5
	1.760	−1.2	.097	D1.41	.16	.0090	−.012	1.4	5
	.884	−1.2	.096	D1.28	.28	.0084	−.010	2.0	7
	.449	−1.3	.096	D1.19	.12	.0098			
	.221	−1.6	.109	D1.15	.37	.0179			
	.112	−1.4		D1.00	.20	.0182			
23012-33	8.000	−1.2	.097	B1.49	.20	.0071	−.010	.6	5
	6.390	−1.2	.098	A1.42	.10	.0075	−.010	.8	5
	3.380	−1.2	.096	D1.26	.23	.0076	−.011	1.0	6
	1.760	−1.2	.096	D1.12	.28	.0071	−.014	.9	3
	.900	−1.2	.094	D1.07	.10	.0084	−.011	.9	0
	.454	−1.4	.096	D1.01	.40	.0096	−.014	.4	−1
$2R_212$	8.370	−.6	.098	A1.61	.10	.0073	.005	1.0	7
	6.310	−.7	.097	D1.55	.02	.0078	.006	1.1	6
	3.540	−.7	.097	D1.44	.11	.0077	.005	1.0	4
	1.770	−.8	.095	D1.28	.23	.0077	.002	.8	0
	.884	−.8	.096	D1.14	.28	.0073	−.001	1.1	0
	.454	−.9	.100	D1.08	.35	.0118			
4409	8.080	−3.9	.096	A1.77	.26	.0073	−.088	.6	2
	5.970	−3.9	.096	D1.70	.26	.0080	−.088	.7	1
	3.340	−4.0	.095	C1.50	.34	.0077	−.090	1.0	−1
	1.700	−4.0	.098	D1.29	.41	.0084	−.092	1.1	−1
	.869	−4.1	.096	D1.26	.40	.0080	−.098	1.4	−4
	.438	−4.1	.097	D1.23	.55	.0097			
	.218	−3.7	.105	D1.21	.57	.0096			
	.110	−2.5	.115	D1.09	.77	.0189			
4412	7.920	−4.0	.098	D1.74	.32	.0082	−.088	.8	2
	6.100	−4.1	.096	D1.70	.22	.0085	−.088	.9	1
	3.270	−4.1	.098	D1.61	.30	.0087	−.091	1.0	−1
	1.680	−4.2	.097	D1.46	.37	.0095	−.095	1.2	−5
	.874	−4.3	.096	D1.36	.36	.0091	−.097	1.1	−8
	.433	−4.3	.094	D1.31	.51	.0109			
	.219	−4.3	.100	D1.32	.57	.0194			
	.111	−2.9	.113	D1.20		.0276			
4415	7.920	−4.0	.097	C1.72	.22	.0090	−.085	1.0	1
	6.280	−4.0	.095	D1.66	.20	.0093	−.086	1.4	1
	3.340	−4.1	.096	D1.56	.23	.0094	−.085	1.4	−2
	1.730	−4.2	.095	D1.48	.31	.0099	−.090	1.7	−4
	.882	−4.3	.094	D1.41	.34	.0103	−.092	1.4	−8
	.431	−4.4	.089	D1.35	.39	.0123			
	.219	−4.4	.089	D1.34	.46	.0198			
	.110	−3.1		D1.34	.68	.0269			
6412	8.210	−5.9	.098	D1.82	.37	.0091	−.133	.9	1
	6.020	−5.9	.096	D1.75	.25	.0096	−.130	1.1	1
	3.350	−6.1	.097	D1.64	.38	.0099	−.131	.8	−3
	1.700	−6.2	.097	D1.54	.52	.0104	−.135	1.0	−2
	.882	−6.3	.097	D1.48	.60	.0096			
	.441	−6.2	.097	D1.47	.55	.0129			
	.219	−5.9	.106	D1.46	.70	.0205			
	.110	−5.4		D1.45		.0160			

[1] Type lift-curve peak:

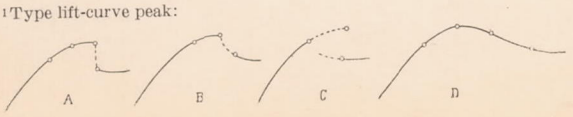

[2] From reference 2.
[3] From reference 7.

TABLE I—Continued

IMPORTANT AIRFOIL SECTION CHARACTERISTICS—Continued

N. A. C. A. airfoil	R_e (millions)	α_{l_0} (deg.)	a_0	$c_{l_{max}}$ [1]	$c_{l_{opt}}$	$c_{d_{0\,min}}$	$c_{m_{a.c.}}$	a. c. x (percent c)	a. c. y (percent c)
6712	8.100	−7.3	0.096	D2.05	0.35	0.0115	−0.199	1.2	−2
	6.120	−7.4	.095	D1.99	.32	.0119	−.197	1.1	−4
	3.380	−7.4	.098	D1.83	.33	.0120	−.198	1.1	−8
	1.750	−7.6	.103	D1.65	.45	.0124	−.210	1.6	−12
	.892	−7.8	.103	D1.52	.82	.0138			
	.449	−5.7		D1.45	.88	.0228			
	.222	−4.6		D1.50	1.01	.0283			
	.112	−3.9		D1.41	−.02	.0411			
8318	8.450	−7.2	.095	D1.59	.24	.0127	−.132	1.5	2
	6.420	−7.3	.092		.10	.0128	−.132	1.8	2
	3.460	−7.4	.093	D1.67	.31	.0128	−.135	1.8	2
	1.790	−7.6	.093	D1.76	.36	.0140	−.137	2.1	3
	.911	−8.7	.088	D1.80	.43	.0173			
	.449	−9.0	.085	D1.78	.58	.0215			
	.224	−9.2	.080	D1.40	.58	.0259			
	.112	−8.0	.077	D1.02		.0332			
0012 (With split flap at 60°.)	8.110	[4] −13.1	[5] .091	A2.35		[7] .167	[8] −.220	.6	3
	5.910			A2.35					
	3.770			A2.30					
	3.430			A2.21					
	1.740			A1.84					
	.919			D1.67					
	.449			D1.63					
23012 (With split flap at 60°.)	8.180	[4] −14.3	[5] .088	A2.48		[7] .166	[8] −.236	1.2	7
	5.970			A2.51					
	3.620 (Average)			A2.39					
	1.740			A2.24					
	.882			A2.07					
	.444			D1.92					
23012 (With split flap at 75°.)	8.100	[4] −15.6	[5] .085	A2.54		[7] .201	[8] −.228	1.2	7
	5.990			A2.52					
	3.800			A2.41					
	1.740			A2.21					
	.887			A2.01					
	.446			A1.90					
23015	8.370	−1.1	.098	A1.73	.10	.0081	−.008	1.1	6
	3.880			C1.60					
23015 (With split flap at 75°.)	8.210	[4] −16.2	[5] .086	A2.70		[7] .198	[8] −2.45	1.1	6
	5.990			A2.69					
	3.830			A2.59					
	1.800			A2.45					
	.924			A2.32					
	.450			A2.11					
23021	8.210	−1.2	.092	B1.50	.07	.0101	−.005	2.3	7
	5.940			A1.54					
	3.770			A1.47					
	1.720			D1.32					
	.892			D1.26					
	.441			A1.20					
23021 (With split flap at 75°.)	8.130	[4] −16.5	[5] .094	A2.74		[7] .191	[8] −.300	2.3	7
	5.960			A2.81					
	3.800			A2.79					
	1.720			A2.58					
	.879			A2.46					
	.435			A2.28					
43012	8.390	−2.3	.100	A1.84	.26	.0079	−.019	1.0	7
	3.890			A1.71					
	.449			A1.44					
43012 (With split flap at 75°.)	8.240	[4] −17.3	[5] .082	A2.65		[7] .200	[8] −.225	1.0	7
	6.040			A2.60					
	3.830			A2.47					
	1.740			A2.39					
	.887			A2.29					
	.449			A2.18					
23012 (With 23012 flap 3° up.)	8.210	−.9	.101	A1.68	.07	.0069	.009	.5	8
	6.150	−.8	.100	A1.62	.15	.0074	.009	1.0	9
	3.300	−.8	.100	A1.54	.19	.0078	.010	1.1	11
	1.680	−.8	.097	A1.39	.13	.0068	.011	1.2	11
	.858	−.8	.096	D1.24	.08	.0093			
	.430	−1.2	.096	D1.12	.08	.0119			
23012 (With 23012 flap set 30°.)	8.140	[4] −13.8	[5] .102	A2.46	.45	.0161	[9] −.260	.5	8
	6.200			A2.40					
	3.410			A2.32					
	1.700	[4] −12.5	[5] .103	[6] C2.13	.70	.0184	[9] −.260	1.2	11
	1.700			[6] D1.95					
	.879	[4] −11.9	[5] .102	D1.75	.60	.0218			
	.441			D1.66					
Clark Y [10] (With Handley Page slot.)	9.900	−4.2	[5] .099	D2.12	.76	.0242			
	8.080	−4.3	[5] .099	D2.06	.76	.0248			
	4.990	−4.2	[5] .098	D2.02	.69	.0260			
	3.090	−4.2	[5] .097	D1.96	.62	.0260			
	2.040	−4.1	[5] .096	D1.98	.65	.0264			
	1.290	−4.1	[5] .092	D1.92	.63	.0272			
	.784	−4.1		D1.82	.64	.0301			
	.520	−4.1		D1.75	.63	.0291			
	.261	−4.1		D1.60	.64	.0322			
	.135	−4.3		D1.41	.63	.0431			

[1] See footnote 1, p. 39.

[4] Angle of zero lift determined from linear lift curve approximating experimental lift curve.

[5] Slope of lift curve determined from linear lift curve approximating experimental lift curve.

[6] Discontinuity present in the scale effect.

[7] Value of the drag that applies approximately over the entire useful range of lift coefficients.

[8] $c_{m_{a.c.}}$ is taken about the aerodynamic center of the plain wing and is fairly constant at high lift coefficients.

[9] $c_{m_{a.c.}}$ is taken about the aerodynamic center of the wing with flap neutral and is fairly constant at high lift coefficients.

[10] Not N. A. C. A.

TABLE II

AIRFOIL SECTION CHARACTERISTICS

N. A. C. A. airfoil	Classification			R_c [4] (Millions)	Fundamental section characteristics							
	Chord [1]	SE [2]	$C_{L_{max}}$ [3]		$c_{l_{max}}$	α_{l_0} (deg.)	a_0, per degree	$c_{l_{opt}}$	$c_{d_{0\ min}}$	$c_{m\ a.c.}$	*a. c.* (percent *c* from *c*/4)	
											Ahead	Above
0009	A	B	A	8.29	1.39	0	0.098	0	0.0064	0	1.0	5
0012	A	C0	A	8.37	1.66	0	.099	0	.0069	0	.6	3
0015	A	D0	A	8.61	1.66	0	.097	0	.0077	0	1.2	4
0018	A	E0	A	7.84	1.53	0	.096	0	.0088	0	1.7	4
2412	A	C2	A	8.24	1.72	−2.0	.098	.14	.0071	−.043	.5	3
23012	A	D2	A	8.16	1.72	−1.2	.100	.08	.0070	−.008	1.2	7
23012–33	A	B6	B	8.00	1.49	−1.2	.097	.20	.0071	−.010	.6	5
$2R_312$	A	C3	A	8.37	1.61	−.6	.098	.10	.0073	−.005	1.0	7
4409	A	B4	A	8.08	1.77	−3.9	.096	.26	.0073	−.088	.6	2
4412	A	C4	D	7.92	1.74	−4.0	.098	.32	.0082	−.088	.8	2
4415	A	D4	C	7.92	1.72	−4.0	.097	.22	.0090	−.085	1.0	1
6412	A	C6	D	8.21	1.82	−5.9	.098	.37	.0091	−.133	.9	1
6712	A	C2	D	8.10	2.05	−7.3	.096	.35	.0115	−.199	1.2	−2
8318	A	E8	D	8.45	1.59	−7.2	.095	.24	.0127	−.132	1.5	2
0012 with split flap at 60°	A	C0	A	8.11	2.35	[5] −13.1	[6] .091	-------	[7] .167	[8] −.220	.6	3
23012 with split flap at 60°	A	D2	A	8.18	2.48	[5] −14.3	[6] .088	-------	[7] .166	[8] −.236	1.2	7
23012 with split flap at 75°	A	D2	A	8.10	2.54	[5] −15.6	[6] .085	-------	[7] .201	[8] −.228	1.2	7
23015	A	D2	A	8.37	1.73	−1.1	.098	.10	.0081	−.008	1.1	6
23015 with split flap at 75°	A	D2	A	8.21	2.70	[5] −16.2	[6] .086	-------	[7] .198	[8] −.245	1.1	6
23021	A	E2	B	8.21	1.50	−1.2	.092	.07	.0101	−.005	2.3	7
23021 with split flap at 75°	A	E2	A	8.13	2.74	[5] −16.5	[6] .094	-------	[7] .191	[8] −.300	2.3	7
43012	A	D4	A	8.39	1.84	−2.3	.100	.26	.0079	−.019	1.0	7
43012 with split flap at 75°	A	D4	A	8.24	2.65	[5] −17.3	[6] .082	-------	[7] .200	[8] −.225	1.0	7
23012 with 23012 flap 3° up	A	D2	A	8.21	1.68	−.9	.101	.07	.0069	.009	.5	8
23012 with 23012 flap set 30°	A	-------	A	8.14	2.46	[5] −13.8	[6] .102	.45	.0161	[9] −.260	.5	8
Clark Y with Handley Page slot [10]	B	-------	D	8.08	2.06	−4.3	.099	.76	.0248	----------	-------	-------

[1] Type of chord. A refers to a chord defined as a line joining the extremities of the mean line.

[2] Type of scale effect on maximum lift.

[3] Type of lift-curve peak as shown in the sketches below:

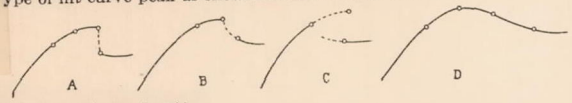

[4] Turbulence factor is 2.64.

[5] Angle of zero lift determined from linear lift curve approximating experimental lift curve.

[6] Slope of lift curve determined from linear lift curve approximating experimental lift curve.

[7] Value of the drag that applies approximately over the entire useful range of lift coefficients.

[8] $c_{m_{a.c.}}$ is taken about the aerodynamic center of the plain wing and is fairly constant at high lift coefficients.

[9] $c_{m_{a.c.}}$ is taken about the aerodynamic center of the wing with flap neutral (−3°) and is fairly constant at high lift coefficients.

[10] Not N. A. C. A.

U. S. GOVERNMENT PRINTING OFFICE: 1937